Optimisation of Floating Offshore Wind Substructures: A Higher-Fidelity Approach

Bart Jan Klootwijk

Delft University of Technology

Optimisation of Floating Offshore Wind Substructures: A Higher-Fidelity Approach

by

Bart Jan Klootwijk

Wednesday 22$^{\text{nd}}$ November, 2023

to obtain the degree of Master of Science in Aerospace Engineering
at Delft University of Technology,

Wind Energy Group, Faculty of Aerospace Engineering, Delft University of Technology

Student number:	4551516	
Thesis committee:	Prof. dr. D. A. von Terzi	TU Delft, chair
	Prof. dr. A. C. Viré,	TU Delft, supervisor
	Ir. F. J. Savenije,	TNO, supervisor
	Dr. ir. G. la Rocca	TU Delft, examiner

Cover: GustoMSC

Preface

This thesis report marks the culmination of my academic endeavors at Delft University of Technology. Embarking on the aerospace engineering programme at the age of seventeen, I was initially drawn by the fascinating technology of aviation. Yet, following explorations into the minor program of electrical sustainable energy systems and the completion of a bachelor thesis on renewable energy systems for Martian habitats, I discovered that my primary interest lies in a specialisation in wind energy - a field that I consider of great and immediate relevance to society.

I am grateful for all the friendships, and opportunities that shaped me into the person I am today, both within and outside the university. I will remember my student days as being vibrant, filled with invaluable learning experiences, and most importantly: fun.

I would like to start off by thanking my supervisors Axelle Viré and Feike Savenije. Axelle, your exceptional expertise in floating wind energy technology has been a continuous source of inspiration to me, and I appreciate your invaluable guidance and ability to always connect me with the right people. Feike, I am grateful for your faith in me, and continued support. The opportunity to conduct my research at a prestigious institution like TNO has been an honour, and I am thankful for the autonomy you afforded me in steering my research project. To all future students, I wish for mentors as dedicated and supportive as you.

I extend my gratitude to my colleagues at TNO for the incredible experience I've had. Working alongside some of the brightest minds on cutting-edge research projects has been truly inspiring, and I've felt welcomed from the very beginning. I enjoyed our dynamic interactions and appreciated your readiness to always offer assistance.

Additionally, I would like to express my gratitude to Matteo Baudino Bessone for his support with OpenMDAO and the optimisation problem setup. Your valuable insights at the right moments have contributed significantly to my work.

A special thank you goes out to my girlfriend, whose love and continuous support have been a driving force behind my success, both professionally and in my personal life. Jolie, thank you for your belief in me, your encouragements, and not to mention: your patience.

Last but not least, I want to recognise and express my heartfelt thanks to my parents. Without your unconditional support in every way, I would never have reached where I am today.

Bart Jan Klootwijk
The Hague, November 2023

Abstract

Floating offshore wind turbines (FOWTs) unlock the potential to harness energy from wind in deeper waters. Despite their potential, the major obstacle to large-scale commercial deployment remains the floating substructure's high cost. Multidisciplinary design, analysis and optimisation techniques are commonly employed to improve their cost-competitiveness, but existing models often use simplified engineering models. This approach risks neglecting design considerations typical of structures subjected to complex aero-hydro-servo-elastic loads.

To address the need for incorporating higher-fidelity analysis methods, an optimisation framework is developed, integrating OpenFAST to simulate the response of the FOWT system under various environmental and operational conditions. Leveraging the flexibility of the Python framework and the wealth of output data contained within the OpenFAST simulation results, this holistic approach offers opportunities to explore novel and cost-effective platform designs with high reliability.

To demonstrate its effectiveness, the optimisation framework is utilised to achieve a significant reduction of the DeepCWind platform's structural mass. Among the considered constraints, the platform pitch motion was critical, reaching maxima for design load cases characterised by the most extreme wind and waves. Although the inclusion of a structural model for the platform comes at considerable computational expense, it enhances the framework's value, as structural integrity can be verified.

The recommended use of the optimisation framework is for in-depth studies, following preliminary design explorations conducted with cheaper models. Future efforts should focus on extending the structural and hydrodynamic model to improve the framework's versatility, and make it applicable to a wider range of platform concepts and turbine sizes.

Contents

List of Figures

List of Tables

Nomenclature

Abbreviations

AEP	Annual Energy Production
BC	Base Column
BEM	Boundary Element Method
BIE	Boundary Integral Equation
BVP	Boundary Value Problem
CAPEX	Capital Expenditures
COBYLA	Constrained Optimisation BY Linear Approximation
COD	Co-Directional
DFT	Discrete Fourier Transform
DLC	Design Load Condition
DOF	Degree of Freedom
ESS	Extreme Sea State
EWM	Extreme Wind Model
FEM	Finite Element Method
FFT	Fast Fourier Transform
FOWT	Floating Offshore Wind Turbine
IEC	International Electrotechnical Commission
IRF	Impulse Response Function
LCOE	Levelised Cost Of Energy
LFEM	Linear Frame Finite Element Model
MC	Main Column
MDAO	Multidisciplinary Design Analysis and Optimisation
MSL	Mean Sea Level
NPV	Net Present Value
NREL	National Renewable Energy Laboratory
NSS	Normal Sea State
NTM	Normal Turbulence Model
OPEX	Operational Expenditures
PSF	Partial Safety Factor
QTF	Quadratic Transfer Function
RAO	Response Amplitude Operator
RNA	Rotor-Nacelle Assembly
SIM	Static-Improvement Method
TLP	Tension Leg Platform
TRL	Technology Readiness Level
UC	Upper Column
VLA	Vertical Load Anchor
WACC	Weighted Average Cost of Capital

Latin Symbols

A	area	(m^2)
a	acceleration	(m s^{-2})
c	Weibull scale parameter	(m s^{-1})
c_A	added mass coefficient	(-)
c_D	drag coefficient	(-)
D	diameter	(m)
d	discount rate	(-)
E	Young's modulus	(Pa)
F	force	(N)
f	frequency	(Hz)
G	shear modulus	(Pa)
g	gravitational acceleration	(m s^{-2})
H	height	(m)
I	mass moment of inertia	(kg m^2)
k	Weibull shape parameter	(-)
L	length	(m)
m	mass	(kg)
p	pressure	(Pa)
R	radius	(m)
T	period	(s)
t	thickness	(m)
U	wind speed	(m s^{-1})
u	velocity in x-direction	(m s^{-1})
V	Volume	(m^3)
v	velocity in y-direction	(m s^{-1})
w	velocity in z-direction	(m s^{-1})

Greek Symbols

γ	peak enhancement factor	(-)
ω	frequency	(rad s^{-1})
Φ	velocity potential	(m^2 s^{-1})
ρ	density	(kg m^{-3})
σ	stress	(Pa)
θ	platform pitch angle	(°)

1

Introduction

Offshore wind energy is regarded as a crucial component of the transition towards a low-carbon energy system. To meet global sustainable energy goals, the installation of offshore wind farms must be drastically increased before 2050. However, conventional offshore wind turbines are fixed to the seabed, which restricts their deployment to shallow waters. According to the IEA, the world's total electricity demand could be met 11 times over if wind turbines could operate in deep water environments [1]. It is for this reason that floating wind turbines have attracted significant attention from researchers, policymakers and industry in recent years.

By eliminating the depth constraint to a large extent, floating wind turbines unlock the potential to harness stronger winds at higher capacity factors, further offshore. But more importantly, they offer access to offshore wind in regions that are close to population centres, where floating foundations are the only option for large-scale deployment, such as the United States or Japan [2]. Other major opportunities exist in installation and maintenance of floating wind turbines, because of their ability to be towed from port to site and back, thereby reducing dependence on large and costly vessels. The technological feasibility of floating wind power has already been demonstrated through the development of two pilot wind farms, Hywind Scotland and WindFloat Atlantic [3], along with several other prototypes. The important next step is to move towards large-scale commercial deployments. This may be achieved through development of standards, building upon experience from the offshore oil and gas industry, and standardisation of floating substructure designs [4].

As such, there is an established potential for floating offshore wind energy. Nonetheless, a major obstacle to large-scale commercial deployment remains the high cost of the floating substructure, which may constitute up to 30% of the total CAPEX [5]. Hence, it is important to assess the technological and economical feasibility of this technology in a precise and reliable manner. This is not a straightforward task, because floating wind is still in its infancy. Techno-economic analyses may provide insight into the sensitivity of the costs and revenues of floating wind farms to different floater concepts or different site locations, but they lack the granularity required to comprehensively address platform design and wind turbine performance aspects.

A more effective strategy to improve the cost-competitiveness of floating substructures is the application of multidisciplinary design, analysis and optimisation (MDAO) techniques. However, existing models often use simplified engineering methods to model the response of the floating platform due to their computational efficiency. This approach risks to neglect design considerations in a problem that is driven by the inherent dynamic nature of a structure subjected to aero-hydro-servo-elastic loads.

This thesis addresses the shortcomings of existing substructure optimisation models by integrating higher-fidelity analysis tools into a holistic and flexible programming framework, in order to enhance the cost-effectiveness of floating wind turbines, ultimately promoting the economic viability of floating wind.

This introductory chapter serves to provide a solid basis for the thesis. First, section 1.1 summarises the findings of a literature study, done prior to this thesis. Then, section 1.2 presents the motivation of the research. Subsequently, the research questions are formulated in section 1.3. And finally, section 1.4 provides an overview of the report structure.

1.1. Literature

Prior to this thesis, a thorough literature review has been carried out. The findings of the literature study that are relevant for the work presented in this thesis report, are outlined in the following sections.

1.1.1. Floating Offshore Wind Energy Technology

Although floating offshore wind energy is not a mature technology yet, floating platforms have been around for many decades already, since the beginning of offshore exploration and production of oil and gas. Hence the floating wind industry can build upon the experience from this sector. However, there are significant challenges to overcome. Oil and gas platforms are uniquely designed for a single location and specific purpose. They are often over-designed, because their reliability is of utmost importance, and profit margins are less stringent. Therefore, platform mass is less critical in these contexts. However, to exploit the offshore wind at large scale in an economically viable way, floating platforms should be standardised, and designed with minimum cost and weight in mind. To achieve this, engineers are pushing boundaries and seeking limits of the design space. In the following paragraphs, some of the challenges associated with offshore wind are discussed, going from bottom-fixed to floating substructures.

From Bottom-Fixed to Floating Wind Turbines

In the offshore wind industry, the marine environment is well understood. Site conditions like wave height and wave period play an important role in the design of bottom-fixed wind turbine foundations (e.g. monopiles, jackets). However, the essential difference between bottom-fixed and floating foundations is that in the former case the wind turbine is constraint and does not move (apart from the aero-servo-elastic deformations), whereas in the latter case, the wind turbine is mounted on a floating platform that is secured to the seabed with mooring lines and anchors. As such, the turbine is able to move in all six degrees of freedom (surge, sway, heave, roll, pitch and yaw), which are visualised in figure 1.1. The compliant motion of the floating platform has a significant impact on turbine performance, fatigue and design loads. Therefore it should not only provide enough buoyancy to support the wind turbine tower and rotor-nacelle assembly (RNA), but also provide stability in the offshore environment, preventing excessive motion due to wind, waves and other environmental loads [6].

Nevertheless, floating wind turbines operate in harsh environmental conditions and encounter more complex interactions with the physical environment compared to their bottom-fixed counterparts, due to the inherent nature of floating platforms. Wind-induced loads on the rotor, coupled with wave-induced loads on the floating system, constitute the primary loads on the floating wind turbine, with both mean and dynamic components. Additional loads are induced by ocean currents, sea level variation due to tides, gravitational loads of the turbine and floater, etc. [7]. As a consequence, floating wind turbines are subject to fully coupled interactions with metocean conditions, leading to complex aero-hydro-servo-elastic loading. Designers must carefully assess metocean data and simulate the system response to a wide range of design load conditions [8], with the aid of high-fidelity models for an accurate representation of the physics involved.

Floater Concepts

Many concepts have been researched and developed that tackle the issues discussed previously, and enable the deployment of wind turbines in deep waters. In a market analysis in 2015 [3], over thirty different concepts have already been identified that are under development, and this number is growing every year.

Floating Foundations

Floating platforms can be classified according to the physical principle that provides their hydrostatic stability [9]. The floating substructures may be:

- **Ballast stabilised**, which relies on heavy ballast at the bottom of the floating substructure. This causes the centre of gravity of the complete system to shift below the centre of buoyancy. When the system is tilted from its equilibrium position, a righting moment counteracts the rotational displacement, hence achieving stability. This is the principle that is utilised by spar-type floating platforms, which usually consist of a deep draft cylindrical structure with ballast at the bottom.
- **Waterplane stabilised** (or buoyancy stabilised), in which case the restoring moment is generated by a horizontal shift in the centre of buoyancy, creating a lever arm between the centre of gravity and centre of buoyancy, opposing the tilting motion.

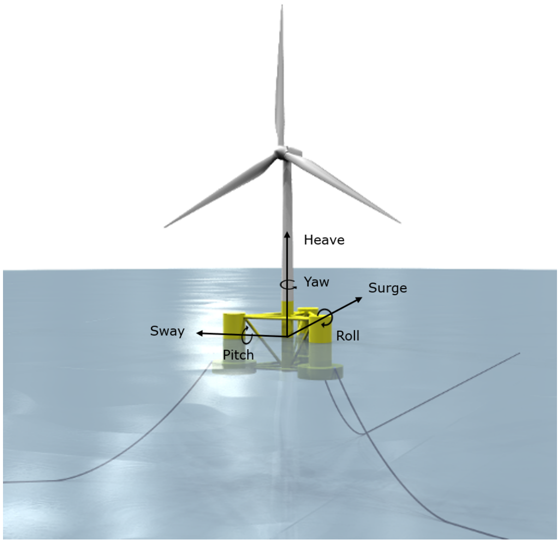

Figure 1.1: Degrees of freedom of a floating offshore wind turbine.

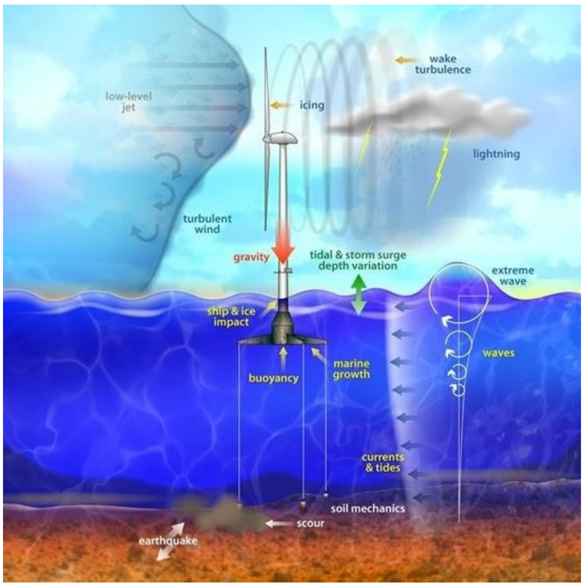

Figure 1.2: Complex physical environment that floating wind turbines have to be designed for [7].

- **Mooring line stabilised**, which achieves stability through vertical mooring lines under high tension, tightly anchored to the seabed to hold the buoyant substructure in its place. Tension Leg Platforms (TLP) thus make use of the restoring force provided by the tension in the mooring system.

The stability triangle diagram, as depicted in figure 1.3, shows the three cornerstones of the possible design space for achieving hydrostatic stability. The spar, barge and TLP mentioned above lie near these corners. The absolute corners of this triangle represent idealised solutions with limited properties to achieve stability. In practice, all floating platforms are to some extent hybrid designs that achieve hydrostatic stability through a combination of all three methods. As such, they are all moored to prevent the platforms from drifting away, and they all require a minimum waterplane area to be able to support the large base of a wind turbine tower. From a more pragmatic design approach, hybrid floating platforms lie further inside the stability triangle, between the primary points. The objective is to identify the best platform in terms of functionality and cost, by finding an optimal balance among the stability options.

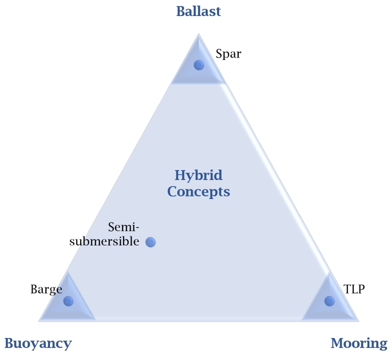

Figure 1.3: Stability triangle showing the available options for achieving hydrostatic stability.

An example of a concept that has attracted a lot of attention in the floating wind R&D community, is the semi-submersible, which is in fact a hybrid solution. In this concept, waterplane stability is achieved with a multi-cylindrical structure, that places three buoyant columns in a triangular configuration. The wind turbine may be mounted on one of the three columns, or on a fourth column in the centre of the structure [9]. The columns are interconnected with braces, and contain ballast material such that part of the structure is submerged and the centre of gravity is lowered, thereby improving stability. to prevent excessive motion due to wave loading. The semi-submersible concept, along with the spar, barge and TLP are illustrated in figure 1.4.

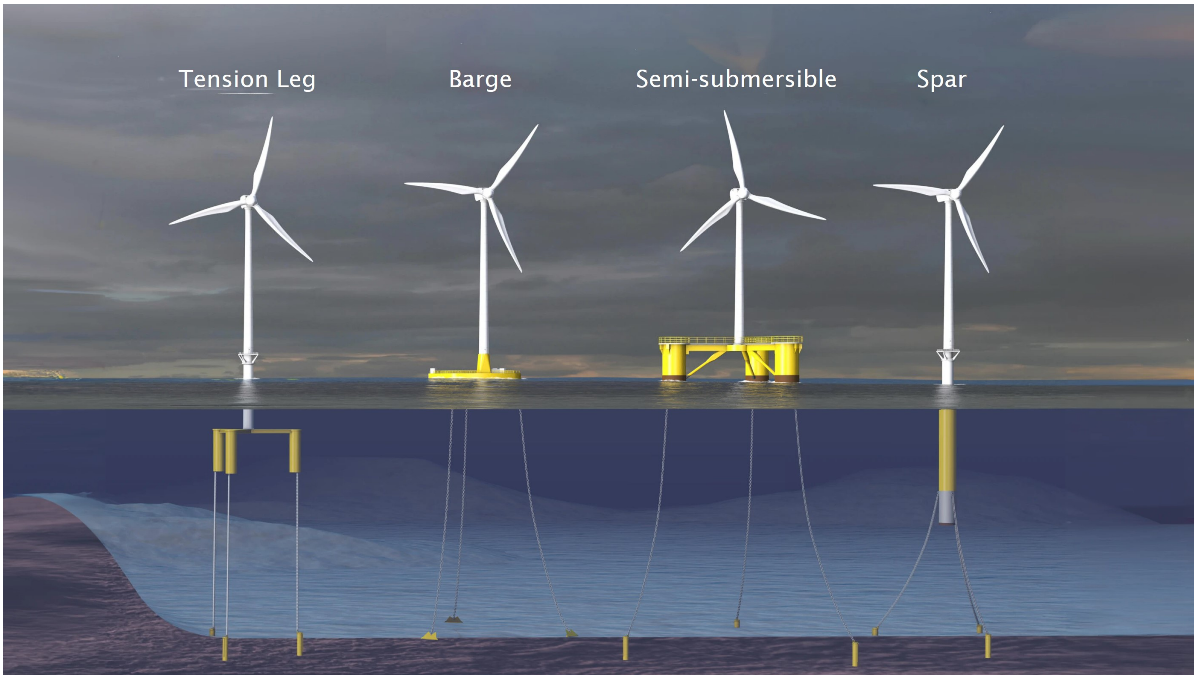

Figure 1.4: Dominant types of floating offshore wind substructures [10].

Each of the concepts that are illustrated in figure 1.4 have their advantages and disadvantages. In [9], the results of a SWOT analysis are presented following a critical review of floating support structures for offshore wind farm deployment. The main aspects from this study are summarised below:

- **TLP**: Due to the shallow draft and stability from the tension in the mooring lines, the resulting structure is small and light. This has the added advantage that it can be assembled onshore or in dry dock. Because the structure is vertically moored to the seabed, its footprint is small and the mooring lines are short. As a result of the tension in the mooring lines, the platform is highly stable and thus performs well in restricting tower top motions. When the platform is submerged, it has little wave sensitivity, thus making it a suitable option for deployment in more severe sea states.

  The stability of this platform is compromised, however, when it is not tightly moored to the seabed. The inherently unstable floating structure is made stable only after commissioning of the anchoring and mooring system. This leads to complex and risky installation procedures. The high tension in the anchoring and mooring system result in large stresses in the structure, with severe consequences in case of failure. This drives the complexity and cost of the system. Finally, the structure may be unsuitable for use in situations where strong tidal currents or storm surges may occur, or for specific soil conditions.

- **Barge**: Because of the shallow draft of barges, they can be deployed in a wide range of water depth. The added advantage of its shallow draft is that the turbine can be assembled at quayside, after which the floating wind turbine is towed to site. The towability of barges make for simple installation and decommissioning of the floating wind turbine, with increased weather windows. Similarly, the floating platform can be towed back to port for maintenance. Simple mooring and anchoring systems reduce the complexity and risk of these substructures.

  Nevertheless, the low draft must be compensated by an increased waterplane area. This requires large and heavy (and thus costly) structures to ensure stability. Because the large platform is not submerged, it is more sensitive to corrosion, and wave loading leads to higher motions, which in turn impacts the wind turbine. Although the mooring and anchoring system is simple, the horizontally-loaded catenary mooring lines are long (and thus expensive), and result in a large footprint.

- **Semi-submersible**: As this floater concept is similar to the barge, the two share many advantages and disadvantages. However, the semi-submersible platform is more stable because of the distributed buoyancy and ballast material below the waterline. Reducing its sensitivity to wave loading, however, comes at the cost of a larger, more complex structure, as can be seen from comparison with the barge in figure 1.4. Nevertheless, the majority of floating wind projects currently in development utilise this concept, which boosts the market potential of this concept [11].

- **Spar**: the low centre of gravity of this concept makes this floater inherently stable, therefore it is suitable for deployment in severe sea states. Both the structure and its mooring and anchoring system are simple, which reduces operational risk. Lastly, it is little susceptible to corrosion and can be deployed independent of soil condition.

  Although the structure is simple, it requires a large volume and mass below the waterline. Because of its deep draft, it is unsuitable for deployment in shallow waters, which in turn complicates float-out and installation. Similar to barges and semi-submersibles, spars use long catenary mooring lines that are costly and result in large seabed footprints. Lastly, the pitch and roll motions of the platform cause relatively large angular displacements of the tower top, and lead to high fatigue loads in the tower base.

It should be made clear that there is no clear winner among these concepts, and the choice for a specific solution may reflect a strong relation with site conditions, such as water depth, soil conditions, wave height and period, proximity of ports, supply chain, etc.

Stationkeeping

The floating wind turbine is kept in its place by a system of mooring lines and anchors. From experience in the offshore oil and gas industry, there are various mooring systems available. The most common are shown in figure 1.5, and are discussed below.

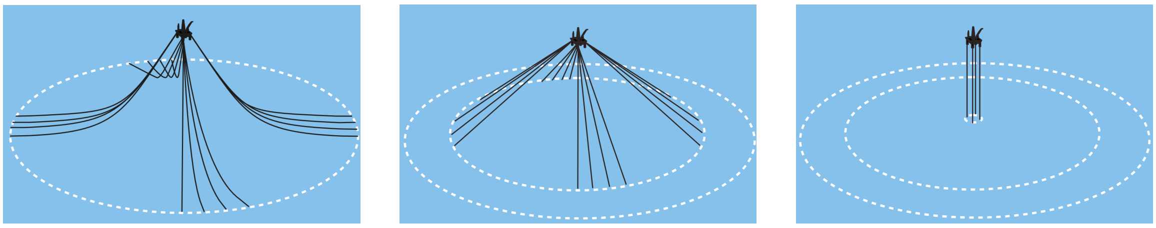

(a) Catenary mooring

(b) Taut leg mooring

(c) Tension leg mooring

Figure 1.5: Different mooring system typologies [12]

- **Catenary** mooring lines are widely used because of their simplicity. Continuing the synergy with the offshore oil and gas industry, this was the choice for shallow to deep water [12]. Long steel chains or wire ropes arrive horizontally at the seabed, hence the loading at the anchoring point is horizontal. The restoring force in this configuration results from the line weight. The catenary mooring system has a damping effect on the floater motion [13], but it still allows for some degree of motion in the surge, sway and yaw directions. As water depth increases, the catenary mooring system becomes less attractive, due to it's long length. With typical line lengths of 3-5 times the water depth, it has not only a large footprint, but the lines also become costly and their weight starts to compromise the buoyancy of the floating platform [12].
- **Taut leg** mooring configurations have reduced footprint with respect to catenary mooring, as the lines arrive at the seabed at an angle instead of horizontally. Therefore, in this configuration, the anchoring point is subjected to both horizontal and vertical loads. The restoring force results not only from the weight of the lines, but also from the pre-tension in the mooring lines [12], resulting in higher loads in the lines. This mooring option requires less material, resulting in lower overall mass and cost. Platform motion is reduced with respect to catenary mooring.
- **Tension leg** mooring is especially useful for very deep water applications, because it has the lowest line length. The lines run vertically to the seabed, where they are connected to anchors capable of withstanding high vertical loads. The high tension in the cables constrains platform motion, which results in the highest platform stability. Its footprint is small, but challenging installation procedures complicate the design trade-off [3].

Depending on the mooring configuration, there are several options for anchoring [3]. The gravity anchor is the oldest in existence, which relies on its own weight to achieve the required holding capacity. The large weight and size may increase cost of installation. This anchor type is mainly used to cope with vertical loads, although it may also be deployed with horizontal loading. For a catenary mooring system, drag-embedded anchors are usually the preferred option because of their capacity to bear horizontal loads. They are simple to install, and recoverable upon decommissioning. For taut leg mooring configurations, they are unsuitable, as the anchors must also withstand vertical loads. In this case, driven piles or suction piles are generally good choices. The former is applicable in a wide range of soil conditions, but requires hammer piling for installation, and is difficult to remove during decommissioning. The latter is easier to install and remove, but is unsuitable in very soft or stiff seabed conditions. Another anchor type that is capable of bearing both horizontal and vertical loads is the Vertical Load Anchor (VLA), which is installed in the same way as the drag-embedded one, but penetrates a lot deeper [12].

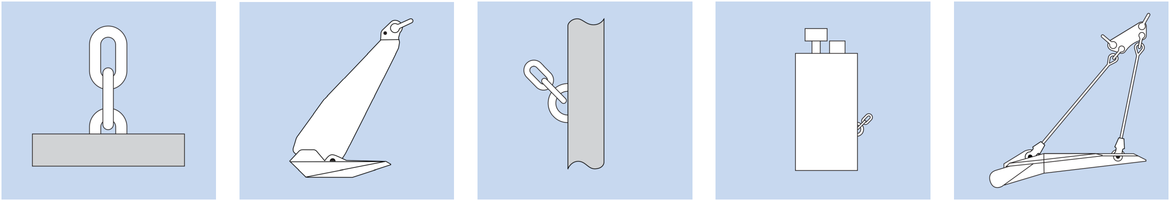

(a) Gravity anchor **(b)** Drag-embedded **(c)** Driven pile **(d)** Suction pile **(e)** VLA

Figure 1.6: Different types of anchoring systems [12]

It should be pointed out that anchor choice is site specific, and often governed by seabed conditions [3]. A schematic representation of the anchor types described above is presented in figure 1.6. These are the main types found in the marine and offshore oil and gas industry, and applicable to floating offshore wind. However, a great variety exists.

Research and Development

In the multidisciplinary field of floating offshore wind technology, industry and academia have partnered to collaboratively develop simulation, verification and validation methods. This becomes apparent in the work performed in the offshore code comparison collaboration projects, which are a part of IEA tasks. Over the past two decades, several reference designs have been provided with detailed documentation for public access to promote R&D and collaboration in this field. As such, they have been used by participants of the offshore code collaboration projects to develop aero-hydro-servo-elastic models. The design of the OC3-Hywind spar, OC4-DeepCwind semi-submersible and VolturnUS-S semi-submersible are defined in [14]–[16].

In another collaborative project, the LIFES50+ Consortium performed an optimisation of four floater concepts for a 10MW wind turbine in deep waters [17]. In this EU-funded project, the design basis of two semi-submersible concepts, a tension-leg platform and a barge with damping pool is presented, together with case studies in site conditions ranging from mild to severe.

1.1.2. Cost of Energy Modelling

Economic viability and technological feasibility of potential projects in the energy sector are commonly assessed by carrying out a techno-economic analysis. The results of such assessments help to make informed decisions about whether to pursue a particular project or not by identifying costs, benefits, risks and opportunities. In techno-economic assessments, Levelised Cost of Energy (LCOE) is a key metric to quantify economic viability, as it can be utilised to determine the minimum energy price required for a project to generate the required return [18]. Furthermore, it allows comparing between alternative energy sources.

Levelised Cost of Energy

The department for Business, Energy & Industrial Strategy defines LCOE as the net present value (NPV) of the expected costs for each year, divided by the NPV of the expected energy generation for each year, summed over the lifetime of the project [19]. The NPV of the expected costs comprises capital- and operation expenses, which are discounted to reflect the future value of money. The annual energy production is equally discounted to evaluate the future benefits of energy produced. A theoretical justification of the widely adopted notion of LCOE is described in [18], and its general expression is given by equation 1.1.

$$LCOE = \frac{NPV_{\text{costs}}}{NPV_{\text{energy}}} = \frac{\sum_{t=1}^{n} \frac{CAPEX + OPEX}{(1+d)^t}}{\sum_{t=1}^{n} \frac{AEP}{(1+d)^t}} \tag{1.1}$$

Where $CAPEX$ are the capital expenditures in year t (€), $OPEX$ the operational and maintenance expenditures in year t (€), d the discount rate (-), AEP the annual energy production (MWh) and n the lifetime of the project in years. Equating costs to energy production results in a value with units of €/MWh. The discount rate should take into account the market value of both equity and debt, and additionally, inflation and tax rates. This is achieved by setting the discount rate to the weighted average cost of capital (WACC) [20]. By addition of the cost of equity, the WACC reflects the investment risk of the project [21].

The terms in equation 1.1 can be broken down further into lower-level cost components, e.g. development and project management, production and acquisition, installation and commissioning, operation and maintenance, and decommissioning and disposal [22]. As for the annual energy production (AEP), numerous factors influence the AEP, including direct factors such as turbine rating and farm size, and indirect factors such as wake losses due to the farms size and layout [23]. In addition to hardware considerations, site specific parameters such as the wind resource also have a significant impact on AEP. Given the complexity of LCOE estimation, a bottom-up engineering approach is commonly utilised.

Review of Life Cycle Costs Calculation

Numerous methods have been proposed in the literature to estimate life cycle costs of floating offshore wind farms. In [23], [24], [25] methodologies are proposed for evaluating the life cycle costs of floating offshore wind farms. They mostly consist of parametric equations, which relate the cost of (sub)system components to their physical dimensions. Unfortunately, not all articles are explicit about the expressions used to calculate LCOE.

These methods prove to be very useful for performing sensitivity studies. For example, in [26] the influence of the wind farm location on life cycle costs is investigated for the north-western area of Spain. Similarly, in [27], the author explores spatial variation of the LCOE for floating offshore wind farms near the European Atlantic coastline. Furthermore, these methods allow to identify cost reduction potential, as shown in [22].

However, it can be argued that the application of these techno-economic models is limited, because their methods are often simplified. They may serve as feasibility study but do not offer reliable results for specific projects. In addition, they are snapshot models, and cost data must be regularly maintained as new technologies are developed, existing technology is improved and material costs change.

In [5], it is concluded that a more accurate breakdown of costs requires a higher-level analysis. In this article, the author performs a hydrostatic analysis for different floater concepts in the context of a techno-economic analysis. In [28], a similar approach with optimisation is chosen to arrive at the LCOE of a hypothetical floating offshore wind farm.

TNO's In-House Cost Model

The in-house cost model of TNO is a tool for assessing economic feasibility of potential offshore wind projects. It consists of a Python-based wrapper, which encapsulates several modules to compute the cost of specific components of the offshore wind farm. Originally, the cost model had been developed for evaluating the performance of a conventional offshore wind farm with bottom-fixed foundations, such as monopiles or jackets. Recently, however, the cost model has been extended with modules for photovoltaics, batteries and hydrogen technology, such that it can be applied to hybrid power plants. Another recent project has led to the addition of a module for floating foundations. The model for conceptual sizing and cost estimation of a floating substructure is based on the application of hydrostatics and vertical equilibrium to achieve a stable structure. The mooring lines are modelled using quasi-static calculation methods. An overview of the cost model structure and its modules is given in figure 1.7.

The model for conceptual sizing and cost estimation of a floating substructure is based on the application of hydrostatics and vertical equilibrium to achieve a stable structure. Three different floating structures can be modelled. One vertical cylinder for a spar, two horizontal cylinders to model a catamaran-type platform, and three vertical cylinders for a semi-submersible platform. The length and diameter of the cylinders is varied to achieve a structure with minimal weight that satisfies the hydrostatic constraints, for a given wind turbine. To arrive at this optimal structure, the displacement, centre of gravity, buoyancy point, metacentric height, added mass and the mass of the floating body are computed. The cost is then incurred from the mass of the substructure, using models that have been verified with data from literature.

Similarly to the floating platform, the mooring system is modelled by means of an optimisation framework. Loads in the mooring lines are determined using quasi-static calculations methods, for a limited number of design conditions. The optimisation is constrained by a prescribed operational heel, a survival heel and maximum excursion of the platform. The design variables are mooring line diameter, length and anchor radius. Ultimately, the line breaking load, wetted mass, axial stiffness and cost are computed to arrive at the lowest mooring cost that satisfies the constraints.

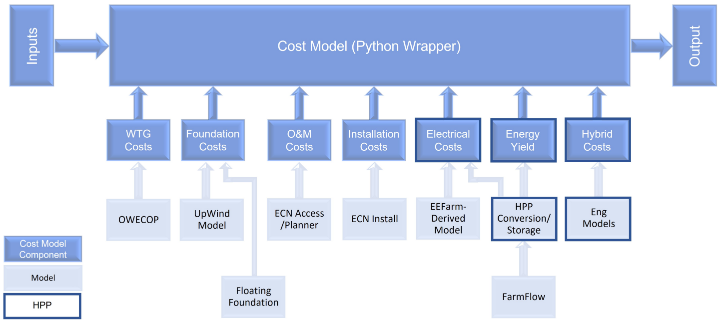

Figure 1.7: Input-output flow diagram of TNO's in-house cost model.

1.1.3. Multidisciplinary Design, Analysis and Optimisation

In recent years, multidisciplinary design analysis and optimisation (MDAO) has gained increasing attention in the research community as a powerful approach for optimising the performance of engineering systems consisting of multiple subsystems or components. MDAO involves a methodical approach to design and analysis to deal with the interface between various disciplines within a system [6]. The primary goal is to optimise the performance of a system by considering the interactions between its various components and subsystems. In [7], it is discussed that a MDAO approach could be highly beneficial for floating offshore wind turbines, given their low Technology Readiness Level (TRL), tight aero-hydro-servo-elastic coupling, and the dynamics of the marine environment (i.e. motion in all six degrees of freedom). The floating substructure accounts for approximately 30% of the total CAPEX [5], hence there is a significant opportunity for cost reduction. By adopting the systems engineering vision put forth in [7], floating wind farms may one day be able to compete with bottom-fixed plants in terms of LCOE.

In [6], a comprehensive review is presented of earlier work involving MDAO of a floating offshore wind turbine. Traditionally, design optimisation involves the use of low-fidelity models, which typically involve the use of steady-state or quasi-static methods, because they are computationally efficient. This approach is used in e.g. [5] and [28], but also in TNO's in-house cost model, as described in the previous section. To better represent the physical behaviour of floating wind turbines, mid-fidelity models are used to simulate the system in the frequency domain. This is a widely used analysis domain, as concluded in [6] and [29]. Although this method allows to capture (linearised) dynamic effects, its suitability for non-linear systems is questionable. The use of frequency domain analysis is often the result of a trade-off between computational expense and model accuracy. Though, to obtain accurate and reliable results, higher-fidelity models should be utilised to simulate the non-linear system in the time domain.

The question of which model fidelity should be used in the design, analysis and optimisation of floating offshore wind turbines does not have a clear answer. For example, recent research suggests that the optimised floating substructure is not driven by hydrostatic constraints, but by dynamic constraints instead [30]. On the other hand, in [31], the author concludes that static constraints governed the design of a spar floater. It may be that the dynamic constraints are activated in the case of relaxation of the static constraints, or in the case of harsh environmental conditions. It is also likely that different results occur when a semi-submersible floater is considered. Besides the platform and wind turbine, studies have also investigated the importance of mooring line model fidelity [32], with similar contradicting results.

Finally, a comprehensive literature review on optimisation techniques applied to floating offshore wind platforms [29] underscores the relatively limited research dedicated to such substructures. At the same time, this review highlights the vast potential for incorporating more in-depth analysis methods into the optimisation work, such as the inclusion of an energy production model, and structural analysis of the platform. Ultimately, this may uncover new and cost-competitive solutions for the future.

1.2. Research Motivation

The literature review prior to this thesis has led to the following insights:

- Cost reduction of the floating substructure is necessary to enhance the economic viability of floating wind energy. Moreover, accurate estimations of the performance of floating substructures are required for decision-making about investments and to ensure that projects are financially sustainable in the long term.
- The in-house model used by TNO for design and cost estimation of the floating substructure is based on hydrostatic analysis. This approach risks to neglect design considerations in a problem that is driven by the inherent dynamic nature of a structure subject to aero-hydro-servo-elastic loads. Furthermore, a limited number of load cases are considered in the cost model, which is insufficient to model the broad range of environmental and operational conditions that the floating wind turbine will encounter during its lifetime.
- It has been shown that the inclusion of dynamic constraints may have a clear impact on the optimised design of a floating substructure. This calls for moving towards higher fidelity models to perform their analysis. Combined with numerical optimisation methods in a holistic programming framework, this approach offers opportunities to investigate cost-effective substructure designs with a high degree of reliability.

1.3. Research Questions

Based on the findings of the previous section, this thesis aims to address the following research question:

"How can advanced computational models and optimisation techniques be leveraged to enhance the cost-effectiveness of floating wind turbine substructures subjected to various environmental conditions?"

To answer this question in a structured and precise way, the following sub-questions are formulated:

1. How can the integration of high-fidelity simulation tools be practically implemented in the optimisation workflow?
2. Which design load cases have the most impact on the optimal floater design, in terms of structural integrity, operational limits and performance?
3. What are the key challenges associated with integrating higher-fidelity computational models into the optimisation of floating wind turbine substructures?

1.4. Report Outline

To address the research questions, a modelling framework will be developed, aimed at optimising the design of a floating wind turbine substructure. Through utilisation of higher-fidelity software tools, the framework shall enable simulation of the fully coupled response of the complete FOWT system to various environmental and operational conditions, thereby examining the performance of the system across a wide range of possible scenarios. This thesis report will present the theoretical foundations, methodology, implementation and outcomes of this undertaking.

Starting with chapter 2, the theoretical concepts underpinning the hydrodynamic and structural modelling of the platform are provided, followed by a short introduction into optimisation techniques. Chapter 3 then elaborates on the research methodology, outlining the general approach used in developing the programming framework, including the software choices made and a description of the optimisation routine. The subsequent chapters take a closer look at the specific software tools used. Chapter 4 offers a detailed explanation of the methods and implementation of the hydrodynamic modelling tool, including its integration within the programming framework, while chapter 5 provides a comprehensive description of the OpenFAST model, exploring the relevant parameters necessary to set up its various modules. Next, the optimisation workflow is detailed in chapter 6, describing the different steps involved in the optimisation process, from configuration and initialisation to post-processing. Then, chapter 7 is dedicated to verification of NEMOH and OpenFAST simulation results, confirming the correct implementation of the models. Furthermore, the results of a sensitivity study on the hydrodynamic mesh size are explained presented. In chapter 8, the outcomes of the optimisation are analysed and discussed. Building on the results, the main findings of the thesis are concluded in chapter 9, and recommendations for further research are summarised in chapter 10.

2

Theoretical Foundation

This chapter discusses theories and concepts needed to understand the theoretical basis of the models used in this research. Section 2.1 gives a brief explanation of the concepts behind the two hydrodynamic models employed in the programming framework. Subsequently, the fundamental concepts underpinning the structural model are outlined in section 2.2. Finally, a brief overview of the theory behind optimisation is provided in section 2.3.

2.1. Hydrodynamics

In the field of offshore wind energy, two widely used methods for modelling the hydrodynamics of offshore wind turbines are strip theory (through Morison's equation), and potential flow theory. In the following sections, the main concepts of these theories are described.

2.1.1. Strip Theory

In the strip theory, a submerged member is divided into smaller segments, to which the Morison equation is applied to calculate the hydrodynamic forces acting on the member due to incoming waves. The Morison equation is semi-empirical, incorporating three main components, and it is given for a cylindrical member in equation 2.1. The first component corresponds to the Froude-Krylov force, which is due to the pressure field generated by undisturbed waves. This is the first term in equation 2.1 [33]. The second component in the strip theory represents the added mass, which is related to the inertia of the surrounding fluid that must be accelerated along with the object. This term corresponds with the second term in equation 2.1. The last term in this equation corresponds to the viscous drag contribution.

$$\mathrm{d}F = \frac{\pi}{4}\rho D^2 \frac{\mathrm{d}u}{\mathrm{d}t}\mathrm{d}s + \frac{\pi}{4}\rho c_{\mathrm{A}} D^2 \left(\frac{\mathrm{d}u}{\mathrm{d}t} - \frac{\mathrm{d}u_{\mathrm{b}}}{\mathrm{d}t}\right)\mathrm{d}s + \frac{1}{2}\rho c_{\mathrm{D}} D\,(u - u_{\mathrm{b}})\,|u - u_{\mathrm{b}}|\,\mathrm{d}s \tag{2.1}$$

Where F is the hydrodynamic force (N), ρ is the water density ($\mathrm{kg\,m^{-3}}$), D is the diameter of the cylindrical member (m), u and u_b are the velocity of the water and the floating body, respectively ($\mathrm{m\,s^{-1}}$), $\mathrm{d}s$ is the infinitesimal length of the strip (m), and c_A and c_D are non-dimensional added mass and drag coefficients.

The Morison equation is applied to the small segments (strips) of the members, and upon summation of the contribution of all strips, the total hydrodynamic force is obtained. Utilising the equation requires the added mass (c_A) and drag coefficients (c_D) to be found empirically. Nonetheless, the Morison equation offers a straightforward approach for solving wave forces in the time domain, making it a widely used method for hydrodynamic calculations.

A fundamental limitation of Morison's equation, though, is that wave diffraction effects are neglected. Therefore, it is applicable primarily to slender structures, requiring that the diameter of the member is small in comparison with the wavelength [33].

2.1.2. Potential Flow Theory

A different approach to modelling a body subjected to hydrodynamic loads, is potential flow theory. In the case of wave-structure interaction, two primary phenomena are oberved: wave diffraction, where incoming waves are deflected, and wave radiation, as the object in motion generates its own waves [33]. These effects become more significant with increasing size, hence for large-volume floating platforms, not only loads from incident waves need to be considered but also those due to wave diffraction and radiation.

These effects can be modelled using potential flow theory, with the fundamental assumption that the flow is inviscid. The scalar potential flow function is introduced such that its partial derivatives represent the fluid velocities:

$$u = \frac{\partial \Phi}{\partial x}, \quad v = \frac{\partial \Phi}{\partial y}, \quad w = \frac{\partial \Phi}{\partial z} \tag{2.2}$$

Where Φ is the velocity potential ($\mathrm{m^2\,s^{-1}}$), and u, v, w are the velocity components in x, y, z direction, respectively. The velocity potential must satisfy the Laplace equation:

$$\frac{\partial^2 \Phi}{\partial x^2} + \frac{\partial^2 \Phi}{\partial y^2} + \frac{\partial^2 \Phi}{\partial z^2} = 0 \tag{2.3}$$

The Laplace equation defines a boundary value problem, which may be solved using different methods. Common solution strategies in the field of hydrodynamics involve panel methods, where the floating platform is discretised into surface elements or panels. By applying sources, vortices and doublets to the surface elements, the problem is turned into a set of algebraic equations. By setting appropriate boundary conditions, the velocity potential can then be determined. After solving the three potential functions, the pressure due to the wave loads on the structure can be computed using Bernoulli's equation:

$$\frac{\partial \Phi}{\partial t} + \frac{p}{\rho} + \frac{1}{2}\left[\left(\frac{\partial \Phi}{\partial x}\right)^2 + \left(\frac{\partial \Phi}{\partial y}\right)^2 + \left(\frac{\partial \Phi}{\partial z}\right)^2\right] + gz = 0 \tag{2.4}$$

Where p stands for pressure (Pa), g is the acceleration due to gravity ($\mathrm{m\,s^{-2}}$), and z is the vertical elevation (m). This equation is solved in the frequency domain, by assuming that the velocity potential is of the form $\Phi = \Phi_0(z)\sin(kx - \omega t)$.

2.2. Structural Dynamics

Presently, the number of studies which include structural flexibility of the platform in preliminary analysis and optimisation of FOWTs using fully coupled aero-hydro-servo-elastic simulations is limited [34]. Different software tools exist which are capable of performing finite element analysis to compute hydroelastic deformations. Examples are the Abaqus-, SESAM- or ANSYS software suites. Despite their robustness in providing solutions for hydroelastic analysis, these programs are computationally intensive, and their integration into a comprehensive simulation framework for fully coupled aero-hydro-servo-elastic simulations is non-trivial.

OpenFAST, on the other hand, provides an efficient and proven framework for simulating the fully coupled response of FOWTs, and recent developments in the SubDyn module have extended its capabilities to model the dynamics and structural flexibility of floating platforms. In the SubDyn module, a combination of engineering approaches is utilised, namely the Linear Frame Finite Element Model (LFEM), and the Craig-Bampton method in conjunction with the Static-Improvement Method (SIM). This approach serves to achieve a good balance between computational efficiency and accuracy. In the following paragraphs, the theoretical framework of SubDyn will be further detailed.

Linear Frame Finite Element Model

In the context of offshore wind turbine substructures, it is often suitable to utilise a LFEM representation [35]. Firstly, because material non-linearity can typically be neglected for offshore support structures due to the prevalent use of steel in their design. These structures are designed such that the maximum stress in the members does not exceed the yield strength, and hence remains in the elastic region. And secondly, because test results from simulations involving several wind turbine configurations have demonstrated that non-linear behaviour has minimal impact on the multi-member support structures. As for the beam elements, two different types can be used with the LFEM representation: Euler-Bernoulli or Timoshenko. The latter, which takes into account shear deformation, is better suited for modelling beams with low aspect ratios often used in frames to transfer loads within the structure.

Craig-Bampton Reduction

Finite element method (FEM) analysis of a floating substructure involves a detailed representation of the complete multi-member structure. Each structural component has multiple degrees of freedom (DOFs), and therefore the total number of DOFs grows quickly in size (to the order of thousands), which in turn requires high computational resources. To address this, the Craig-Bampton method is implemented, which is a technique to reduce the large substructure physical DOFs into a smaller set of modal and interface (also referred to as boundary) DOFs [35]. Through this method, only the fundamental low-frequency response modes of the structure are preserved, thus significantly enhancing computational efficiency while maintaining good accuracy in the system's overall response. When this technique is applied, the SubDyn module exclusively solves the equations of motion of the modal DOFs. The equations of motion of the interface DOFs are solved in ElastoDyn. In SubDyn, the number of modes to be retained can be controlled by the user. If all modes are retained, the full finite-element model will be resolved. When zero modes are retained, the process is referred to as a Guyan reduction, where the Guyan modes represent the global motion of the structure as a whole, in terms of translational and rotational displacements.

Static Improvement Method

Despite its effectiveness, the Craig-Bampton reduction might exclude high-frequency axial modes, which are essential for capturing static load effects like gravity (member self-weight) and buoyancy. To address this limitation, the static improvement method is implemented [35]. The SIM concept relies on the evaluation of two static solutions at each time step. One static solution is based on the full system stiffness matrix, and the other is based on the reduced system stiffness matrix. Subsequently, the time-varying dynamic system is solved using the Craig-Bampton method, which is then combined with the difference between the two static solutions. This superposition effectively accounts for the contribution of the vibration modes that were not directly included in the dynamic solution. In this manner, the effects of gravity and buoyancy are captured quasi-statically, enhancing the overall efficiency of the FEM process.

Guyan Load Correction

Lastly, the FEM formulation requires adjustments because of two considerations. Firstly, because the loads are applied within SubDyn at the displaced positions, whereas the FEM formulation expects the loads to be applied at the undisplaced positions. And secondly, because the rigid body motions of the floating platform must be considered as well. By implementing the Guyan load correction, a rotating frame of reference is utilised, which follows the rigid body motion of the Guyan modes. The Craig-Bampton and static modes are then solved within this rotating reference frame. Furthermore, the forces on the deflected structure are applied directly to the reference nodal positions, although extra moments are introduced at these reference positions as part of the mapping process, which are also adressed with the Guyan load correction. To reduce complexity, it is assumed that loads are applied at the Guyan position, rather than the fully deflected position. These considerations are visualised in figure 2.1, and additional information on the Guyan load correction procedure is described in the SubDyn theory section of the OpenFAST manual [35].

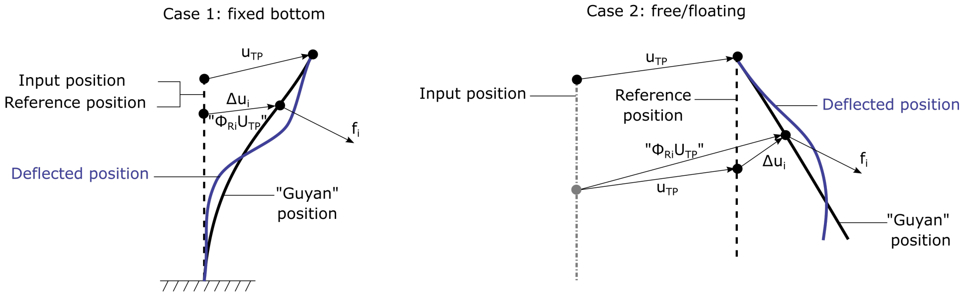

Figure 2.1: Visual representation of how additional moments are introduced by motion and deflection of the structure

2.3. Optimisation

Optimisation techniques encompass a broad range of mathematical and computational methods designed to find the best solution among a set of possible options. At its core, optimisation seeks to find the values of one or more variables, typically subject to certain boundaries and constraints, that minimise or maximise a specific performance measure, formulated as the objective function (often also referred to as the cost function). Optimisation techniques can be classified in different ways.

Firstly, a distinction can be made between linear and non-linear optimisation. Linear optimisation deals with problems where the objective function and constraints are linear. Typical examples of linear optimisation methods are the Simplex method, or the interior point method. non-linear optimisation, on the other hand, addresses problems involving non-linear objectives or constraints. non-linear optimisation techniques, such as the gradient descent, or Newton's method, are used when relationships between the variables are more complex.

Secondly, optimisation techniques can be classified into gradient-free methods and gradient-based methods. The essential difference between the two is in their names. As such, gradient-based methods are used when gradient information is available or can be computed reliably, resulting in a more efficient solution. When gradient information is unavailable or difficult to compute however, as might be the case for complex problems, gradient-free methods may be employed that do not require partial derivative calculation.

As floating offshore wind turbines are complex non-linear systems, gradient information is difficult to obtain, and hence a gradient-free method is considered the best approach. The results of a review of optimisation techniques applied to floating offshore wind platforms support this conclusion [29]. The results of this paper point out that evolutionary algorithms are the most commonly applied optimisation methods, because of their robustness in finding the global optimum, and their independence on gradient information. Another popular optimisation algorithm is COBYLA (Constrained Optimisation BY Linear Approximation) [36].

The COBYLA algorithm is designed to minimise an objective function $F(X)$ subjected to inequality constraints of the form $g(X) \geq 0$, where X is a vector of N variables. The method supports only inequality constraints, but in cases where equality constraints of the type $g(X) = 0$ are desired, they can be implemented as a pair of inequality constraints $g(X) \geq 0$ and $-g(X) \geq 0$. As for the variable bounds, they can be incorporated as well by reformulating them as inequality constraints.

The COBYLA method relies on linear approximation of the objective and constraint functions. These approximations are conducted through linear interpolation at $N+1$ points in the variable space, treating the interpolation points as vertices of a simplex. The size of the simplex is controlled by a parameter ρ, automatically decreasing from the initial value ρ_{beg} to the final ρ_{end}. The goal is to find the best set of variables for each simplex size. The reduction of the simplex size then continues until the specified ρ_{end} is reached. Convergence of the problem might depend on the values of the initial and termination criteria, which may require experimenting. A notable feature of the COBYLA optimisation algorithm is that the constraints are treated individually after each change of variables, rather than considering all of them together in a single penalty function.

3

Methodology

In order to set the basis for answering the research question, a framework is developed for the multidisciplinary design, analysis and optimisation of a floating offshore wind turbine. The building blocks of this framework are described in [37]. This paper presents a holistic framework, which can be utilised for automated simulation and optimisation to handle the extensive number of simulations needed in the design process of a wind turbine system. The general idea behind the holistic approach described in the article is to account for all system components, including their fully coupled aero-hydro-servo-elastic behaviour. In addition, it reduces the need for approximations, being based on physical principles rather than simplified engineering methods. Lastly, the programming framework described is flexible, implementing systematic methods that could be extended to any level of detail and applied to any optimisation problem.

This chapter describes the higher-level methodologies of the employed programming framework, and offers an explanation of the software choices made. Furthermore, the main optimisation problem is outlined, including decisions made for the optimisation objectives and constraints. Furthermore, supplementary studies that build upon the core optimisation problem are described. It should be noted that specific choices related to the external software tools will not be discussed in this chapter, but will be addressed in dedicated chapters, namely chapters 4 and 5.

3.1. Programming Framework

As described in the first paragraph of this chapter, the programming framework developed during the thesis employs the same general methodology as described in [37]. This framework is visualised in figure 3.1 below.

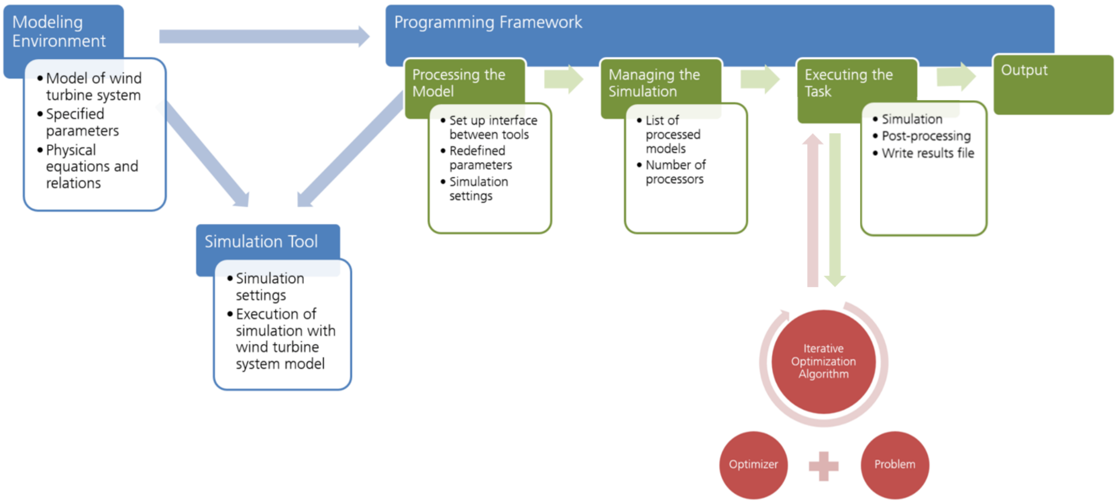

Figure 3.1: Components of the framework for automated simulation and their relations, including optimsation functionalities. Adapted from [37].

The figure describes the interaction between three main components: a modelling environment, a simulation tool and a programming framework. The modelling environment is needed to represent the physics of the wind turbine system, and should include models for its fully coupled aero-hydro-servo-elastic response. Therefore, the modelling environment focuses on the physical equations and relations. The simulation tool on the other hand, as described in [37], is necessary to characterise and execute the simulation, considering aspects like simulation duration, solver type, step size etc. It is noted that this tool could be integrated together with the software that provides the modelling environment for the wind turbine (for example in the case of Bladed, FAST and HAWC2), or it could be a stand-alone tool, such as Dymola, which is used in [37]. Lastly, the programming framework should serve as an interface between the modelling environment and simulation tool, and allow for scripting in order to set up the model, manage its simulation, and process the results. The programming framework is essential for manipulating and automating tasks within the overall optimisation problem. In effect, the optimisation routine is also integrated within the programming framework.

The rationale behind the choice of software used within the programming framework is explained below. For the sake of accessibility and reproducibility, the choice was made to only make use of open-source software.

- The selected modelling environment is OpenFAST, which is also the simulation tool. Developed by NREL, OpenFAST is an open-source software package, that is capable of performing coupled nonlinear, aero-hydro-servo-elastic simulation of wind turbines in the time domain [38]. It has gained widespread adoption in the wind energy research and development community for its versatility and extensive modelling capabilities. OpenFAST consists of various computational modules for aerodynamics, hydrodynamics for offshore structures, control and electrical system dynamics, and structural dynamics. Input files are utilised to define the simulation set-up and specify e.g. the geometry of the turbine, relevant simulation parameters, degrees of freedom etc.
- Using the potential flow model within the hydrodynamics module of OpenFAST, requires hydrodynamic coefficients of the floating substructure to be computed in a pre-processing step. For this purpose, the open-source boundary element methods (BEM) code of NEMOH is used [39], which is capable of computing first- and second-order wave loads for a meshed geometry.
- The programming framework will be written in Python, because of its versatility, broad area of application and open-source character. The Python glue code will enable scripting to define and change settings in the input files, allow the different software modules to interact, and post-process results. Furthermore, the use of Python eases integration with TNO's in-house cost model, as it also uses Python glue code.
- For the optimisation problem, the open-source Python library OpenMDAO will be used [40]. Developed by NASA, OpenMDAO is a computing platform used for systems analysis and multidisciplinary optimisation with efficient parallel numerical methods. The optimisation algorithm that will be implemented is the COBYLA method, which offers a proven and efficient gradient-free method in the context of a highly non-linear system.
- Because the higher-fidelity simulation with OpenFAST will require high computing power, the computer cluster of TNO will be utilised. Each cluster node encompasses 32 physical processors for performing simulations in parallel, allowing the simulation of a broad range of environmental and operational conditions.

In the presented work, the approach taken involves a step-by-step development of the framework. The development commences with the setup of a reference model in NEMOH and OpenFAST, which is tested and verified to eliminate inconsistencies at an early stage. Then, the floating platform is parametrised, which allows the geometry to be defined at a higher level, and translated into the right inputs for NEMOH and OpenFAST. The two software tools are coupled to the Python framework, allowing the NEMOH and OpenFAST simulations to be run sequentially, as the OpenFAST model depends on the hydrodynamic coefficients output by NEMOH. At this point, the response of the floating platform is found by automated simulation using a single design load case (DLC). Again, after verification, the next step is to further develop the model by defining multiple DLCs and writing the code for parallel processing of multiple OpenFAST simulations. To be able to verify the results, the OC4 semi-submersible platform introduced in section 1.1.1 will be modelled, because a lot of data is available in the literature for this platform. The geometry of this platform is shown in figure 3.2.

After successful simulation, the geometry or physical description of the DeepCWind platform will be altered to test the robustness of the program. In the next step, an optimisation method will be incorporated into the program to minimise the structural mass of the semi-submersible platform design. The ensemble of modelling choices implemented along the way provide the insights to answer the first research sub-question. The results of the optimisation problem will showcase the possibilities and flexibility of the developed model. Finding an answer to the second sub-question will require a combination of model testing and literature study. The goal is twofold: not only does it provide a better understanding of the effect of environmental and operational conditions on the platform design, it will also allow to run the simulation for a selected set of DLCs to reduce computational effort. Drawing conclusions from the optimisation results and insights of the modelling process, the third sub-question may be answered by reflecting on the strengths and weaknesses of the developed model.

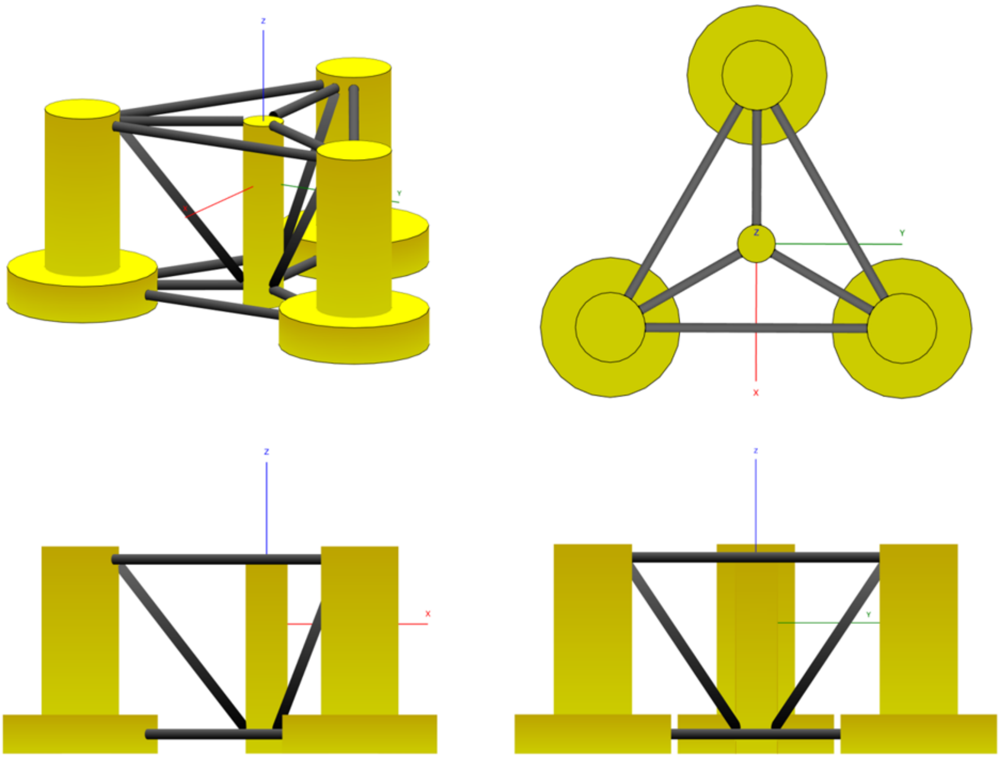

Figure 3.2: From top left to bottom right: perspective-, top-, side- and front view of the DeepCWind platform.

3.2. Optimisation Problem

The main purpose of the optimisation is to achieve a floating substructure design which has the lowest cost. As introduced in section 1.1.2, the final cost of a floating wind turbine is constituted by many components. Besides the CAPEX, which include manufacturing costs like raw materials and labour, there are expenses linked to installation, operation and maintenance, which will also vary depending on the floating platform design. For example, it is argued in [41] that shipyard costs increase with a larger footprint of the structure.

Objectives

Including all of these cost components in a single cost function is impractical. For that reason, the simplification is often made that the cost of the platform is directly and solely proportional to the structural mass of the platform. The underlying principle is that reducing material usage leads to cost reduction. Sometimes, a complexity factor is included which may account for the cost of welds, painting, etc. While it is understood that there could be value in broadening the cost function, the choice has been made to focus on reducing structural mass, to maintain simplicity.

Design Variables

The independent variables that will function as design variables for the optimisation problem, are the distance between the centre column and the outer column, also called the offset radius, and the diameter of the outer columns. This choice was made because the voluminous outer columns have a large impact on both the buoyancy and structural weight of the platform, while the offset radius significantly influences the stability. Because the outer columns of the DeepCWind platform consist of an upper- and base section with different dimensions, the ratio between the two is kept the same, and the base column diameter is treated as a dependent variable.

It is worth noting at this point that the optimisation problem focuses solely on the substructure. Although many components of the complete system have an impact on stability, such as the mooring system, turbine characteristics and controller, they are excluded from the optimisation routine. Of course, these elements are indispensable in the simulations to ensure an accurate representation of the entire system, but their characteristics remain unchanged throughout the process.

Constraints

Constraints that are frequently imposed on the optimal platform design in the literature include nacelle acceleration, platform motion, design variables, stability, mooring and structural limitations [29]. Now, because the mooring system remains unchanged during the optimisation, there will be no constraints related to the mooring lines in this project. As for the rest:

- Although it is mentioned in [29] that including a nacelle acceleration constraint is questionable, it is a common consideration in the design of floating wind turbine substructures, because excessive accelerations are believed to reduce fatigue life of turbine components, and may cause damage to equipment housed inside the nacelle. According to [42], common values for this constraint are 20-30% of the gravitational acceleration. For this project, because survival load cases are included, a value at the higher end of this spectrum is chosen: $3\,\mathrm{m\,s^{-1}}$.
- Regarding the platform motion, common constraints include a maximum surge excursion, and maximum values on the floater pitch angle. Because the restoring force in the surge direction is generated by the mooring system only, this will not be considered here. The maximum pitch constraint however, is an important parameter. On the one hand, because the FOWT system becomes unstable beyond a certain limit, but also because high pitch angles induce large moments at the tower base. In addition, power generation is compromised at high floater pitch angles. To stay within acceptable limits, a maximum pitch angle of 10° is set.
- The design variables are bound to predetermined upper and lower limits to narrow down the design space, and prevent unrealistic designs from being generated. In this project, the upper column diameter is restricted to values between 6 and 20 m, while the offset radius is limited between 20 and 50 m.
- Stability constraints in the literature encompass restrictions on the draft and freeboard height, but also on metacentric height, or a restoring coefficient for the pitch DOF [29]. For the optimisation routine in this project, no such constraints are explicitly considered. The draft is kept constant for practical reasons (a variation in draft requires cascading changes to many other parameters in NEMOH and OpenFAST). This is achieved by adjusting the ballast in response to a change in substructure buoyancy. This will be explained in more detail in section 6.2.1. Similar to the draft, the freeboard height of the platform remains constant. Then, as for the metacentric height and pitch restoring parameter: they are implicitly accounted for in the maximum pitch angle (i.e., if the restoring force of the pitch DOF is insufficient, the constraint will certainly be violated), but also in a unique constraint introduced in this project. This unique constraint serves as a failure flag, which signals whether the simulation has failed or not. An unstable platform will inevitably lead to the OpenFAST software aborting simulation, resulting in a violation of the $failure$ constraint.
- Structural limitations are considered in this project, but due to imperfections in the full-scale design of the DeepCWind platform, in combination with limitations of the OpenFAST software, the structural analysis could not be used to its full potential, hence the floating platform design is not directly constrained by structural limits in the optimisation process. Nonetheless, the opportunity to analyse internal forces in the structural components of the platform would allow future optimisation studies to account for e.g. limits in the maximum allowable stresses in the members, enabling the optimisation algorithm to converge to a platform design that is structurally sound.

The formal definition of the optimisation problem in this project is as follows:

$$
\begin{aligned}
\text{minimize} \quad & m(X) \\
\text{w.r.t.} \quad & X = \begin{bmatrix} R_{\text{offset}} \\ D_{\text{UC}} \end{bmatrix} \\
\text{subject to} \quad & 20\,\text{m} \leq R_{\text{offset}} \leq 50\,\text{m} \\
& 6\,\text{m} \leq D_{\text{UC}} \leq 20\,\text{m} \\
& \theta_{\text{max}} \leq 10^{\circ} \\
& a_{\text{nac,max}} \leq 3\,\text{m}\,\text{s}^{-2} \\
& failure = 0
\end{aligned}
$$

where $m(X)$ is the structural mass of the platform (kg), as function of the topology and cross-sectional properties of the members, and a function of the design variables X of the optimisation problem. Furthermore, R_{offset} is the radius between the centre column and the outer columns (m), D_{UC} is the diameter of the upper columns (m), θ_{max} is the maximum observed floating platform pitch angle (°), $a_{\text{nac,max}}$ is the maximum nacelle acceleration ($\text{m}\,\text{s}^{-2}$), and $failure$ is a flag which takes the value 1 if an OpenFAST simulation crashes, and 0 in case all simulations terminate successfully.

As discussed previously, the failure flag is necessary because in some limiting cases, the optimiser might pick a set of design variables that results in an unstable platform. This instability might lead to the wind turbine tipping over during the simulation, thereby causing an abrupt termination of the OpenFAST simulation. In such situations, it is essential to communicate to the optimiser that the selected set of design variables is inadequate.

The existing constraints, which are based on the maximum pitch angle and nacelle acceleration, cannot fulfill this role, primarily because these constraint values are obtained only after the post-processing of successful OpenFAST simulations. In the event of a simulation failure, these constraint values are unavailable. Hence, a failure flag has been introduced, enabling communication back to the optimiser, signalling that one or more OpenFAST simulations have failed.

Additionally, in cases where a simulation fails, the pitch and nacelle acceleration constraints are set to their maximum allowable values. This adjustment was made after experimenting with a "dummy" optimisation problem, revealing that utilising limiting constraint values (e.g. a maximum pitch value of 10 degrees) yielded faster convergence compared to values indicating constraint violations (e.g. a maximum pitch value of 15 degrees).

The optimisation process will be conducted twice: once with SubDyn enabled and a second time without the sub-structural model. In the former case, the process requires significantly higher computational overhead, but it provides the ability to perform structural analysis when post-processing the results. In the latter case, consideration of structural integrity is neglected, as the focus shifts to modelling solely the overall dynamics of the floating wind turbine. Furthermore, after an optimal solution has been found, a small optimisation study is performed to test how the pontoons and braces, interconnecting the outer and centre columns, should be redesigned to cope with the internal stresses present in the substructure. Finally, sensitivity of the results to simulation length and the impact of second order wave forces is checked.

4

NEMOH Model

To model the hydrodynamic loads on the floating platform, and its resulting motion, OpenFAST's HydroDyn module is used. As explained in section 2.1, various approaches exist for modelling hydrodynamic loads on a floating body. Within HydroDyn, it is possible to use potential flow theory, strip theory (via Morison's equation), or a combination [35]. Fundamentally, strip theory should only be applied to slender structures, such as a truss element, whose diameter is much smaller than the wavelength [43]. However, because semi-submersible platforms typically comprise large-volume columns with significant waterline length, one cannot get away with using just strip theory to model the full semi-submersible platform. Thus, a potential-flow model is needed.

In order to utilise the potential-flow model in HydroDyn, it is necessary to first simulate the hydrodynamic response of the floating platform using a Boundary Element Method (BEM) solver, covering a wide range of wave frequencies and directions. A widely used tool for this purpose is WAMIT, which is a commercial program for wave load- and motion analysis. The output files generated by WAMIT contain a comprehensive hydrodynamic database of the floating platform, including hydrodynamic stiffness matrix, added mass and radiation damping coefficients, wave excitation force components, and optionally, second order difference- and sum-frequency wave loads. Besides WAMIT, there are alternative open-source BEM solvers available, such as NEMOH and HAMS, that offer similar capabilities for hydrodynamic modelling. It is important to note that while these alternatives provide better accessibility, OpenFAST, specifically, requires hydrodynamic data to be provided in the WAMIT file format, which differs from the formats used by NEMOH and HAMS.

As mentioned in chapter 3, it was decided to use NEMOH instead of WAMIT, which automatically introduced the additional task of converting the NEMOH output files to the WAMIT file format. The sections in this chapter will provide some background info on NEMOH, and explain in more detail how the software is used to create the hydrodynamic database.

4.1. Theoretical Overview

NEMOH is a software tool that employs a 3D boundary element method in the frequency domain to solve wave-structure interaction problems. The recently released version 3.0 consists of two main modules: NEMOH1, which solves first-order linear diffraction and radiation problems, and NEMOH2, an extended module for computing second-order Quadratic Transfer Functions (QTFs) for fixed or floating structures.

In NEMOH1, the underlying theoretical foundation is potential flow theory, assuming an inviscid fluid, incompressible and irrotational flow [44]. The equations solved must satisfy free-surface conditions, impermeable bottom conditions, diffraction and radiation conditions on the body hull, as well as radiation wave conditions in the far field. The total potential is decomposed into incident, diffraction and radiation potentials to capture the various effects of the structure on the surrounding fluid and vice-versa.

The 3D linear potential flow problem is formulated as a Boundary Integral Equation (BIE), and transformed into a two-dimensional problem considering the distribution of sources on the body surface. The BIE is expressed using Green's second identity and the appropriate Green function, and through its solution, the diffraction potential, radiation potential, and corresponding velocities can be determined. Based on the obtained potentials, the added mass and radiation damping coefficients are derived, as well as the excitation force. Finally, in a post-processing step, the Impulse Response Functions (IRFs) are computed, as well as the

Response Amplitude Operators (RAO).

NEMOH2, the second-order module, focuses on the computation of QTFs. The second-order loads are divided into quadratic and potential parts. The quadratic part is formulated based on the near-field method, while the potential part utilises the indirect method.

To solve the BIE in NEMOH1 numerically, a constant panel method with quadrilateral mesh is employed, and influence coefficients are computed using Gauss-quadrature integration. The linear system resulting from the discretisation is solved using a numerical solver, with e.g. Gauss elimination or LU-decomposition. The second-order QTF module can be run only after having computed the first-order hydrodynamic coefficients with NEMOH1. The second-order wave loads can be analysed for both bi-directional and uni-directional waves, but multi-body problems have not been extensively tested yet.

The general workflow of NEMOH is visualised in figure 4.1. Both NEMOH1 and NEMOH2 comprise several modules: a pre-processor, solver and a post-processor, which are intended to be run in this respective order. NEMOH1 also includes a module for performing hydrostatic calculations.

In NEMOH1, the *preProc* executable is responsible for processing the input mesh file and generating the necessary body conditions for each calculation case. The *hydrosCal* executable calculates hydrostatic parameters of the input mesh, such as the stiffness matrix and inertia matrix. The *Solver* numerically solves the boundary value problems provided by *preProc*, and calculates the hydrodynamic coefficients. Lastly, *postProc* processes the output from the solver to compute e.g. IRF, infinite-frequency added mass, the Kochin coefficient, free-surface elevation and RAOs.

Using the first-order results as input, NEMOH2's *QTFpreProc* performs calculations of the total potential, perturbed potential, normalised radiation potential, as well as the associated velocities on the body panels, waterline, and free-surface panels. Subsequently, the *QTFsolver* is run to compute the quadratic part and potential part of the second-order loads. Inclusion of the free-surface integrals in the potential part is optional. Finally, *QTFpostProc* combines the computed components of the QTFs to generate the total QTF.

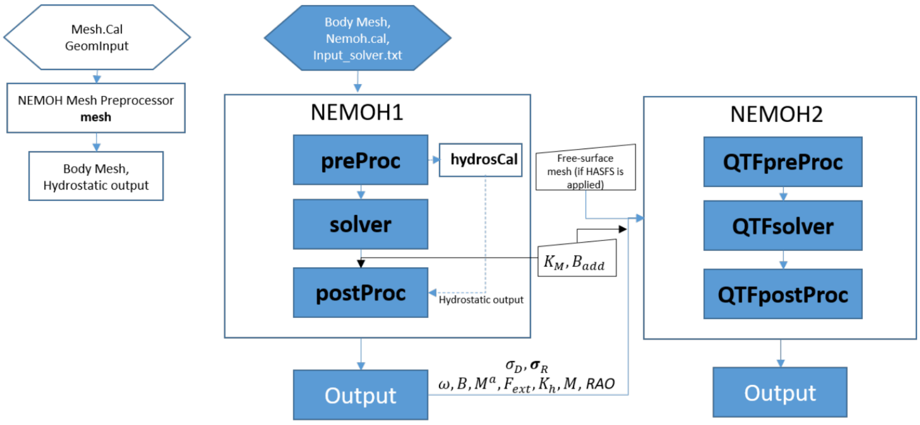

Figure 4.1: Global flowchart of the NEMOH software suite [44]

Lastly, there is a *mesh* pre-processor executable, which can be used to refine a coarse input mesh, estimate its properties, and write an input *Mesh.cal* file that can subsequently be used with the BEM solver. Properties calculated include displacement volume, buoyancy centre, hydrostatic stiffness, and the mass- and inertia matrices. For additional information on the workflow of the NEMOH software and a detailed description of the underlying physical principles, the reader is referred to the user manual [44].

4.2. Practical Application

While the default method to run NEMOH involves using the command-line, the third release of NEMOH comes with a number of accompanying MATLAB scripts that wrap the software. These scripts offer several useful functionalities, such as the ability to generate an appropriate mesh for NEMOH calculations from a coarse body description. Furthermore, they facilitate execution of the software and include functionalities for post-processing of the results. These functionalities would be useful in the context of this thesis. However, due to their implementation in MATLAB, they do not match well with the developed programming framework, which is written in Python. Hence, a Python wrapper for the NEMOH software was developed, converting the relevant portions of the MATLAB scripts to Python code. Additionally, the scripts were adjusted or extended to the needs of this project.

The Python wrapper for NEMOH adopts an object-oriented approach, utilising a class structure that encapsulates various functionalities, which will be explained in more detail in the following paragraphs. Upon instantiation of the NEMOH class, a set of input parameters is provided that are related to the physical environment, including water depth, water density, gravitational acceleration, and the desired range of wave frequencies and directions. Furthermore, the class expects inputs to set the configuration of the NEMOH modules, such as flags to enable calculation of hydrostatic parameters and second-order QTFs.

4.2.1. Mesh Generation

The *generate_mesh* method takes as input the geometry of the floating platform for which the hydrodynamic coefficients are to be computed. The geometry input may be provided by the user when the NEMOH wrapper is used as a standalone program, or it may be automatically defined and provided at a higher level when integrating the wrapper with the optimisation framework.

The semi-submersible platform comprises multiple cylindrical components that are arranged according to a specific topology. In the case of the DeepCWind platform, the central column and the offset columns are two distinct components with different shape. The shape is determined by a number of design variables, including diameter and height for different sections of the two components. The topology is established in such a way that the central column is aligned with the z-axis of the cartesian body reference frame. Next, three offset columns are positioned in a triangular arrangement around the central column, at a prescribed distance from the centre. This distance is known as the offset radius, which is another important design variable.

The description of the design variables (i.e. diameter and height of the different sections), in combination with an estimate of the draft of the floating platform, results in a coarse description of the distinct components by defining the vertices in z- and r-coordinates in 2D space, as shown in figure 4.2. Furthermore, the location of the offset columns with respect to the body reference frame is described by using translation and rotation operations. Finally, a few parameters are defined that influence the quality of the mesh, such as the azimuthal discretisation, or the target number of panels. This information combined is passed to the *generate_mesh* method, which will create a mesh from the coarse body description, suitable for performing NEMOH calculations. This mesh is then generated in two steps.

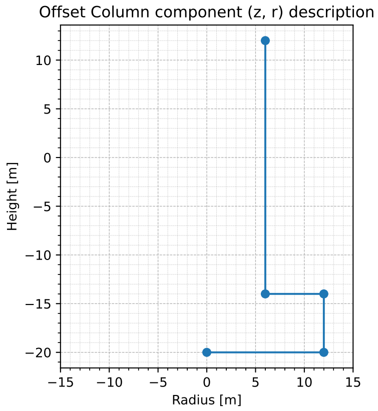

Figure 4.2: Coarse description of the offset column component in terms of its vertices in (z, r) coordinates.

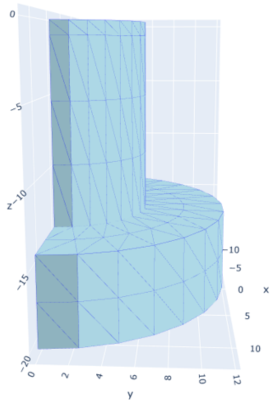

Figure 4.3: Meshed representation of the offset column component. The x-axis is used as symmetry plane

First, a function "axiMesh" is called for each component (i.e. central column, offset column), which creates a mesh for the axisymmetric body. The coarse description of each component in terms of 2D $z-$ and $r-$coordinates (as shown in figure 4.2) is further refined by adding points. Subsequently, the array of points is revolved around the local $z-$axis to obtain a 3-dimensional description of the component mesh. When this 3D description is passed to the axiMesh function, the mesh pre-processor from figure 4.1 is utilised to generate a quadrilateral mesh with a user-defined target number of panels. The resulting mesh of the offset column is depicted in figure 4.3. Two important features of the mesh pre-processor can be observed from this

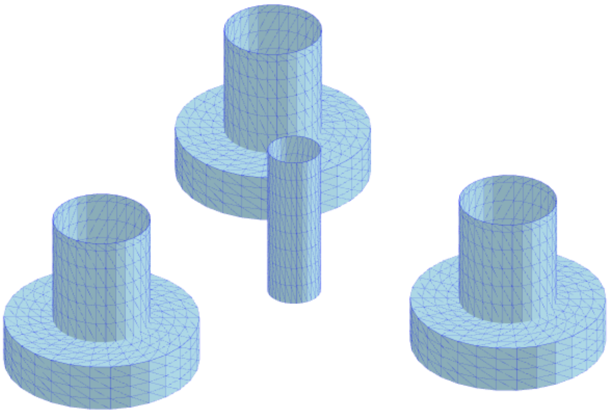

Figure 4.4: Mesh of the DeepCWind platform created with the developed Nemoh wrapper in Python

figure. Firstly, in this process, the mesh section above the waterline is removed, as it does not contribute to the calculation of wave loads. Secondly, to save on computational resources, only one half of the component is generated, taking advantage of symmetry.

In the second step, a single instance of the central column along with three copies of the offset column mesh are created, resulting in four individual meshes. The function "Mesh" positions the different components according to the predetermined topology, using a combination of translation and rotation operations. Hereafter, the panels of each individual mesh are broken down, and reassembled into a final, cohesive main mesh, as shown in figure 4.4. In this final step, the mesh can again be refined according to a user-defined target number of panels.

In addition to creating the mesh, the Mesh functions also produce NEMOH input files in the project directory. These include *Mesh.cal, Nemoh.cal, input_solver.txt, [meshfile].dat,* hydrodynamic stiffness matrix *KH.dat, Inertia.dat* and *Hydrostatics.dat*

4.2.2. Results Generation and Processing

The *run_solver* method of the NEMOH wrapper is rather straightforward. It uses the subprocess module in Python to call and run the NEMOH executables in a separate process, in the order described in section 4.1. The project directory is passed as an argument to the solver, in order to locate the various NEMOH input files generated with the *generate_mesh* method. The *Nemoh.cal* file is the main input file, which includes flags to enable or disable post-processing options (e.g. IRF calculation) and second-order QTF calculations. Furthermore, it provides a description of the range of wave frequencies and directions that the Boundary Value Problems (BVP) will be solved for.

Results Processing

The *process_results* method reads the input- and output files of the NEMOH simulation to extract the results. With some basic post-processing, the dimensional added mass and radiation damping coefficients are obtained as a function of wave frequency. Similarly, the excitation force amplitude and phase, IRFs, and second-order sum- and difference frequencies are derived. These results can be used for further analysis of the floating platform, or rewritten in the WAMIT file format, to be used in an OpenFAST simulation with HydroDyn.

Writing the Results to the HydroDyn Input Format

Most quantities in the NEMOH output files are expressed in S.I. units and are dimensional, whereas the output from WAMIT is non-dimensional. Therefore, all NEMOH results are non-dimensionalised. To make the added mass matrix $\mathbf{A}_{ij}$ and radiation damping matrix $\mathbf{B}_{ij}$ non-dimensional, the following equations are utilised:

$$\overline{\mathbf{A}}_{ij} = \frac{\mathbf{A}_{ij}}{\rho L^k} \qquad \overline{\mathbf{B}}_{ij} = \frac{\mathbf{B}_{ij}}{\rho L^k \omega} \tag{4.1}$$

where L is the characteristic length scale in (m), ω is the wave frequency in ($\mathrm{rad\,s^{-1}}$) and $k = 3$ for $i, j = 1, 2, 3, k = 4$ for $i = 1, 2, 3, j = 4, 5, 6$ or $i = 4, 5, 6, j = 1, 2, 3$ and $k = 5$ for $i, j = 4, 5, 6$. Because L is conveniently set to unity, L^k will be equal to 1, regardless of the matrix indices i and j. Then, the added mass and damping coefficients are written to a *'.1'* file using the following column structure:

$$\boxed{T \quad i \quad j \quad \overline{\mathbf{A}}_{ij} \quad \overline{\mathbf{B}}_{ij}}$$

where indices i, j point to the degrees of freedom (surge, sway, etc.), and T is the wave period in (s), related to the wave frequency as follows:

$$T = \frac{2\pi}{\omega} \tag{4.2}$$

The first lines of the *'.1'* file must contain the zero- and infinite-frequency added mass coefficients. The infinite-frequency (or zero-period) coefficients are provided by NEMOH. The zero-frequency (or infinite-period) coefficients, however, are derived from the added mass coefficients by means of quadratic extrapolation. Now, moving on to the excitation force, the non-dimensionalisation is performed using:

$$\overline{\mathbf{X}}_i = \frac{\mathbf{X}_i}{\rho g A L^m} \tag{4.3}$$

where $\mathbf{X}_i$ is the excitation force in (N), A is the wave amplitude in (m) and $m = 2$ for $i = 1, 2, 3$ and $m = 3$ for $i = 4, 5, 6$. It should be noted that in NEMOH, the force output is already normalised with the unit wave amplitude [44], hence A can be omitted from equation 4.3. The excitation forces are written to a *'.3'* file according to the following column structure:

$$\boxed{T \quad \beta \quad i \quad \mathrm{Mod}\left(\overline{\mathbf{X}}_i\right) \quad \mathrm{Pha}\left(\overline{\mathbf{X}}_i\right) \quad \mathrm{Re}\left(\overline{\mathbf{X}}_i\right) \quad \mathrm{Im}\left(\overline{\mathbf{X}}_i\right)}$$

where β is the wave direction in (°), and $\mathrm{Mod}(\overline{\mathbf{X}}_i)$, $\mathrm{Pha}(\overline{\mathbf{X}}_i)$, $\mathrm{Re}(\overline{\mathbf{X}}_i)$ and $\mathrm{Im}(\overline{\mathbf{X}}_i)$ denote the modulus, phase, real part and imaginary part of the excitation force, respectively.

As for the hydrostatic stiffness matrix elements, they are non-dimensionalised using the following relation:

$$\overline{\mathbf{C}}_{ij} = \frac{\mathbf{C}_{ij}}{\rho g L} \tag{4.4}$$

The *'.hst'* file is then formatted as follows:

$$\boxed{i \quad j \quad \overline{\mathbf{C}}_{ij}}$$

Finally, the second-order sum- and difference frequencies are rewritten to the *'.12s'* and *'.12d'* WAMIT output file format, respectively. Because the second-order results in NEMOH have already been non-dimensionalised with respect to g and ρ, the non-dimensionalisation step can be omitted, and the results can be rewritten directly to the output files, adopting the following column structure:

$$\boxed{T_1 \quad T_2 \quad \beta_1 \quad \beta_2 \quad i \quad \mathrm{Mod}\left(\overline{\mathbf{F}}_{ij}^{+}\right) \quad \mathrm{Pha}\left(\overline{\mathbf{F}}_{ij}^{+}\right) \quad \mathrm{Re}\left(\overline{\mathbf{F}}_{ij}^{+}\right) \quad \mathrm{Im}\left(\overline{\mathbf{F}}_{ij}^{+}\right)}$$

where $\overline{\mathbf{F}}_{ij}^{+}$ is the sum-frequency QTF value, and i again denotes the DOF. For the difference-frequency QTF values, the + symbol is replaced by a minus: $\overline{\mathbf{F}}_{ij}^{-}$.

5

OpenFAST Model

The OpenFAST software is a physics-based engineering tool developed by NREL [35]. It consists of various modules, which correspond to distinct physical domains of the wind turbine model (i.e. aerodynamics, hydrodynamics, control, etc). Coupled together, these modules allow computing the aero-hydro-servo-elastic solution of the wind turbine system. The different modules and their coupling are visualised in figure 5.1. In the subsequent sections of this chapter, the simulation setup is elaborated. Section 5.1 explains the rationale behind the environmental and operational conditions. Subsequently, section 5.2 describes the metocean conditions, which the floating platform is designed for. Next, section 5.3 details the initial platform design, which will be subject to optimisation. Finally, section 5.4 elaborates the relevant parameters for the different modules.

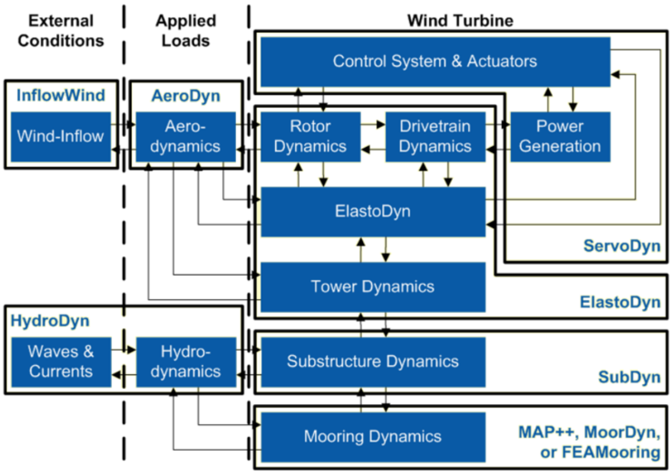

Figure 5.1: Diagram of OpenFAST and the couplings between its modules [45]

5.1. DLC Selection

As introduced in chapter 1 already, a FOWT must be designed to withstand the broad range of operational and environmental loads that it may encounter during its operational lifetime. In preliminary discussions on the upcoming IEC standard IEC 61400-3-2 on the design requirements for floating offshore wind turbines, it is noted that the FOWT operational lifetime may be effectively represented through a collection of design scenarios that cover the most significant conditions that may occur. These design load cases (DLCs) should encompass all relevant situations with a reasonable probability of occurrence, which includes normal operational situations in normal or extreme environmental conditions, the occurrence of faults, and transportation, installation and maintenance situations in appropriate weather circumstances. A complete description of all the design situations to be simulated is provided in the upcoming IEC 61400-3-2 standard. The standard provides guidelines and requirements on e.g. the number of simulations to be performed, the length of simulated time, etc. It is prescribed that each DLC is simulated for a duration of at least 1 hour, to capture the effects of any slowly varying response. Furthermore, it is required that simulations are repeated at least six times, with different stochastic wind fields and sea states, to avoid dependence of seed. Additionally, multi-directionality of wind and waves may play an important role in the loads acting on the floating substructure. Hence, it is prescribed to consider wind-wave misalignment in assessing the FOWT response.

Thus, it becomes clear that a large number of DLCs is required for evaluating the design of a FOWT, with the number of simulations potentially reaching up to more than a thousand. It is needless to say that performing this many simulations inside an optimisation loop is unfeasible. Methods exist to reduce the number of load cases to test the FOWT response, for example by utilising an importance sampling method with two-stage filtering [46], or by developing a reduced non-linear model to identify the most critical load cases [47]. These methods, however, are outside the scope of this project. Instead, a subset of DLCs is selected, with load conditions that are expected to cause the most extreme loads on the FOWT, and that have the biggest impact on fatigue life.

Because the optimisation problem in this project focuses on the support structure, rather than the wind turbine, the decision has been made to consider only design load cases that are expected to be most relevant to the design of the substructure, or to the complete system. In order to further narrow down the scope of the exercise, only normal operating conditions will be considered, which means that fault conditions are not accounted for. Furthermore, transient conditions like start-up, shutdown and emergency stop are disregarded. The main reason for this is the limited availability of cores for parallel processing. The choice for the reduced set of design situations is in line with those described in [16] and [17].

Table 5.1: Subset of Design Load Cases used to evaluate the FOWT response

DLC	Wind Type	V_{Hub} [m/s]	H_s [m]	T_p [s]	γ [-]	Metocean Directionality	Sea Currents	Other Conditions	Partial safety factor	# Seeds	Total # sims
1.2	NTM	3.00	0.92	6.69	1.03	COD	None	-	1.00	1	1
		5.00	1.09	6.90	1.13				1.00	1	1
		7.00	1.29	7.14	1.23				1.00	1	1
		9.00	1.52	7.41	1.33				1.00	1	1
		11.00	1.80	7.70	1.44				1.00	1	1
		13.00	2.12	8.02	1.55				1.00	1	1
		15.00	2.50	8.38	1.65				1.00	1	1
		17.00	2.96	8.78	1.76				1.00	1	1
		19.00	3.49	9.23	1.86				1.00	1	1
		21.00	4.13	9.74	1.96				1.00	1	1
		23.00	4.87	10.32	2.05				1.00	1	1
		25.00	5.76	10.98	2.12				1.25	1	1
1.6	NTM	3.00	3.35	9.12	1.84	COD	None	-	1.25	1	1
		5.00	3.55	9.28	1.87				1.25	1	1
		7.00	3.79	9.48	1.91				1.25	1	1
		9.00	4.11	9.73	1.96				1.25	1	1
		11.00	4.66	10.16	2.02				1.25	1	1
		13.00	5.27	10.62	2.09				1.25	1	1
		15.00	6.01	11.17	2.14				1.25	1	1
		17.00	6.88	11.80	2.19				1.25	1	1
		19.00	7.86	12.49	2.22				1.25	1	1
		21.00	8.71	13.08	2.24				1.25	1	1
		23.00	9.78	13.81	2.26				1.25	1	1
		25.00	10.37	14.21	2.26				1.25	1	1
6.1	EWM 50 yr	45.0	10.90	14.60	2.25	COD	None	Yaw +/- 8°	1.25	1	2
6.3	EWM 1 yr	37.5	7.80	12.40	2.24	COD	None	Yaw +/- 20°	1.25	1	2

In this project, DLC 1.2 will be simulated to assess the fatigue life of the floating substructure during normal operation. With DLC 1.6, the ultimate loads are simulated, during power production in a severe sea state. Furthermore, DLCs 6.1 and 6.3 are simulated to test the FOWT response in storm conditions, with yaw misalignment in extreme wind and waves with a return period of 50 years and 1 year, respectively. For DLCs 1.2 and 1.6, the range of wind speeds considered runs from cut-in to cut-out, in steps of $2\,\mathrm{m\,s^{-1}}$. The wind fields are generated with TurbSim [48]. They are stochastic, and in accordance with the IEC normal turbulence model (NTM). The sea state is modelled by means of the JONSWAP spectral model. The specific metocean conditions utilised are summarised in table 5.1, and are further explained in section 5.2. For DLCs 6.1 and 6.3, the extreme wind model (EWM) is utilised, with a return period of 50 years and 1 year respectively. For these storm cases, the wind turbine rotor is at an angle with respect to the incoming wind. The yaw misalignment angle, and the corresponding marine conditions are also provided in table 5.1. Finally, for the load assessment, a partial safety factor of 1.25 will be applied to the ultimate loading cases, whereas a factor of 1 will be used in the assessment of fatigue loading.

For the load cases described, a number of simplifications is made. Firstly, the effect of sea currents is neglected. Secondly, only co-directional wind and wave conditions will be considered, with a wind/wave heading of zero degrees with respect to the FOWT reference frame in OpenFAST. This simplification was made because the occurrence of aligned wind and waves is most common, and although it might not result in the most severe loading case, it greatly reduces the number of simulations to be performed. Also, because it is not known beforehand which combination of wind/wave heading causes extreme loading.

Furthermore, the time simulated for each load case is shortened to ten minutes, instead of a full hour, to reduce computational cost. Because the aim is to obtain estimates of the fatigue life and ultimate loads in the context of an optimisation problem, rather than performing detailed analyses for e.g. certification purposes, a ten-minute simulation is assumed sufficient for obtaining decent estimates.

Lastly, although standard practice is to run each load case six times with different wind and wave seeds, the limited number of CPU cores available restricts the analysis to only a single simulation per load case.

5.2. Metocean Conditions

In order to prepare a relevant subset of DLCs, a comprehensive and representative dataset of metocean conditions should be utilised. This data is sourced from the metocean design basis of the Hywind pilot farm at Buchan Deep [49], because of the extensive assessment of the site conditions, and because it is a representative site in the North Sea where FOWT technology has already been demonstrated.

The data presented in [49] has been obtained by hindcasting, and contains detailed information and analyses about both the short-term and long-term wind and wave statistics, including the correlation between the two. Furthermore, site characteristics such as water levels, marine growth, icing, temperature and salinity are analysed. However, the influence of these aspects on the structural integrity and performance of the FOWT will be neglected in the simulations. Most of the data covers the period 1958 - 2010, representing a total of 53 years. The sample interval of the wind and wave data is 3 hours.

5.2.1. Wind Resource

The long-term wind climate is best represented by a Weibull distribution. The shape and scale parameters for the Buchan Deep site have been derived for the altitude of 10 m above sea level. However, the wind speeds considered in table 5.1 are given for the hub height, at which the distribution of wind speeds is different. Now, the Weibull parameters at hub height can be computed, starting from the following equation [50]:

$$\overline{U} = c\Gamma\left(1 + 1/k\right) \tag{5.1}$$

where $\overline{U}$ is the mean wind speed ($\mathrm{m\,s^{-1}}$), c is the scale parameter ($\mathrm{m\,s^{-1}}$), k is the shape parameter (-), and Γ denotes the complete gamma function. Assuming that the shape parameter does not vary with altitude, the scale parameter at hub height can be computed after extrapolating the mean wind speed. At the Buchan Deep site, the wind profile as function of height z is given by:

$$U_z = U_0\left(1 + C \cdot \ln\frac{z}{z_r}\right) \tag{5.2}$$

where U_0 is the mean wind speed at the reference elevation of z_r = 10 m, and C is given by:

$$C = 5.73 \cdot 10^{-2}\sqrt{1 + \frac{3}{2}\frac{U_0}{U_{\mathrm{ref}}}} \tag{5.3}$$

with U_{ref} =10 $\mathrm{m\,s^{-1}}$, being the reference wind speed. Then, by combining equations 5.1 to 5.3, the extrapolated value of the scale parameter, can be found. The Weibull parameters at the reference height and at hub height are summarised in table 5.2:

Table 5.2: Wind speed Weibull parameters at the reference- and hub height

	k	c
z_{10}	2.235	10.03
z_{hub}	2.235	11.96

5.2.2. Sea State

The marine conditions in DLC 1.2 represent the so-called Normal Sea State (NSS). The marine conditions depend on the wind speed, as there is a strong correlation between wind speed and wave height. This relation is found for the NSS by fitting an exponential function to the metocean data, as presented in [49]:

$$H_{\mathrm{s}} = 0.719e^{0.0832U_{100}} \tag{5.4}$$

where H_s is the significant wave height (m), and U_{100} is the 1-hour mean wind speed at 100 m above sea level. The mean spectral peak period $\overline{T_{\mathrm{p}}}$ is then computed from:

$$\overline{T_{\mathrm{p}}} = e^{\mu+\frac{1}{2}\sigma^2} \tag{5.5}$$

where:

$$\mu = 1.307 + 0.567H_{\mathrm{s}}^{0.369} \tag{5.6}$$

$$\sigma^2 = 0.005 + 0.119e^{-0.425\cdot H_{\mathrm{s}}} \tag{5.7}$$

And lastly, the peak-enhancement factor γ is calculated using:

$$\gamma = \max\left[1.0, 42.2\left(\frac{2\pi H_{\mathrm{s}}}{gT_{\mathrm{p}}^2}\right)^{6/7}\right] \tag{5.8}$$

For DLC 1.6, the marine conditions represent a Severe Sea State (SSS). This means that for each wind speed in the range from cut-in to cut-out, the 50-year return wave height H_{s50} is utilised. This value is derived statistically from the wind-wave correlation data presented in [49].

5.3. Initial Design: DeepCWind Semi-Submersible Platform

The optimisation problem considers the 5 MW offshore reference wind turbine on top of the DeepCWind semi-submersible platform. The relevant data of these systems are presented in tables 5.3 and 5.4. For a more detailed understanding of the turbine and platform characteristics, the reader is referred to [15] and [51].

Figure 5.2 shows a schematic representation of how the platform design variables from table 5.3 define its physical dimensions. The platform geometry is defined with respect to the global reference frame, where the x-axis is aligned with the mean sea level (MSL), and the z-axis coincides with the centreline of the undisplaced tower. The acronyms "MC", "UC" and "BC" point to the Main Column, Upper Column and Base Column, respectively. Furthermore, as the cross-sectional properties of the pontoons and brace are equal, the words are sometimes used interchangeably.

5.4. Simulation Setup

The simulation setup is based on FAST certification test #25. The OpenFAST input files of this simulation can be found via the OpenFAST GitHub repository [38]. The settings and parameters used for the OpenFAST simulation in this project will be explained in the following subsections, where specific sections of the input files are provided. In this chapter, all input file sections are from DLC1.2 with a mean wind speed of 11 $\mathrm{m\,s^{-1}}$. Throughout the chapter, only the main changes incorporated with respect to the reference case are described: the ones which are relevant to this project. Some settings are DLC-specific, it is mentioned when this is the case.

Table 5.3: Physical properties of the DeepCWind semi-submersible platform

Platform Design Variables						
		MC	UC	BC	brace	
Diameter	D	6.5	12	24	1.6	(m)
Height	H	30	6	26	N/A	(m)
Wall thickness	t	0.03	0.06	0.06	0.0175	(m)
Offset radius	R_{offset}	28.868				(m)
Young's modulus	E	21000				(GPa)
Shear modulus	G	80.769				(GPa)
Density	ρ_{material}	7850				($\mathrm{kg\,m^{-3}}$)
Density	ρ_{ballast}	1025				($\mathrm{kg\,m^{-3}}$)
Fill location	$z_{\text{ballast,UC}}$	6.17				(m)
Fill location	$z_{\text{ballast,BC}}$	14.89				(m)
Draft	$Draft$	20				(m)

Table 5.4: Relevant characteristics of the 5 MW offshore reference turbine [51].

Wind Turbine Properties			
Rotor diameter	D_{rotor}	126	(m)
Mean chord	c_{mean}	3.48	(m)
Tower base diameter	$D_{\text{towerbase}}$	6	(m)
Tower top diameter	D_{towertop}	3.87	(m)
Tower base wall thickness	$t_{\text{towerbase}}$	0.027	(m)
Tower top wall thickness	t_{towertop}	0.019	(m)
Hub height	z_{hub}	90	(m)
Transition piece height	z_{TP}	10	(m)
Cut-in wind speed	$U_{\text{cut-in}}$	3	($\mathrm{m\,s^{-1}}$)
Rated wind speed	U_{rated}	11.4	($\mathrm{m\,s^{-1}}$)
Cut-out wind speed	$U_{\text{cut-out}}$	25	($\mathrm{m\,s^{-1}}$)
Total mass	M_{turbine}	599107	(kg)

5.4.1. Main Settings

The high-level simulation settings are defined in the main *.fst* input file. Adhering to the guidelines on the simulation length, sufficient transient time is used to ensure that initial simulation transients are dampened out, and to allow for the buildup of an adequate response of the full FOWT system to the environmental conditions. Therefore a total run time of 1000 seconds is used, of which the first 400 will be discarded. This results in an exploitable window of 600 seconds, in accordance with what has been described in section 5.1. The global time step used in OpenFAST is intrinsically related to the rotor speed and the full system natural frequencies that are being modelled. For modelling the fully coupled response, i.e. all flexible modes are enabled, a time step small enough should be chosen in order to prevent the simulation from becoming numerically unstable. A rule of thumb for choosing the time step has been suggested by J. Jonkman [52] as follows:

$$\texttt{DT} \leq \frac{1}{10 f_{\max}} \tag{5.9}$$

where $f_{\max}$ is the highest full system natural frequency in Hz, which can be found by performing a FAST linearisation analysis. Such an analysis however, is unfeasible within the scope of this optimisation project, considering that a change in dimensions automatically leads to a change in system frequencies. The recommended time step for the initial design is 0.0125 seconds. A sensitivity analysis was conducted where the simulation was run with different values of `DT`. The findings showed that the simulation remained stable for the recommended time step, even after modest adjustments to the platform geometry. Yet, increasing it beyond 0.02 seconds introduces numerical instabilities. Therefore, it was chosen to stick with the recommended time step, leaving some margin to avoid possible numerical instabilities.

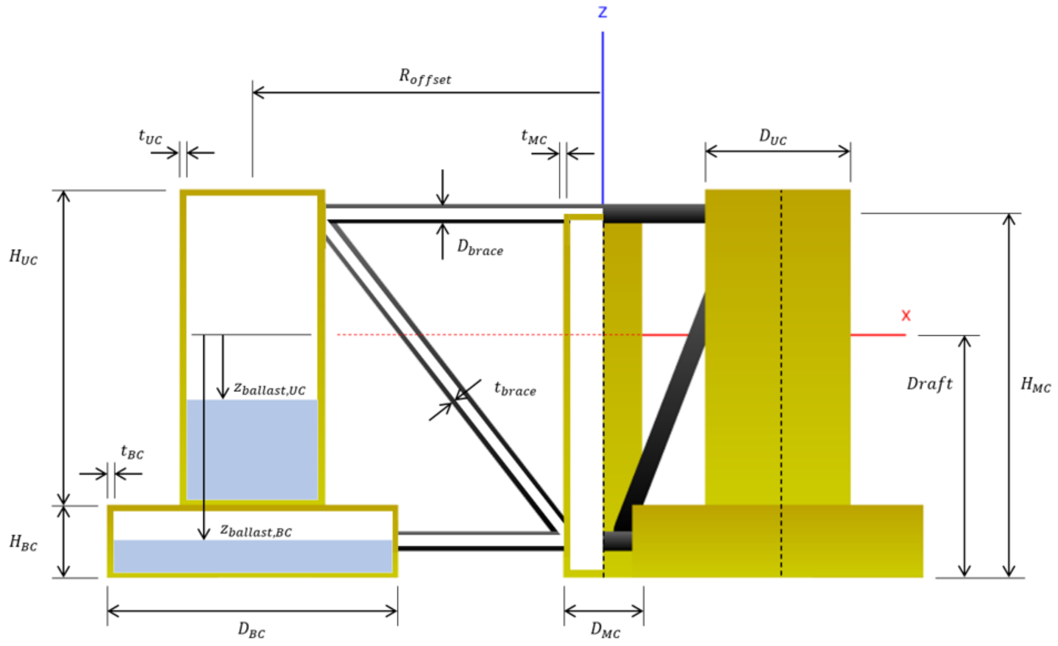

Figure 5.2: Representation of the platform design variables

In the context of modelling the sub-structural dynamics of floating platforms in OpenFAST, it is essential to consider several other simulation control parameters, which may not hold as much significance when modelling bottom-fixed turbines. The parameter `NumCrctn` defines how many correction steps should be taken by the OpenFAST integrator. It has been advised by developers of OpenFAST[1] to set this value to 1, or otherwise the time integration will fail. Furthermore, in the coupling between ElastoDyn, HydroDyn and SubDyn, a Jacobian matrix is utilised to resolve the connection between acceleration and load interactions. The parameter `DT_UJac` determines the frequency of the Jacobian updates. In most models, this value may be larger than the total run time. For floating platforms, however, it is advised to set this value according to the following relation:

$$\texttt{DT\_UJac} = \frac{1}{10 f_{\mathrm{n}}} \tag{5.10}$$

where f_n is the natural frequency in Hz corresponding to the roll, pitch or yaw mode with excessive motion. For the initial platform design, it is sufficient to use a value of 2.7 seconds, which corresponds with the natural frequency in pitch (0.037 Hz). However, because it is not known beforehand what the platform natural frequencies will be for different platform geometries in the optimisation, a conservative value of 1.0 seconds is used. Lastly, the scaling factor `UJacSclFact` is applied to scale down the load components within the Jacobian matrix, to reduce them to a comparable magnitude as the acceleration components. It is advised to set this approximately to the same scale as the total system mass expressed in kg (including ballast) [35]. The simulation control parameters are summarised below.

```
---------------------- SIMULATION CONTROL --------------------------------------
1000          TMax            - Total run time (s)
0.0125        DT              - Recommended module time step (s)
1             NumCrctn        - Number of correction iterations (-)
1.0           DT_UJac         - Time between calls to get Jacobians (s)
1.4E+07       UJacSclFact     - Scaling factor used in Jacobians (-)
```

In the simulation configuration, the environmental conditions are aligned with those utilised in the NEMOH hydrodynamic model. However, it is essential to note that any changes to the water depth will directly impact the mooring response, which requires that the MoorDyn input file is updated accordingly.

---

[1] https://github.com/OpenFAST/openfast/discussions/801#discussioncomment-1139658

```
---------------------- ENVIRONMENTAL CONDITIONS --------------------------------
9.80665       Gravity       - Gravitational acceleration (m/s^2)
1.225         AirDens       - Air density (kg/m^3)
1025          WtrDens       - Water density (kg/m^3)
1.464e-05     KinVisc       - Kinematic viscosity of working fluid (m^2/s)
335           SpdSound      - Speed of sound in working fluid (m/s)
103500        Patm          - Atmospheric pressure (Pa)
1700          Pvap          - Vapour pressure of working fluid (Pa)
200           WtrDpth       - Water depth (m)
0             MSL2SWL       - Offset between still-water level and mean sea level (m) [positive upward]
```

5.4.2. TurbSim

To simulate the FOWT response to different wind conditions, the InflowWind module is used in conjunction with TurbSim. In section 5.1, these wind conditions have already been outlined. The following paragraphs elaborate on the specific configuration settings used in TurbSim. Using this module, turbulent wind fields are generated that replicate real-world atmospheric conditions encountered on site. These synthesised inflow conditions allow assessment of the FOWT's performance under a wide range of wind scenarios. In the runtime options of the input file, the effects of tower shadow and tower aerodynamic loads must be enabled, hence the synthesised wind domain must include tower data points.

```
---------Runtime Options-----------------------------------
True          WrADFF        - Output full-field time-series data in TurbSim/AeroDyn form?
True          WrADTWR       - Output tower time-series data?
```

In the model specifications, the grid height and width are set to 1.25 times the rotor diameter. A larger factor is chosen here than the typically suggested value of 1.1 [48], in order to account for potentially excessive platform motions, which could otherwise cause the wind turbine to exceed the predefined grid boundaries. The number of grid points in the Z- and Y-direction are set equal to the nearest odd integer to the grid height/width divided by the mean chord of the turbine's blades. The analysis time is set equal to the OpenFAST total run time, and the time step for discretisation of the turbulent wind field can be set slightly higher, because the OpenFAST integrator will interpolate between the instantaneous values. Because in this project only aligned wind and waves at a heading angle of zero degrees is considered, there will not be any uptilt or skew angle in the mean flow. The settings listed below are shared between each simulation. The meteorological boundary conditions, however, differ between DLC.

```
--------Turbine/Model Specifications-----------------------
47            NumGrid_Z     - Vertical grid-point matrix dimension
47            NumGrid_Y     - Horizontal grid-point matrix dimension
0.05          TimeStep      - Time step [seconds]
1000          AnalysisTime  - Length of analysis time series [seconds]
"ALL"         UsableTime    - Usable length of output time series [seconds]
90.0          HubHt         - Hub height [m] (should be > 0.5*GridHeight)
157.5         GridHeight    - Grid height [m]
157.5         GridWidth     - Grid width [m] (should be >= 2*(RotorRadius+ShaftLength))
0             VFlowAng      - Vertical mean flow (uptilt) angle [degrees]
0             HFlowAng      - Horizontal mean flow (skew) angle [degrees]
```

Due to the offshore location of the wind turbine, turbulent wind field data is generated in compliance with the IEC standard 61400-3. The selected turbulence model is the IEC Kaimal spectrum, and turbulence class C is chosen for the wind turbine. For DLCs 1.2 and 1.6, the NTM is used, while DLCs 6.1 and 6.3 utilize the EWM with return periods of 50 years and 1 year, respectively. The hub height is utilised as reference height for the wind velocity, and default values are chosen for the power law exponent and surface roughness length, associated with the chosen `IEC_WindType`. For the NTM type, the power law exponent is 0.14, whereas it is 0.11 for the EWM type. In both cases, the surface roughness length is set to 0.03 m.

For DLCs 6.1 and 6.3, it was observed that by setting `IEC_WindType` to "EWM50" and "EWM1" for a class I turbine, the wind speeds from table 5.1 were automatically overridden with values of 50 m/s and 40 m/s, corresponding to return period of 50 years and 1 year, respectively. This behaviour originates from the fact that TurbSim uses standard values defined in the chosen IEC standard. To work with the actual extreme wind speeds derived from the Buchan Deep site measurement campaign, a workaround was implemented. Instead of using the EWM type, the NTM type was chosen, where the power law exponent is manually set to 0.11 (instead of using the default option), and the characteristic value of hub turbulence intensity was set manually by setting `IECturbc` to 11%. This workaround led to the same wind field characteristics of the EWM, except for the mean wind speed, which is now equal to the values defined in table 5.1 for the reference height. Lastly, it should be noted that the wind seed is selected using a pseudo-random generator, resulting in consistent wind fields across the different optimisation iterations. This deterministic feature enhances the robustness of the optimisation.

```
--------Meteorological Boundary Conditions-------------------
IECKAI        TurbModel     - Turbulence model
"3"           IECstandard   - Number of IEC 61400-x standard
C             IECturbc      - IEC turbulence characteristic
NTM           IEC_WindType  - IEC turbulence type
default       WindProfileType - Velocity profile type
90.0          RefHt         - Height of the reference velocity (URef) [m]
11.0          URef          - Mean (total) velocity at the reference height [m/s]
default       PLExp         - Power law exponent [-] (or "default")
default       Z0            - Surface roughness length [m] (or "default")
```

5.4.3. ElastoDyn

The ElastoDyn module is OpenFAST's backbone for conducting aero-hydro-servo-elastic analyses. In the ElastoDyn input file, the degrees of freedom govern the flexibility characteristics of various components of the FOWT. For example, by setting `FlapDOF1`, `FlapDOF2` and `EdgeDOF` to "False", the rotor blades are modelled as rigid blades, thus neglecting any deflections caused by aerodynamic forces acting on the blades. As for the platform degrees of freedom, setting any of them to "False" restricts motion along that particular direction. To maintain a high level of fidelity in the optimisation problem for this project, most of these DOFs are set to "True", except for the drivetrain rotational flexibility DOF. It was observed that enabling this particular DOF led in some cases to numerical instabilities during the OpenFAST simulation, although the exact reasons remain uncertain to the author. Given that drivetrain rotational flexibility is not expected to significantly impact floater motion or wind turbine performance, it was deactivated in the simulation. Another exception exists for DLCs 6.1 and 6.3, during which the FOWT is simulated in parked mode with misaligned yaw. To prevent the rotor from spinning, and to maintain a fixed yaw angle, both `GenDOF` and `YawDOF` are set to "False".

```
--------------------- DEGREES OF FREEDOM --------------------------------------
True          FlapDOF1      - First flapwise blade mode DOF
True          FlapDOF2      - Second flapwise blade mode DOF
True          EdgeDOF       - First edgewise blade mode DOF
False         TeetDOF       - Rotor-teeter DOF [unused for 3 blades]
False         DrTrDOF       - Drivetrain rotational-flexibility DOF
True          GenDOF        - Generator DOF
True          YawDOF        - Yaw DOF
True          TwFADOF1      - First fore-aft tower bending-mode DOF
True          TwFADOF2      - Second fore-aft tower bending-mode DOF
True          TwSSDOF1      - First side-to-side tower bending-mode DOF
True          TwSSDOF2      - Second side-to-side tower bending-mode DOF
True          PtfmSgDOF     - Platform horizontal surge translation DOF
True          PtfmSwDOF     - Platform horizontal sway translation DOF
True          PtfmHvDOF     - Platform vertical heave translation DOF
True          PtfmRDOF      - Platform roll tilt rotation DOF
True          PtfmPDOF      - Platform pitch tilt rotation DOF
True          PtfmYDOF      - Platform yaw rotation DOF
```

The ElastoDyn input file also defines the initial conditions for the simulation. During the simulation setup, it became evident that selecting appropriate initial conditions was paramount in order to prevent the occurrence of early-stage numerical instabilities. It was observed that inadequate initial conditions often led to high component deflections, violations of small angle approximations and negative damping, causing the simulation to abort prematurely. It should be pointed out that, on the one hand, it is unfeasible to tailor the initial conditions for each DLC, because the optimiser will generate floating platforms with varying geometries anyway, which in turn require new sets of initial conditions. On the other hand, there is no universally applicable solution. Nonetheless, by experimenting with different values, a set of initial conditions was identified that proved effective across all floating platform designs, provided that sufficient transient time is used to let the initial transients dampen out.

The set of initial conditions below is applied to DLCs 1.2 and 1.6 where the wind speed is below U_{rated}. Beyond the rated wind speed, the rotor speed is set to 12.1 rpm, and the initial (collective) blade pitch angle is set to 20 degrees. Concerning DLCs 6.1 and 6.3, additional changes are made to the input file. In the extreme wind speeds simulated during these storm cases, the rotor is parked, which requires the blades to be feathered to 90 degrees, and the rotor speed to be initialised at 0 rpm. Because a yaw misalignment angle is modelled in both cases, an initial or fixed nacelle-yaw angle is set as specified in table 5.1. Lastly, depending on the sign of this angle, an initial sway translational displacement of ± 5 m is set.

```
--------------------- INITIAL CONDITIONS ---------------------------------------
0             BlPitch(1)    - Blade 1 initial pitch (degrees)
0             BlPitch(2)    - Blade 2 initial pitch (degrees)
0             BlPitch(3)    - Blade 3 initial pitch (degrees) [unused for 2 blades]
9             RotSpeed      - Initial or fixed rotor speed (rpm)
0             NacYaw        - Initial or fixed nacelle-yaw angle (degrees)
5.0           PtfmSurge     - Initial surge translational displacement of platform (meters)
0             PtfmSway      - Initial sway translational displacement of platform (meters)
0             PtfmHeave     - Initial vertical heave translational displacement of platform (meters)
0             PtfmRoll      - Initial roll tilt rotational displacement of platform (degrees)
2.0           PtfmPitch     - Initial pitch tilt rotational displacement of platform (degrees)
0             PtfmYaw       - Initial yaw rotational displacement of platform (degrees)
```

In the turbine configuration section of the ElastoDyn file, the height of the tower and tower base are specified. The latter should coincide with the interface node in the SubDyn file, because it is cantilevered to the platform at this location. This means, that the parameter `TowerBsHt` should be updated in case a change in the platform geometry causes the platform to be positioned higher relative to the waterline. It is noteworthy that for this project both platform draft and platform height are kept constant by adjusting the ballast mass to changes in buoyancy, therefore the turbine configuration as given below will not change throughout the optimisation process. Lastly, the relative distances to the platform centre of mass are set to zero, as these will be calculated within the SubDyn module.

```
--------------------- TURBINE CONFIGURATION ------------------------------------
87.6          TowerHt       - Height of tower above MSL (meters)
10.0          TowerBsHt     - Height of tower base above MSL (meters)
0             PtfmCMxt      - Downwind distance from MSL (meters)
0             PtfmCMyt      - Lateral distance from MSL (meters)
0             PtfmCMzt      - Vertical distance from MSL (meters)
0             PtfmRefzt     - Vertical distance from MSL (meters)
```

Similarly, the platform mass and platform roll-, pitch- and yaw inertia are zeroed, to prevent double accounting in both ElastoDyn and SubDyn. An exception is made for the platform yaw inertia. Since ElastoDyn does not currently consider the rotational inertia of the undeflected tower about its centreline [35], setting the `PtfmYIner` to match the tower's rotational inertia serves to avoid possible division-by-zero errors when `PtfmYDOF` is enabled. Calculation of the tower mass moment of inertia about its centreline is rather straightforward, and by integration over the different tower sections in the *ElastoDyn_Tower.dat* file, the tower rotational inertia is calculated as $1.638\,89 \times 10^{6}\,\mathrm{kg\,m^{2}}$

```
--------------------- MASS AND INERTIA -----------------------------------------
0             PtfmMass      - Platform mass (kg)
0             PtfmRIner     - Platform inertia for roll tilt rotation about the platform CM (kg m^2)
0             PtfmPIner     - Platform inertia for pitch tilt rotation about the platform CM (kg m^2)
1638890.0     PtfmYIner     - Platform inertia for yaw rotation about the platform CM (kg m^2)
```

5.4.4. SubDyn

The structural characteristics of the floating platform are defined within the SubDyn module, which has recently been updated with new capabilities to model sub-structural flexibility and member-level loads, including the possibility to model the structural dynamics of floating platforms [45]. Because at the time of writing, no floating substructure model was available in the public domain yet, the semi-submersible platform model had to be built from scratch. This was achieved by closely adhering to the platform definitions provided in the report [15], and evaluating its response against the reference model in OpenFAST. Furthermore, in some cases guidance was provided by experts from NREL.

Firstly, the simulation control settings were chosen as follows. Firstly, the local integration step is set to the global time step. Following guidance from developers[2], the Adams-Bashforth-Moulton 4th-order explicit predictor-corrector (ABM4) integration method was utilised, as it provides the best numerical stability in SubDyn. Hence `IntMethod` is set to 3. Furthermore, `SttcSolve` is enabled in order to employ the static improvement method described in section 2.2. Lastly, the `GuyanLoadCorrection` is activated to ensure that the FEM representation is expressed within the rotating frame of reference of the floating platform. Furthermore, by enabling the Guyan load correction, the added moment resulting from the lever arm created by the Guyan deflection of the structure is considered, as outlined in section 2.2. The simulation control settings are summarised below.

```
------------------------- SIMULATION CONTROL ---------------------------------
"DEFAULT"     SDdeltaT      - Local Integration Step. If "default", the glue-code step will be used.
3             IntMethod     - Integration Method [1/2/3/4 = RK4/AB4/ABM4/AM2].
True          SttcSolve     - Solve dynamics about static equilibrium point
True          GuyanLoadCorrection - Include extra moment from lever arm at interface
                                    and rotate FEM for floating.
```

As for the structural analysis model, the FEM model will be employed with 2-node Timoshenko beam elements, by setting `FEMMod` to 3. Then, the structural model can be further discretised by setting `NDiv`. This parameter uniformly divides all structural members into the entered number of sub-elements. After experimenting with various values for this parameter, it was observed that the required CPU time increased considerably as the number of sub–elements increased. To expedite the optimisation process, the structural members as entered in the SubDyn input file were not further discretised, therefore keeping the number of sub-elements per member at 1. The Craig-Bampton formulation is utilised to reduce the size of the finite element model while retaining essential dynamic characteristics.

The `NModes` parameter specifies the number of internal modes to retain. To model substructure flexibility, the number of modes should be large enough to capture the predominant platform modes, generally up frequencies of 5 to 10 Hz. Since the exact structural frequencies are unknown before executing the simulation, it is often necessary to experiment with the number of modes. However, based on guidance from developers, this number is typically less than 10 or 20 modes for most floating platforms.

By zeroing this parameter, the Guyan Reduction is applied, and only the rigid body motions of the platform are simulated. Although it would be interesting to account for deformation of the platform, the choice for zero internal modes reduces the computational overhead, making the optimisation problem in this project more manageable. Although it is expected that flexibility of the structural members will have an impact on their sizing (especially for the slender pontoons and cross-braces), the approach is suitable for studying the overall dynamic response of the FOWT.

The parameter `JDampings` determines the damping ratios for the flexible modes. A single value can be given for all retained modes, or individual values can be specified. The damping ratios should be tuned to match known full-system damping ratios. If these values are unknown, a value of 1 serves as a reasonable approximation. Lastly, Guyan damping is disabled for the floating platform model. The FEM settings for the SubDyn module are summarised below.

```
-------------------- FEA and CRAIG-BAMPTON PARAMETERS--------------------------
3             FEMMod        - FEM switch: element model in the FEM. [3= 2-node Timoshenko]
1             NDiv          - Number of sub-elements per member
True          CBMod         - [T/F] If True perform C-B reduction, else full FEM dofs will be retained.
0             Nmodes        - Number of internal modes to retain. If Nmodes=0 --> Guyan Reduction.
1             JDampings     - Damping Ratios for each retained mode (% of critical)
0             GuyanDampMod  - Guyan damping {0=none, 1=Rayleigh Damping, 2=user specified 6x6 matrix}
```

Modelling of the physical components in SubDyn is done in the subsequent sections of the input file, by defining structure joints, members who are connected by the joints, cross-sectional properties of the members, etc. The complete SubDyn input file for the initial design is provided in appendix A. The platform's structure is shaped by the connections between the joints, while its size is determined by the (x, y, z) coordinates of the joints and the cross-sectional dimensions of the connecting members. A visualisation of the joints and the connecting members is provided in figure 5.3.

Based on the offset radius R_{offset}, platform draft, and diameter D and height H of the members, the joint coordinates are calculated and added to the corresponding table in the input file. Besides their coordinates,

---

[2] `https://github.com/OpenFAST/openfast/discussions/801#discussioncomment-1139658`

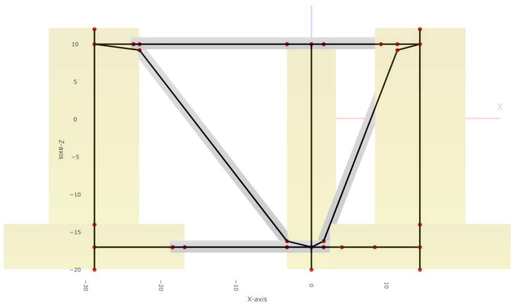

Figure 5.3: 2-D side view of the DeepCWind semi-submersible platform design, where the structural joints (red markers) and the connecting members (black lines) depict how the platform's topology and dimensions are defined within SubDyn

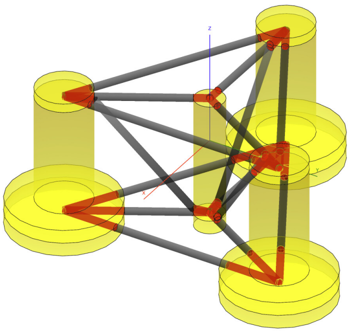

Figure 5.4: 3-D representation of the DeepCWind semi-submersible platform design, showing the virtual members in red, which serve as rigid links with negligible mass between the large-volume columns and the pontoons/braces.

each joint has a unique identifier. Additionally, the joint types must be specified, establishing the boundary conditions or constraints for all the members connected to the joints. In order to ensure the structural rigidity of the floating platform, all joints are set to type 1 (cantilever).

The connection between the FOWT substructure and the tower (or transition piece) is determined by the interface joints. At the uppermost joint of the main column, the tower is rigidly connected to the substructure. In situations involving a bottom-fixed substructure, the connection between the structure and the seabed is established by defining base reaction joints. However, in this project there are none, and SubDyn conveniently considers the structure to be floating in the absence of reaction nodes.

After fixing the joint coordinates, the next step involves the interconnection of these joints using members. Each member is associated with a pair of start and end joints, and can be discretised with additional nodes by subdividing each element with the `NDiv` parameter mentioned previously. Similar to the joints, each member is assigned a unique identifier. In the model created for this project, two member types are distinguished. The main components of the substructure model are cylindrical beam elements (`MType` = 1) with physical properties defined by the `MPropSet` parameters. They are the physical members of the platform.

In SubDyn, the member connections are represented through the centrelines of the cylindrical beams. In order to stay true to the original design, additional joints must be introduced into the structure, ensuring the accurate placement of the component endpoints (see figure 5.3). To ensure the establishment of an effective load path between all the beam elements, new connections should be made between the newly added joints. To prevent additional mass from being introduced to the system due to member overlap (a limitation inherent in SubDyn) the connectivity between the beam elements is addressed by introducing rigid links (`MType` = 3). These rigid links have negligible mass, and establish a link of high stiffness, so as to directly transmit loads between two (elastic) beam elements. The rigid links (in this project sometimes also referred to as virtual members) are visualised in figure 5.4.

The member properties are defined separately for the beam elements and the rigid links. Regarding the beam elements, four distinct member types correspond to the main column, upper columns, base columns and the pontoons/braces, in accordance with the values provided in table 5.3. As for the rigid links, they have a uniform mass of 1 $\mathrm{kg\,m^{-1}}$, to simulate any added mass associated with the beam connections.

Lastly, because the beam elements are hollow cylindrical elements without end caps, the mass- and inertia contribution of the column top- and bottom caps must be modelled separately, which is done in the "Joint Additional Concentrated Masses" section of the SubDyn input file. A visual representation of these cylinder caps is provided in figure 5.5. Based on this figure, and the values from table 5.3, the mass and inertia corresponding to each cylinder cap can be derived. The values are summarised in table 5.5. These mass- and inertia values are lumped to each structure joint corresponding to the cylinder endpoint.

In the last section of the SubDyn file, the member output channels are defined. In the input file in appendix A, the static force and moment components in the local x-, y-, and z-direction at the start and endpoints of the upper- and base column members are requested as output channels.

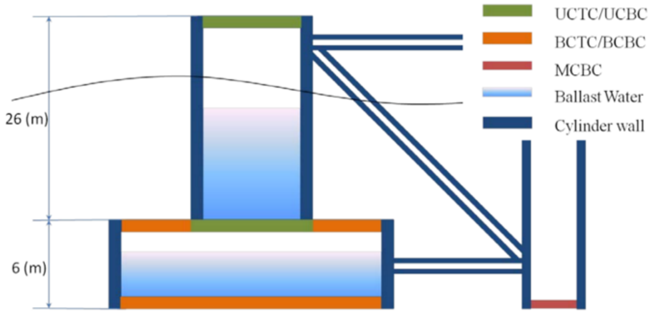

Figure 5.5: Side view of the platform's cylindrical walls and caps [15]

Table 5.5: Mass and inertia values about the principal axes of the cylinder caps.

Name	Abbreviated	Mass (kg)	I_{xx} (kgm^2)	I_{yy} (kgm^2)	I_{zz} (kgm^2)
Main Column Bottom Cap	MCBC	7.671e+03	1.988e+04	1.988e+04	3.977e+04
Upper Column Top Cap	UCTC	5.221e+04	4.605e+05	4.605e+05	9.211e+05
Upper Column Bottom Cap	UCBC	5.327e+04	4.794e+05	4.794e+05	9.588e+05
Base Column Top Cap	BCTC	1.577e+05	7.039e+06	7.039e+06	1.408e+07
Base Column Bottom Cap	BCBC	2.110e+05	7.518e+06	7.518e+06	1.504e+07

5.4.5. HydroDyn

The hydrodynamics module of OpenFAST is employed to simulate the coupled response of the platform to dynamic effects caused by the wind turbine at the tower base, as well as to hydrodynamic loads resulting from currents and wave excitation. The HydroDyn module can be exploited for the generation of regular (periodic) or irregular (stochastic) waves, and comes with many options for modelling sea states, including different wave spectra, and the possibility to model second-order waves through time-domain calculations of sum- and difference-frequency terms. The waves act on the substructure as excitation forces, and as introduced in chapter 4 already, HydroDyn offers three different methods for calculating hydrodynamic loads on the structure [35]:

- **Potential Flow Theory:** this is the preferred method for large substructures, whose members are large in comparison to the wavelength. The potential flow solution involves the transformation of frequency-dependent hydrodynamic coefficients into the time domain, which, in this project, is provided by the frequency-domain panel code NEMOH during a pre-processing step. The potential flow solution includes the linear hydrostatic restoring matrix, added mass and radiation damping, and incident wave excitation from first- and second-order diffraction [35].
- **Strip Theory:** this option is most suitable for structures with members that are small compared to the wavelength. Through the application of strip theory, hydrodynamic loads are calculated directly from the undisturbed wave (and if applicable: current-) kinematics at the substructure's undisplaced position [35]. The strip theory approach requires the user to enter specific coefficients for dynamic pressure, added mass and viscous drag. Then, Morison's equation is applied to account for the effects of distributed fluid-inertia, added mass and viscous drag components, along with distributed loads due to static buoyancy. The strip theory formulation in HydroDyn also allows the user to model the effects of flooding or ballasting, or marine growth.
- **Hybrid Combination:** in setting up the HydroDyn file, the user has the option to specify for each member whether its contribution to the hydrodynamic response of the platform is modelled using potential flow theory or strip theory.

In summary, the choice of which model to use depends on the outer dimensions of the structural members that are considered. Given the platform's varying member sizes, the hybrid combination is selected as the preferred method for this project. The following paragraphs will provide an overview of the HydroDyn module setup by exploring various sections of the input file.

```
--------------------- WAVES -----------------------------------------------
2             WaveMod       - Incident wave kinematics model
                              {2: JONSWAP/Pierson-Moskowitz spectrum (irregular)} (switch)
4600          WaveTMax      - Analysis time for incident wave calculations (sec)
0.2           WaveDT        - Time step for incident wave calculations (sec)
1.8           WaveHs        - Significant wave height of incident waves (meters)
7.7           WaveTp        - Peak-spectral period of incident waves (sec)
1.44          WavePkShp     - Peak-shape parameter of incident wave spectrum (-)
0.314159      WvLowCOff     - Low cut-off frequency of the wave spectrum (rad/s)
1.570796      WvHiCOff      - High cut-off frequency of the wave spectrum (rad/s)
0.0           WaveDir       - Incident wave propagation heading direction (degrees)
0             WaveDirMod    - Directional spreading function {0: none, 1: COS2S} (-)
```

The first aspects to discuss are related to generation of the wave input signals. As introduced in section 5.1, irregular waves are modelled using the JONSWAP frequency spectrum. The time series of the incident waves is derived from the inverse Fast Fourier Transform (FFT). Two important factors that affect the resolution of the resulting time series are the parameters `WaveTMax`, which determines the duration of the incident wave kinematics time series, and `WaveDT`, which sets both its time step, and the maximum frequency in the inverse FFT. Setting these parameters to 4600 s and 0.2 s respectively, ensures adequate resolution for the wave spectrum and kinematics [35]. The parameters `WaveHs`, `WaveTp` and `WavePkShp` are DLC specific, and therefore vary for each simulation as specified in table 5.1. It is noteworthy, that if a Pierson-Moskowitz wave spectrum is desired, one would have to set the wave peak-shape parameter to a value of 1. The lower and upper boundaries of the first-order frequency spectrum are governed by the parameters `WvLowCOff` and `WvHiCOff`. Outside this range, the wave component amplitudes are zeroed. On the one hand, this ensures efficient use computational resources, and on the other hand, it avoids non-physical effects in the strip theory solution at high frequencies. Lastly, the parameters `WaveDir` and `WaveDirMod` are zeroed to generate a long-crested sea state propagating in the positive X-direction, without directional spreading. The first-order wave parameters are summarised above.

Second-order contributions to the incident wave kinematics are specified in the next section of the HydroDyn input file, by setting `WvDiffQTF` and `WvSumQTF` to "True", enabling the full difference- and sum-frequency QTFs, respectively. This setting only affects members for which hydrodynamic loads are calculated using strip theory, as second order forces are activated separately for the potential flow model. Similarly to the cut-off frequencies of the first-order waves, appropriate settings for `WvHiCOffD`, `WvLowCOffS`, `WvLowCOffS` are chosen to minimise computational overhead. An exception is for `WvLowCOffD`, which is advised to set to zero, in order to prevent the mean-drift term from being eliminated [35]. The parameters are summarised below.

```
--------------------- 2ND-ORDER WAVES -----------------------------------------
False         WvDiffQTF     - Full difference-frequency 2nd-order wave kinematics (flag)
False         WvSumQTF      - Full summation-frequency 2nd-order wave kinematics (flag)
0             WvLowCOffD    - Low frequency cutoff used in the difference-frequencies (rad/s)
1.256637      WvHiCOffD     - High frequency cutoff used in the difference-frequencies (rad/s)
0.618319      WvLowCOffS    - Low frequency cutoff used in the summation-frequencies (rad/s)
3.141593      WvHiCOffS     - High frequency cutoff used in the summation-frequencies (rad/s)
```

The floating platform section within the HydroDyn input file relates to the potential flow model. Because the large-volume columns are modelled with NEMOH, the potential-flow model is enabled by setting `PotMod` to 1. Because state space models are not considered in this project, the wave-excitation model is based on Discrete Fourier Transform (DFT), and the radiation memory effect model is based on convolution. The accuracy of the radiation memory effect is influenced by the parameter `RdtnTMax`, which governs for how long the effect is tracked. According to the modelling guidelines, a value of 60 s is enough. Furthermore, the time step used for the radiation calculations is set by `RdtnDT`, which must be set equal to the global OpenFAST time step. The potential flow model consists of a single body, hence the `NBody` parameter is set to 1. Furthermore, as mentioned previously in section 4.2.2, the characteristic body length scale used in the NEMOH model and conversion to WAMIT files is 1.

Although the submerged volume of the platform is computed directly by NEMOH, this value is not entered in the HydroDyn setup directly, as it is underestimated due to the coarse azimuthal discretisation. Instead, the displaced water volume is calculated analytically from physical member dimensions in a pre-processing step. For the potential flow body, the value of `PtfmVol0` approximates to 13 557 m^3 in its undisplaced position.

Lastly, since no offset is applied to the representation of the body reference point or the centre of buoyancy, all other parameters within the floating platform section are set to zero.

```
---------------------- FLOATING PLATFORM ---------------------------------------
1             PotMod        - Potential-flow model
                              {1: frequency-to-time-domain transforms based on WAMIT output} (switch)
1             ExctnMod      - Wave-excitation model {1: DFT} (switch)
1             RdtnMod       - Radiation memory-effect model {1: convolution} (switch)
60            RdtnTMax      - Analysis time for wave radiation kernel calculations (sec)
0.0125        RdtnDT        - Time step for wave radiation kernel calculations (sec)
1             NBody         - Number of WAMIT bodies to be used (-)
1             WAMITULEN     - Characteristic body length scale to redimensionalize WAMIT output (meters)
0.0           PtfmRefxt     - The xt offset of the body reference point(s) from (0,0,0) (meters)
0.0           PtfmRefyt     - The yt offset of the body reference point(s) from (0,0,0) (meters)
0.0           PtfmRefzt     - The zt offset of the body reference point(s) from (0,0,0) (meters)
0.0           PtfmRefztRot  - The rotation about zt of the body reference frame(s) from xt/yt (degrees)
13556.76      PtfmVol0      - Displaced water volume when the body is in its undisplaced position (m^3)
0.0           PtfmCOBxt     - The xt offset of the centre of buoyancy (COB) from (0,0) (meters)
0.0           PtfmCOByt     - The yt offset of the centre of buoyancy (COB) from (0,0) (meters)
```

As mentioned before, the second-order wave forces are activated separately for the potential flow body. This is done in the following section in the HydroDyn input file. Of the options `MnDrift`, `NewmanApp` and `DiffQTF`, only one can be enabled. Given that the difference- and sum-frequencies are computed using NEMOH and subsequently converted into the WAMIT output file format, the second order floating platform forces are activated by specifying the corresponding WAMIT file within the input section of HydroDyn.

```
---------------------- 2ND-ORDER FLOATING PLATFORM FORCES ----------------------
0             MnDrift       - Mean-drift 2nd-order forces computed {0: None}
0             NewmanApp     - Mean- and slow-drift 2nd-order forces computed with Newman’s approximation
                              {0: None}
12            DiffQTF       - Full difference-frequency 2nd-order forces computed with full QTF
                              {0: None; [10, 11, or 12]: WAMIT file to use}
                              [Only one of MnDrift, NewmanApp, or DiffQTF can be non-zero]
12            SumQTF        - Full summation -frequency 2nd-order forces computed with full QTF
                              {0: None; [10, 11, or 12]: WAMIT file to use}
```

On top of the hydrodynamic terms computed by HydroDyn in the potential flow- and strip theory solutions, additional loads on the platform can be generated using 6-DOF vectors and matrices in the "platform additional stiffness and damping" section of the HydroDyn input file. This becomes necessary in certain situations to account for effects that are not adequately represented by the used modelling approaches. When modelling potential flow members, for instance, the viscous drag contribution due to flow separation is neglected, as the potential flow method is based on the assumption of inviscid flow. Similarly, in the case of strip theory, hydrostatic restoring coefficients should be introduced as additional linear stiffness to enhance the accuracy of the platform's response. The additional forces are accounted for in HydroDyn through the following equation:

$$\mathbf{F}_{\mathrm{Add}} = \mathbf{F}_0 - \mathbf{C}\mathbf{q} - \mathbf{B}\mathbf{q} - \mathbf{B}_{\mathrm{quad}} \|\dot{\mathbf{q}}\| \dot{\mathbf{q}} \tag{5.11}$$

where $\mathbf{F}_0$ corresponds to the `AddF0` vector for additional pre-loading, **C** points to the `AddCLin` matrix for additional linear stiffness, **B** refers to the additional damping matrix `AddBLin`, and $\mathbf{B}_{\mathrm{quad}}$ is the additional quadratic drag matrix, which corresponds to `AddBQuad`. Lastly, **q** denotes the displacement vector of the potential flow body reference point, in all 6 translational and rotational directions.

In the process of setting up of the HydroDyn module, the hydrostatic restoring matrix is calculated for the strip theory members. This is necessary because of an inherent limitation of the strip theory where substructure buoyancy is only computed for the undisplaced position, and not recomputed after the platform has displaced.

Although the addition of quadratic damping would be needed to represent the real system accurately, the methods for determining the matrix coefficients as suggested in [15] are not feasible in the context of an optimisation problem. Consequently, the viscous effects acting on the large-volume columns are not considered in the additional linear- and quadratic damping matrices. It should be noted, however, that these effects are not entirely disregarded. The damping effect of the heave plates is addressed by introducing an axial drag coefficient at the bottom nodes of the base columns. This will be further explained in the subsequent paragraphs.

Now, the coefficients for the additional linear stiffness matrix are computed using equation 5.12 below. Its derivation is provided in appendix B.

$$\texttt{AddCLin} = \begin{bmatrix} 0 & 0 & 0 & 0 & 0 & 0 \\ 0 & 0 & 0 & 0 & 0 & 0 \\ 0 & 0 & \rho g A_0 & 0 & 0 & 0 \\ 0 & 0 & 0 & \rho g \iint_{A_0} y^2 dA + \rho g V_0 z_b & 0 & 0 \\ 0 & 0 & 0 & 0 & \rho g \iint_{A_0} x^2 dA + \rho g V_0 z_b & 0 \\ 0 & 0 & 0 & 0 & 0 & 0 \end{bmatrix} \tag{5.12}$$

where A_0 is the undisplaced waterplane area of all strip-theory members combined (m^2), V_0 is the undisplaced volume of all strip-theory members combined (m^3), and z_b is the vertical coordinate of the centre of buoyancy of the undisplaced structure composed by all strip-theory members (m).

Because the floating platform comprises members of simple geometry, analytic calculation of the remaining terms is straightforward. The resulting matrix coefficients are $76.6 \times 10^3\,\mathrm{N\,m^{-1}}$ for heave, and $-41.371 \times 10^6\,\mathrm{N\,m\,rad^{-1}}$ for roll and pitch.

In the member and joints sections, the platform geometry in HydroDyn is specified similarly to SubDyn, with one significant difference. In HydroDyn, the primary purpose of geometry specification is to provide accurate inner and outer dimensions for computing hydrodynamic loads, rather than to establish connectivity between members. Since HydroDyn primarily simulates external loads and not internal loads, there is no requirement for a continuous connection between all the individual members. In that regard, the virtual members that were present for the structural representation, have been left out of the HydroDyn file. A notable difference with SubDyn in the member definition, is that there are additional columns: one to specify whether the member is included in the NEMOH potential flow model or that it has to be represented in the strip theory solution (`PropPot`); one that points to which table is used for the member-based coefficients (`MCoefMod`), and one that determines the dimension used in discretising the member for the strip theory method (`MDivSize`). The members and joints defined for the hydrodynamic model can be found in the HydroDyn input file in appendix A.

The strip theory solution of HydroDyn consists of hydrodynamic contributions from viscous drag, added mass, fluid inertia and static pressure loads, which are all lumped to the member joints. The coefficients involved with calculating the hydrodynamic loads are defined in the axial coefficients table of the input file. `AxCd` represents the viscous drag coefficients, while `AxCp` denotes the dynamic pressure coefficient. The added mass and fluid inertia loads are both captured in the `AxCa` parameter. While the latter two parameters are exclusive to the strip theory method, the axial viscous drag loads are calculated for all designated member joints, including those belonging to potential flow members. In this model, the primary purpose of the axial coefficients is to simulate the damping effect of the heave plates. In this regard, an axial viscous drag coefficient of 9.6 has been applied at the bottom joints of the three base columns.

The hydrodynamic coefficients in the transverse direction are specified in the member-based hydrodynamic coefficients. The same drag coefficients are used for all the strip theory members, which are assigned a value of 0.63. All other coefficients in this table are set to 0, in accordance with the reference DeepCWind model.

As the contribution of marine growth is not considered in this project, the final section of the input file to discuss concerns the ballasting and flooding of the columns. The six members subject to water ballast are the upper columns and base columns. Their unique identifiers are entered in the filled-member groups table in the HydroDyn input file, along with the ballast depth (z-location) and density. Since sea water is used as the ballast material, a fill density of $1025\,\mathrm{kg\,m^{-3}}$ is utilised.

5.4.6. MoorDyn

The mooring system in OpenFAST can be represented in five different ways. The simplest approach involves adding linear stiffness into the hydrodynamic model DOFs to account for the mooring system's restoring force. Alternatively, one of the following modules can be coupled with OpenFAST:

1. MAP++: A quasi-static, multi-segmented mooring line model;
2. FEAMooring: A non-linear, dynamic mooring model based on the elastic rod model;
3. MoorDyn: A dynamic mooring model utilising a lumped-mass approach;
4. OrcaFlex: A commercial software package designed for high-fidelity mooring analysis.

Among these possibilities, MoorDyn was chosen as it offered the best trade-off between accuracy and computational efficiency. Given the project's primary focus on the floating platform itself, rather than the mooring system, only a brief overview of the mooring setup will be provided. However, it is important to note that modifications to the platform geometry inevitably lead to corresponding adjustments in the positions of the fairleads and anchor points in the MoorDyn file. The fairlead points are positioned on the platform's outermost radial points, extending along the Y-pontoons, on the top side of the base columns. The anchor points extend in the same direction, and are located on the seabed at a depth of 200 meters. The (x, y, z) coordinates of the mooring line attachment points are summarised below.

```
---------------------- POINTS ---------------------------------
ID     Attachment    X          Y         Z      M      V       CdA   CA
(-)    (-)         (m)        (m)       (m)    (kg)   (m^3)   (m^2)  (-)
1      Fixed     418.8      725.383   -200.0      0      0       0     0
2      Fixed    -837.6        0.0     -200.0      0      0       0     0
3      Fixed     418.8     -725.383   -200.0      0      0       0     0
4      Vessel     20.434     35.393     -14.0     0      0       0     0
5      Vessel    -40.868      0.0       -14.0     0      0       0     0
6      Vessel     20.434    -35.393     -14.0     0      0       0     0
```

6

Optimisation Workflow

The programming framework developed for this project comprises several Python scripts, each serving a distinct purpose and executed in a specific order. A flowchart of the model is provided in Figure 6.1. Yellow blocks represent Python scripts, named in accordance with the model's convention. Dark blue blocks signify external simulation tools integrated into the global model through Python interfaces. The NEMOH software is executed through the NEMOH wrapper script, responsible for pre- and post-processing of the BEM solution. OpenFAST simulations are executed using the runner script, handling the multiprocessing of various DLCs and monitoring the simulation's overall progress. OpenFAST input files, presented as grey blocks in the flowchart, are text files written and read by the pre-processing script. Along with the hydrodynamic database generated by NEMOH, these files serve as inputs to the OpenFAST simulation. The red block represents the OpenMDAO optimisation driver, responsible for executing the optimisation routine, evaluating the objective function and constraints, and adjusting the independent variables. The subsequent sections of this chapter will elaborate on the different modules and scripts comprising the optimisation workflow. The purpose and methods of *nemoh_wrapper* will not be further mentioned, as this has already been explained in detail in chapter 4.

6.1. Configuration and Initialisation

To create a model with a clear and user-friendly structure, two distinct scripts, with names beginning with the prefix "config_", have been created to establish the OpenFAST simulation settings and the configuration of the floating platform to be optimised. In the *config_simulation* script, settings are established for the different components involved in the NEMOH and OpenFAST simulation. The high-level settings encompass naming conventions for the folders and data structure, the number of cores available for parallel processing, and environmental parameters that are shared among the different model components. For NEMOH, the frequency range to be used for generation of the hydrodynamic database is given, and options are provided to enable or disable the effects of second order waves, calculation of hydrostatic parameters, etc. In addition, the metocean conditions are entered for each sea state and wind speed model, along with other parameters specific to each DLC, as detailed in table 5.1. Finally, the script configures input settings for the various OpenFAST modules, as described in chapter 5.

The ensemble of these settings is passed to the *initialise_openFAST* script, which generates the directories and file structure for parallel simulation of the OpenFAST model for the specified DLCs. The input files are generated by writing the settings to template files, and saved to dedicated folders for each load case using an appropriate naming convention. The load case folders are in turn grouped by the iteration number, which is particularly convenient when the simulation is conducted within the optimisation routine. In the initialisation script, the binary output files containing the turbulent wind fields are also generated, and stored in a separate, common folder. Because the input data for the optimisation should be deterministic, the wind fields utilised in the OpenFAST simulation remain consistent for each iteration and do not need to be regenerated.

The initialisation of the floating platform geometry is performed in the *config_floater* script. To streamline the process of adjusting the platform geometry, an object-oriented approach is adopted. In this approach, an instance is created of the semi-submersible substructure, with its geometrical design variables as main

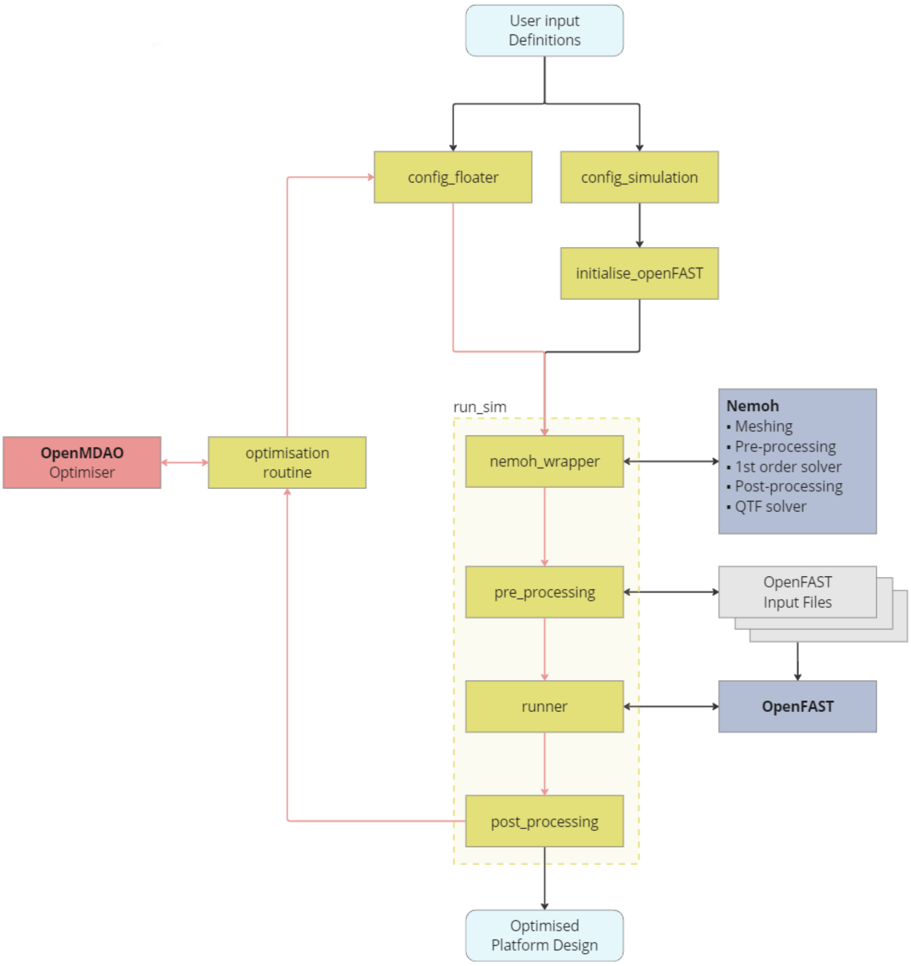

Figure 6.1: Global flowchart of the programming framework.

attributes. The design variables, as listed in table 5.3, are entered upon initialisation of the class. The resulting class object, hereafter referred to as the "floater object", incorporates methods for reformatting these design variables, in preparation to pre-processing of the NEMOH and OpenFAST simulations. Regarding the NEMOH model, this includes setting the azimuthal discretisation and target number of panels used for generating the hydrodynamic mesh for NEMOH, and specification of the radial and z-coordinates of the different potential flow components. As for the OpenFAST model, it entails generation of the structure joints in the global reference frame, definition of the member connections and performing preliminary calculations of physical properties of the platform, following directly from the platform design variables. Generation of the joints, as introduced in section 5.4.4, is an automated process, where the joint (x, y, z) coordinates are derived directly from the design variables. The member connections, however, are set up manually in the configuration script, and remain unaltered throughout the optimisation process.

6.2. Pre-Processing

The pre-processing methods are different based on whether the substructure is modelled within SubDyn or as a rigid body in ElastoDyn.

6.2.1. SubDyn-Based Substructure Model

The main purpose of the pre-processing script is to prepare the input files to the OpenFAST simulation, by writing the geometric representation of the platform to the relevant sections of the text files, thereby incorporating any changes that have been made to the platform geometry. This process necessitates a series of calculations, as adjustments to the platform design have a cascading impact. In the first place, a change in the platform dimensions requires regeneration of both the structural- and hydrodynamic joint locations. This process has been integrated within the *config_simulation* script as a class method of the floater object, which is called from the pre-processing script. Besides the member joints, the member properties are updated, and for the SubDyn formulation the mass and inertia of the cylinder caps in the joint additional masses section are recomputed.

As for HydroDyn, the pre-processing methods are slightly more sophisticated. The submerged platform volume parameter, specific to the potential flow model, is calculated analytically from the member representation, instead of relying on the output of the NEMOH model. This was necessary because the NEMOH model underestimates the submerged platform when the azimuthal discretisation is too coarse. Underestimating the displaced water volume of the platform quickly leads to considerable impact on the neutral stability of the platform. Furthermore, in the pre-processing step, the hydrostatic restoring coefficients for the strip theory members from equation 5.12 are recalculated.

In addition, the ballast must be recomputed for HydroDyn in response to a change in the platform mass. This is necessary as a result of the decision to keep the platform draft constant. If the platform mass changes while the ballast mass remains constant, the actual draft will inevitably change as the platform sinks deeper below the waterline. The change in draft needs to be incorporated into the member joint definition. Neglecting this would result in a difference between the undisplaced position, around which the HydroDyn model is defined, and the static equilibrium position in the heave direction, deteriorating solution accuracy. Not to mention that a new equilibrium positions affects the hub height, requiring additional adjustments to be made to the wind inflow files, the turbine representation in AeroDyn and ElastoDyn, etc. The ballast is featured in the hydrostatic equilibrium equation:

$$F_{\text{buoyant}} = F_{\text{weight}} + F_{\text{mooring}} \tag{6.1}$$

$$\rho g V_0 = (m_{\text{steel}} + m_{\text{ballast}})\, g + F_{\text{mooring}} \tag{6.2}$$

where F_{buoyant} is the buoyant force of the floating platform (N), resulting from the displaced water volume, F_{weight} is the total platform weight (N), including the structural mass of the platform and the water ballast, and F_{mooring} is the vertical mooring pre-tension (N) caused by the weight of the mooring line (the part that is not resting on the seabed) exerting a downward force on the platform. As the mooring system remains unchanged in the optimisation problem, the mooring pre-tension remains constant. Its value is computed using the relation described in equation 6.1, substituting known values for the DeepCWind platform. This calculation yields a mooring pre-tension of 1.8625×10^6 N.

Now, the ballast mass is governed by the platform design variables $z_{\text{ballast,UC}}$ and $z_{\text{ballast,BC}}$, which specify the depth to which the columns are filled with water, as illustrated in figure 5.2. These values are recomputed in a subroutine that optimises them, in order to come to a total ballast mass that satisfies the hydrostatic equilibrium equation. The definition of the optimisation subroutine is as follows:

$$\begin{aligned}
\text{minimize} \quad & \left|F_{\text{weight}}(Z) + F_{\text{mooring}} - F_{\text{buoyant}}\right| \\
\text{w.r.t.} \quad & Z = \begin{bmatrix} z_{\text{ballast,UC}} \\ z_{\text{ballast,BC}} \end{bmatrix} \\
\text{subject to} \quad & z^{\text{lb}}_{\text{ballast,UC}} \leq z_{\text{ballast,UC}} \leq z^{\text{ub}}_{\text{ballast,UC}} \\
& z^{\text{lb}}_{\text{ballast,BC}} \leq z_{\text{ballast,BC}} \leq z^{\text{ub}}_{\text{ballast,BC}} \\
\text{where} \quad & z^{\text{lb}}_{\text{ballast,UC}} = z_{\text{draft}} + H_{\text{BC}} + MDS \\
& z^{\text{ub}}_{\text{ballast,UC}} = z_{\text{draft}} + H_{\text{BC}} + H_{\text{UC}} - t_{\text{UC}} \\
& z^{\text{lb}}_{\text{ballast,BC}} = z_{\text{draft}} + t_{\text{BC}} + MDS \\
& z^{\text{ub}}_{\text{ballast,BC}} = z_{\text{draft}} + H_{\text{BC}} - t_{\text{BC}}
\end{aligned}$$

where the superscripts lb and ub correspond to the lower boundary and upper boundary, and z_{draft} is the z-location, in the global reference frame of the undisplaced platform, which corresponds to the platform's $Draft$ as provided in table 5.3. MDS corresponds to the parameter `MDivSize` in the members table of the HydroDyn file, governing the length of the sub-elements for discretised members. It is important to include this parameter in the constraints, because OpenFAST doesn't allow partial flooding/ballasting of a member if the first sub-element is not fully flooded/ballasted. Therefore, there should be either no ballast at all, or a minimum amount of ballast corresponding to the `MDivSize` parameter.

In practice, the formulation of this optimisation subroutine implies that the z-location of the ballast in both the upper and base columns is constrained within the physical boundaries of these components. The total ballast mass is then taken as the sum of the masses in each column, which can be calculated from the ballast density, the inner dimensions of the columns and the z-location of the ballast. To prioritise a low centre of mass, positively impacting platform stability, the initial z-values are chosen such that:

$$Z_0 = \begin{bmatrix} z^{\text{lb}}_{\text{ballast,UC}} \\ z^{\text{ub}}_{\text{ballast,BC}} \end{bmatrix}$$

which implies that the base column is completely filled, and the upper column is filled only up to the minimum height of MDS. The new z values are written to the "filled members" section in HydroDyn. Lastly, the attachment points of the mooring system need recomputing. As outlined in section 5.4.6, the fairlead coordinates coincide with the outermost radial point, on the top side of the base column, extending along the Y-pontoons. For the second column, which extends along the negative x-direction, the coordinates are:

$$\mathbf{r}_{\text{fairlead},2} = \begin{bmatrix} -\left(R_{\text{offset}} + \frac{1}{2}D_{\text{BC}}\right) \\ 0 \\ z_{\text{draft}} + H_{\text{BC}} \end{bmatrix}$$

The other two fairlead locations are then found by rotating these coordinates around the $z-$axis by $\pm 120°$ by means of a rotation matrix. In order for the mooring response to remain constant, the anchor points need to be translated by the same amount as the fairlead points, with respect to the original mooring system definition of the DeepCWind platform, which is achieved by adopting a similar approach.

A summary of all the SubDyn, HydroDyn and MoorDyn sections and parameters affected by the adjusted platform geometry and updated in the pre-processing step is given in the following table:

Table 6.1: Summary of the OpenFAST inputs that need updating after platform geometry adjustments

Input file section affected	Changes Incorporated
SubDyn	
Structure Joints	(x,y,z) coordinates
Member Properties	Cross-sectional diameter and wall thickness
Concentrated Masses	Cylinder cap mass and inertia
HydroDyn	
Member Joints	(x,y,z) coordinates
Member Properties	Cross-sectional diameter and wall thickness
Submerged Volume	Displaced water volume of the potential flow members
Fill Groups	Ballast fill location
Additional Linear Stiffness Matrix	Hydrostatic restoring coefficients in heave, roll and pitch direction
MoorDyn	
Attachment Points	Fairlead and anchor (x,y,z) coordinates

6.2.2. ElastoDyn-Based Substructure Model

In cases where the floating platform is modelled as a rigid body, and internal forces within the members are not a concern, the need for a coupling with SubDyn is eliminated. As a result, the optimisation process can be greatly sped up by switching to an ElastoDyn-based platform model. However, this transition necessitates the manual computation of platform properties like mass, centre of mass, and inertia, as these are no longer automatically calculated within SubDyn. While the structure joints and members are no longer taken into account by SubDyn, their formulation is retained within the Python model. Utilising the coordinates of the member start- and endpoints, along with information on diameter, radius, and material density, the necessary calculations for these properties can be performed. The total platform mass is the sum of the member masses, which are simply calculated by computing the product of their cross-sectional area, length and material density. The structural centre of mass is then determined by averaging the centroids of all members, weighted by their respective masses. The centroids of the cylindrical member elements are found using simple vector operations, placing the centroids midway between the start and endpoint of the beams. Calculating the inertia of the platform, being a composite structure, is a little more intricate due to the consideration of member orientations. The process of computing the total platform inertia in roll, pitch and yaw direction is explained in detail in appendix B.

6.3. Running OpenFAST

A run script was developed to run OpenFAST simulations in parallel from within the Python model, drawing inspiration from the existing runner in the pyfast toolbox. The decision to create a new runner, as opposed to using the existing one, was driven by the need for additional features. In the existing runner, simulations were launched in chunks using subprocesses, allowing multiple OpenFAST executables to be run concurrently. However, the global process would wait for all OpenFAST simulations to complete before progressing to the next block of code. This approach had drawbacks. Firstly, it lacked insight into the progress of individual simulations, as the OpenFAST output messages were not logged in real-time. Secondly, the code would continue running until all subprocesses had completed, even if one or more simulations had failed.

An example scenario that illustrates this issue involves a platform design with a righting moment that is insufficient to counteract the moment caused by rotor thrust at e.g. rated wind speed. As a result, the wind turbine would likely tip over, leading to simulation failure. However, for wind speeds below the rated value, this tipping may not occur, as the FOWT might remain within its stability limits. Recognising this as an inadequate platform design, it would make more sense to terminate all simulations in progress when an issue is detected, rather than waiting for the ones that were still running to complete. This early termination feature saves a significant amount of computational time, especially given the lengthy duration of the OpenFAST simulations.

The additional features that have been added into the new *runner* script address these shortcomings. Python's "Concurrent Futures" module is utilised to initiate and manage multiple subprocesses in parallel, distributing the workload across a user-defined number of CPU cores. Each subprocess is responsible for executing a single OpenFAST simulation. Within the subprocess, the standard output is captured, (in OpenFAST also referred to as screen messages) which is generated during these subprocesses as text messages. This facilitates debugging and analysis of the individual simulations. Moreover, it continuously monitors this text output for the presence of a specific message "Aborting OpenFAST", which indicates simulation failure. Upon detecting this message, an event is set using the multiprocessing module, communicating failure of the simulation. This event is shared across all subprocesses, resulting in their early termination. The global process continually checks the status of this event flag, and upon activation, it shuts down the parallel process executor. Finally, a log message is written to the global log file, indicating that one or more OpenFAST simulations have crashed. If failure does not occur, the global process will continue and wait until all subprocesses have terminated normally, after which the simulations can be post-processed.

6.4. Post-Processing

The primary objective of the post-processing script is to analyse the time series data generated by OpenFAST simulations and extract various parameters and metrics, serving to quantify the overall performance of the floating wind turbine system, including platform motion, power generation, sub-structural integrity, etc. In the context of the optimisation script, the post-processing script is essential for obtaining and evaluating the constraints. Post-processing is performed using the pCrunch toolbox, which is a Python post-processing interface for OpenFAST results, developed by NREL [53].

Upon initialisation of the *post-processing* script, the directory containing the OpenFAST binary output files is provided. The data processing methods of the pCrunch toolbox are then leveraged to create a structured dataset containing summary statistics for the output channels of OpenFAST, including minima, maxima, averages, etc. for each output channel. Using this data, some of the limit states can be extracted directly, such as the maximum observed platform pitch. By defining the nacelle acceleration as the magnitude of the combined accelerations in x-, $y-$ and z-direction, the maximum nacelle acceleration can also be derived. The limit states with respect to structural integrity of the platform, however, requires further post-processing.

6.4.1. Structural Analysis

In assessing the structural integrity of the platform, the analysis focuses on the extreme stresses observed in each survival load case (DLCs 1.6, 6.1 and 6.3). Furthermore, the structural analysis includes the fatigue damage accumulated during the operational load cases (DLC 1.2). However, prior to this analysis, it is necessary to calculate the internal stresses in the members based on the internal forces. While the SubDyn output channels provide data on internal member axial and shear forces, bending moments, and torsion, the analysis will only consider stresses resulting from axial forces. This simplification is made to maintain manageable complexity in the post-processing methods within the scope of this project. To convert from axial force to axial stress, the internal force is divided by the cross-sectional area of the member. Furthermore, when evaluating extreme stresses, the partial safety factor is applied. The maximum stress in each member is then calculated using the following formula:

$$\sigma_{\max} = \frac{F_{\max}}{A} \cdot PSF \tag{6.3}$$

where $F_{\max}$ (N) represents the maximum axial force observed during the OpenFAST simulations, A is the cross-sectional area (m^2) of the member, and PSF denotes the partial safety factor.

Fatigue analysis is conducted using pCrunch's implementation of MLife [54], a tool which adopts rainflow counting of time series data to compute damage equivalent loads and accumulated damage. These calculations are performed based on user-provided values of the slope m of the Wöhler S-N curve, and the material yield stress (σ_{yield}) as the stress-axis intercept. Furthermore, the Goodman correction is applied for equivalent stress calculation. After processing the time series of all DLC 1.2 load cases, a data structure is obtained containing the accumulated damage for each member within the 10-minute simulation time. In this project, the material value for the fatigue exponent is set to a conservative value of $m = 3.0$, which corresponds to a steel hollow cylindrical section with defects (i.e. welds) [55]. The maximum allowable stress is the yield stress, which is set equal to a value of $\sigma_{\text{yield}} = 3.55 \times 10^8$ Pa.

In order to compute the damage values for the complete lifetime, a few steps are taken. Firstly, the probability distribution of the simulated wind speeds of DLC 1.2 needs to be calculated. This is accomplished using the Weibull cumulative distribution function, which calculates the probability of wind speeds falling within the bin of $U \pm 1\ \mathrm{m\,s^{-1}}$:

$$P(U) = e^{-\left(\frac{U-1}{c}\right)^k} - e^{-\left(\frac{U+1}{c}\right)^k} \tag{6.4}$$

where k is the Weibull scale parameter ($\mathrm{m\,s^{-1}}$) and c is the Weibull shape parameter (-) as defined in table 5.2. The probability of occurrence of each wind speed is depicted in figure 6.2.

In the next step, the number of occurrences of the ten-minute simulations is counted for each wind speed over a 25-year lifetime. These counts are weighted based on their probability of occurrence. By multiplying the accumulated damage of the ten-minute simulations by their respective occurrence counts, the accumulated damage for each wind speed is determined. The cumulative lifetime damage is then obtained by summing the accumulated damages for all wind speeds.

One limitation of SubDyn is its capability to output results for only up to nine members. Therefore, a decision had to be made which members were included in the structural analysis. In order to make this choice, a series of OpenFAST simulations was conducted for the original platform design, each focusing on different sets of members as output channels. These simulations allowed examination of the time series of internal axial forces, assessing their magnitude and variability. These forces were converted into stresses, providing insights into which members had potential for optimisation, in terms of cross-sectional properties. The internal stresses in the structural members due to the axial force are provided in appendix C, in figures C.1 to C.3 for DLC 1.2 with a mean wind speed of $11\ \mathrm{m\,s^{-1}}$.

The figures show the axial stress at the extremities of the member (nodes 1 and 3), and at the member midpoint (node 2). For describing the members, the same naming convention is utilised as the one described in [15], and the member IDs correspond with the identifiers tabulated in the members section of the SubDyn input file in appendix A. From the figures, it can be observed from the sign of the stresses that the columns (both the upper and base sections) are loaded in compression, just like the delta- and Y-pontoons that are located above MSL. In contrast, the lower delta- and Y-pontoons, as well as the cross-braces, are loaded in tension.

A closer look at the magnitudes of the stresses reveals that the axial stress in the pontoons is notably high. In some cases, the mean stress is in the same order of magnitude as the yield stress ($\sigma_{\text{yield}} = 3.55 \times 10^8$ Pa).

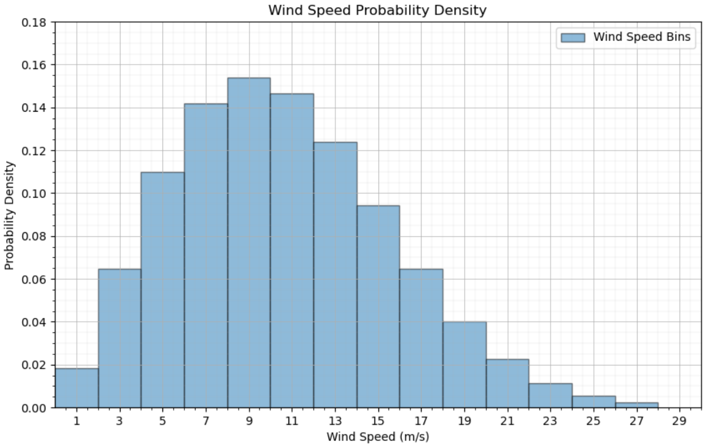

Figure 6.2: Probability density of the 2 m s^{-1} wind speed bins used in DLC 1.2

These high mean stresses imply that even minor fluctuations could lead to fatigue failure. These findings suggest that the sizing of the pontoons and braces has been inadequate in the original design. This issue was acknowledged by the authors in the OC4 definition report [15], and is likely a consequence of their choice to enhance bending stiffness by virtually increasing material stiffness, rather than enlarging the cross braces and pontoons during the transition from a model-scale to a full-scale platform.

As a result, it is considered less meaningful to perform structural analysis of the pontoons and cross-braces of the DeepCWind platform. Furthermore, considering that the heaviest components of the floating platform structure are the large-volume columns, and recognising that the most substantial reduction in platform mass can be achieved by adjusting the wall thickness here, it was chosen to focus the structural analysis on the offset column members.

For this structural analysis of the outer columns, baseline values were first determined by calculating the maximum stress and maximum lifetime fatigue damage observed in the members of the initial platform design. Subsequently, a stress and fatigue analysis was incorporated into a separate subroutine performed after the OpenFAST simulations. This analysis determined which adjustments to the thickness value should be made to ensure that the structural performance matches that of the original platform.

Given the assumption that the members are rigid, and the changes in thickness are modest, it was considered a reasonable assumption that the internal forces in the member remained relatively constant. The inclusion of this subroutine in the post-processing serves two main purposes. First, it demonstrates the potential for adding structural constraints into the optimisation process. Secondly, it illustrates the sensitivity of the platform mass to the loads within the substructure.

7

Verification

In this chapter, the modelling approach is verified by comparing the results with data available from NEMOH validation campaigns and OpenFAST certification tests. In section 7.1, the model results are compared to those of a reference NEMOH and WAMIT simulation, and a sensitivity study is performed on the mesh size to find the best balance between accuracy and CPU time required. Furthermore, in section 7.2, the OpenFAST simulation results are compared to a reference test case.

7.1. Verification of the NEMOH Model

In chapter 4, the development of a wrapper script has been outlined to automatically create a mesh of the floating platform based on a few input variables, and perform a hydrodynamic analysis in NEMOH, based on a given range of wave frequencies and wave directions. In developing the NEMOH model, the DeepCWind platform was used as reference. The mesh is again shown in figure 7.1. Before the NEMOH model is implemented in the optimisation workflow, the outcomes are verified against two cases.

In the first case, the model results were compared with the results of a reference model provided with the distribution of NEMOH v3; an irregular mesh of the DeepCWind created with GMSH, as documented in [56] and shown in figure 7.3. By using the same software with two different meshes, the quality of the mesh created with the developed NEMOH wrapper could be tested.

In the second case, the model results are compared with results from hydrodynamic modelling of the DeepCWind platform with WAMIT, as described in the technical report by NREL [15]. As the WAMIT output files are included in the regression tests of OpenFAST, the hydrodynamic coefficients can be compared, and the performance of the NEMOH model is tested. The mesh is illustrated in figure 7.2

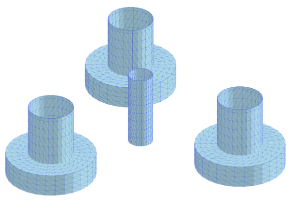

Figure 7.1: Mesh developed with NEMOH wrapper

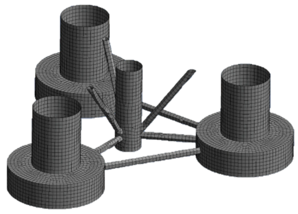

Figure 7.2: Complete mesh similar to WAMIT reference [57]

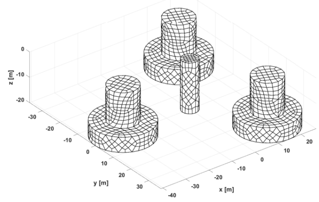

Figure 7.3: NEMOH reference mesh [56], created with GMSH

As such, in all three simulations the same platform is modelled, with similar representative simulation settings, as summarised in table 7.1. For each case, the hydrodynamic added mass and radiation damping coefficients are analysed for the six degrees of freedom, including the infinite-frequency added mass matrix. Furthermore, the wave excitation force is compared.

Table 7.1: Simulation settings for verifying the hydrodynamic modelling approach.

	NEMOH model	WAMIT	NEMOH reference
Meshed components	main- & offset columns	complete geometry	main- & offset columns
# Panels	2100	avg. panel size of 2 m	2196
# Wave frequencies	100	498	100
Wave frequency range [rad/s]	0.05 – 5.0	0.01 – 4.98	0.0628 – 6.28
Wave headings [deg]	0, 30	-180, -170, ..., 170, 180	0, 30
Water depth [m]	200	200	200

7.1.1. Infinite-Frequency Added Mass

The infinite-frequency added mas matrix $\mathbf{A}_\infty$ characterises the floater's instantaneous response to acceleration. The matrix has been given below for the NEMOH model results and the reference WAMIT data. Upon comparison, it can be recognised that the surge-surge and sway-sway elements are identical, just like the roll-roll and pitch-pitch. As noted in [15], this is due to the platform's symmetry, resulting in equal responses at wave headings of 0, 120 and 240 degrees.

However, it is worth noting that the NEMOH-computed matrix shows subtle differences between the surge-pitch and sway-roll components when compared to their pitch-surge and roll-sway counterparts. These discrepancies are likely a consequence of overlapping nodes within the NEMOH mesh at the start- and end-points, resulting from the azimuthal discretisation of the cylindrical components.

$$(\mathbf{A}_\infty)_{\text{NEMOH}} = \begin{bmatrix} 6.47\times10^6 & 0 & 0 & 0 & -84.35\times10^6 & 0 \\ 0 & 6.47\times10^6 & 0 & 84.35\times10^6 & 0 & 0 \\ 0 & 0 & 13.82\times10^6 & 0 & 0 & 0 \\ 0 & 84.25\times10^6 & 0 & 6.98\times10^9 & 0 & 0 \\ -84.25\times10^6 & 0 & 0 & 0 & 6.98\times10^9 & 0 \\ 0 & 0 & 0 & 0 & 0 & 4.98\times10^9 \end{bmatrix}$$

$$(\mathbf{A}_\infty)_{\text{WAMIT}} = \begin{bmatrix} 6.49\times10^6 & 0 & 0 & 0 & -85.10\times10^6 & 0 \\ 0 & 6.49\times10^6 & 0 & 85.10\times10^6 & 0 & 0 \\ 0 & 0 & 14.70\times10^6 & 0 & 0 & 0 \\ 0 & 85.10\times10^6 & 0 & 7.21\times10^9 & 0 & 0 \\ -85.10\times10^6 & 0 & 0 & 0 & 7.21\times10^9 & 0 \\ 0 & 0 & 0 & 0 & 0 & 4.87\times10^9 \end{bmatrix}$$

To compare the added mass coefficients at infinite frequency, the percent error is computed between the modelled infinite-frequency added mass matrix and the reference matrix obtained from NREL. The results of the comparison are presented below. As can be seen from the percent error matrix, there is a good match between the surge and sway elements. Similarly, the match between surge-pitch and sway-roll is quite accurate. However, there are noticeable errors in the roll and pitch direction. And particularly in the heave direction, where a considerable error of 6.12% is observed.

$$\varepsilon = \begin{bmatrix} 0.31 & 0 & 0 & 0 & -0.82 & 0 \\ 0 & 0.31 & 0 & 0.82 & 0 & 0 \\ 0 & 0 & 6.12 & 0 & 0 & 0 \\ 0 & 0.94 & 0 & 3.19 & 0 & 0 \\ -0.94 & 0 & 0 & 0 & 3.19 & 0 \\ 0 & 0 & 0 & 0 & 0 & 2.26 \end{bmatrix}$$

7.1.2. Hydrodynamic Coefficients and Wave Excitation Force

The frequency variation of the added mass coefficients are plotted in figure 7.4 for the frequency range of 0 to 0.8 Hz. From these figures, it can be seen that the trends of the curves for the different cases matches very closely. There is a good fit for the surge, sway and surge-pitch and sway-roll coefficients. However, the same discrepancies as before are observed in the heave, roll, pitch and yaw direction. The figure shows a one-to-one match between the developed NEMOH model, and the reference NEMOH model. The blue curve, which corresponds to the developed NEMOH model, can hardly be seen in the plot, as it coincides with the NEMOH reference curve. This suggests that the implementation of the DeepCWind mesh in NEMOH is correct.

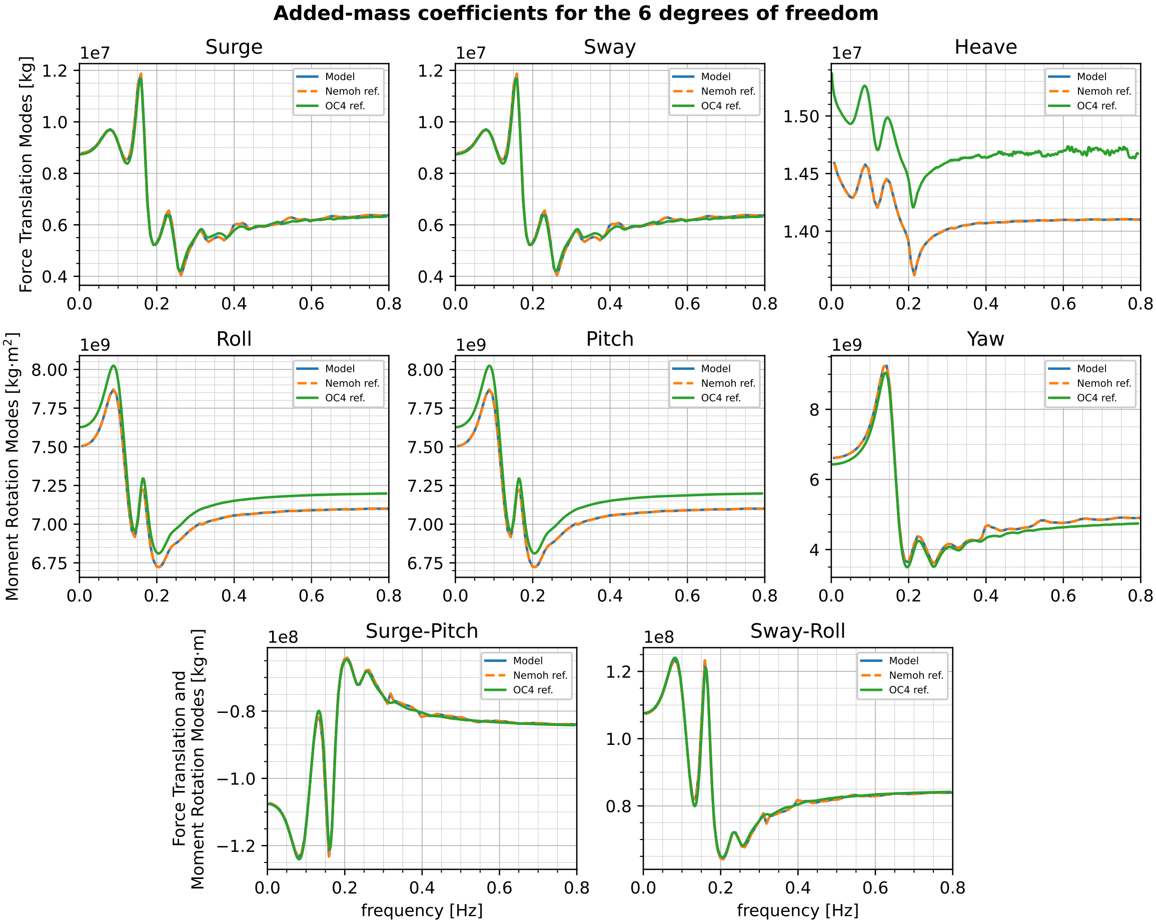

Figure 7.4: Added mass coefficients for the model results, NEMOH reference case and OC4 (WAMIT) reference case.

Concerning the error between the model results and the WAMIT reference case; this can be explained by the presence of pontoons and braces in the mesh for the WAMIT model, which are absent in the NEMOH model mesh. These additional components contribute to the added mass and radiation damping coefficients, and because they are mostly aligned with the xy-plane, the effect is most pronounced in the heave, pitch and roll directions.

The above conclusions are supported by the radiation damping plots, presented in figure 7.5, where again a close match is observed in the trends of the curves, but considerable discrepancies exist in the peak amplitudes for the radiation damping coefficients in the heave, roll and pitch directions.

A notable aspect of the trends in figures 7.4 and 7.5 is that for the NEMOH model and NEMOH reference, the curve shows some irregularities near distinct frequencies (i.e. for the surge and sway radiation damping coefficients at frequencies near 0.4 Hz and 0.53 Hz). These irregularities are attributed to what are called "irregular frequencies", and cause under- or overestimation of hydrodynamic parameters at particular excitation frequencies due to ill-conditioning in BIEs [58].

Lastly, a comparison of the wave excitation forces for the different cases, displayed in figure 7.6, shows that there is a good correspondence in force amplitude. Nonetheless, inconsistencies in the phase become noticeable beyond frequencies of 0.3 or 0.4 Hz. However, it should be noted that beyond these frequencies, the force amplitude is negligible, and therefore this is not expected to significantly impact the platform behaviour.

In conclusion, the comparison of results reveals that NEMOH results generally correspond well with the WAMIT results in terms of the frequency-dependent hydrodynamic response. However, some discrepancies persist, mainly attributed to the absence of pontoon and brace elements in the NEMOH model. It is important to note that these pontoons and braces are not entirely excluded from the model. Instead, their hydrodynamic contribution are accounted for in the hybrid potential flow and strip theory model of HydroDyn.

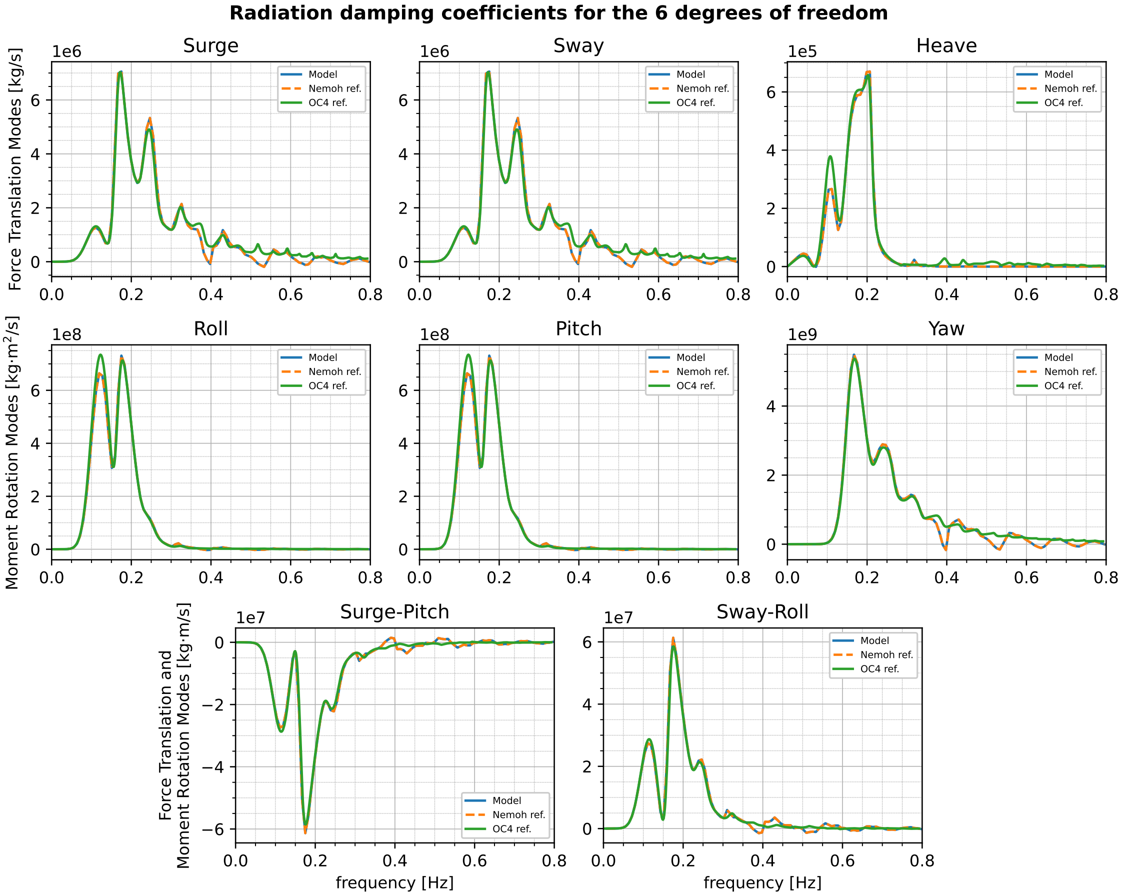

Figure 7.5: Radiation damping coefficients for the model results, NEMOH reference case and OC4 (wamit) reference case.

7.1.3. Hydrostatic Stiffness

Before utilisation of the hybrid model in HydroDyn, the hydrostatic stiffness matrix of the NEMOH results and the WAMIT results should be compared. Again, it is anticipated that discrepancies arise from the absence of pontoons and braces in the NEMOH model. However, with the inclusion of additional linear stiffness elements, as computed using equation 5.12, the differences between these matrices are expected to decrease. Therefore, a comparative analysis of the elements within the hydrostatic stiffness matrix is done, both with and without the contribution of the additional linear stiffness, originating from the strip theory members in HydroDyn. Considering the importance of hydrostatic stiffness for the degrees of freedom related to water piercing, given the platform's symmetry, the analysis will focus on the heave, roll, and pitch directions. These DOFs displayed the most significant differences in the previous section.

The hydrostatic stiffness elements are presented in table 7.2. It can be observed that without inclusion of the additional linear stiffness elements, the error between the NEMOH and WAMIT results is substantial. However, upon inclusion of these elements, the hydrostatic stiffness elements of the hybrid model align more closely with the reference data from WAMIT. The robustness of the hybrid model is improved by this enhanced consistency, accounting for the absent pontoon- and brace components in the NEMOH simulation.

Looking at the sign of the roll- and pitch restoring coefficients, one might be inclined to think that they should be positive instead of negative, in order for the system to be stable. However, it is important to note that the hydrostatic restoring coefficients are affected by various factors, including the waterplane area of the undisplaced platform, centre of buoyancy, and the effects of body weight (taking into account the vertical distance between centre of buoyancy and centre of mass). These factors are handled by different modules in OpenFAST. The body weight terms, excluding ballast and marine growth (which are automatically calculated by HydroDyn), are computed by the ElastoDyn module. Factoring in the mass terms, the restoring coefficients would be positive for stable platforms. However, to prevent double booking, these terms are omitted from the hydrostatic restoring matrix input to HydroDyn.

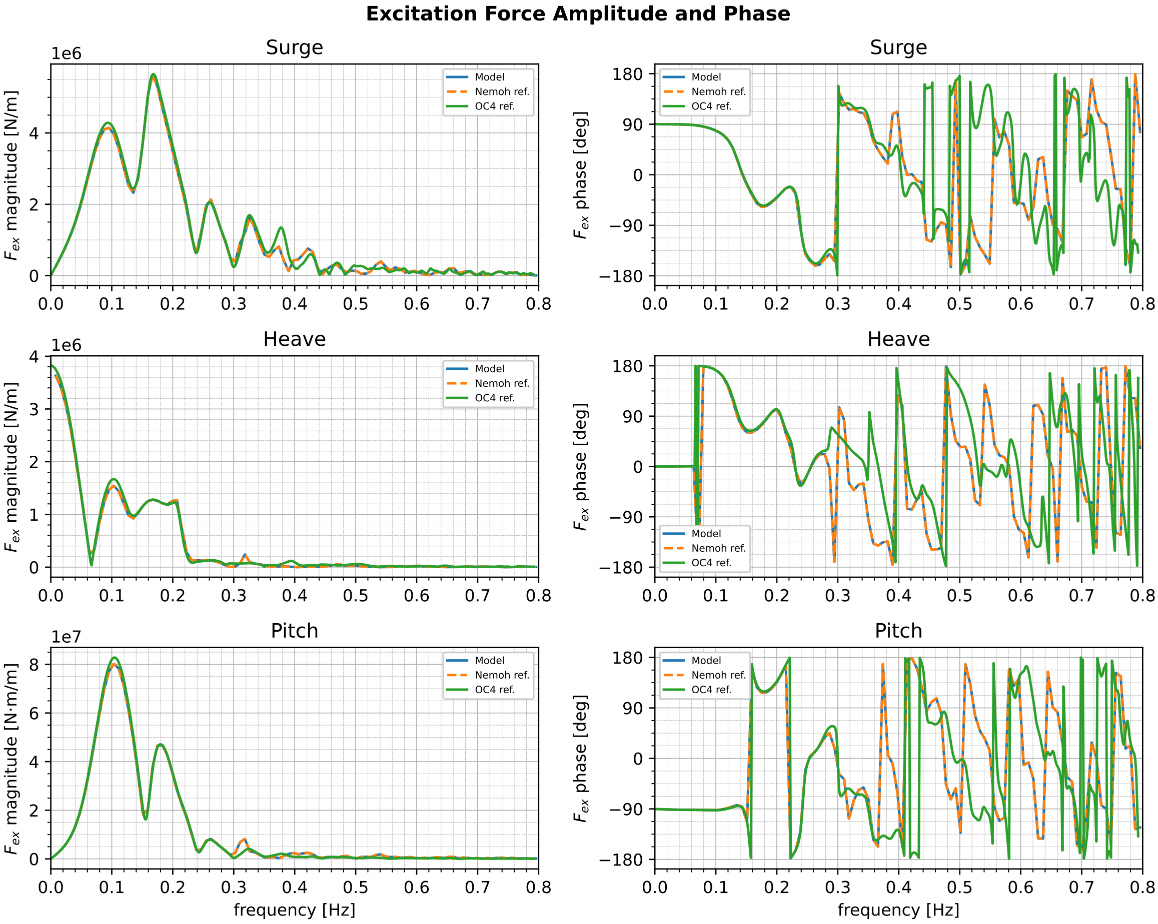

Figure 7.6: Wave excitation forces for waves propagating along the positive X-axis for the model results, NEMOH reference case and OC4 (wamit) reference case. As the wave forces lie in the XZ plane, the forces corresponding to the sway, roll and yaw directions are not shown.

Table 7.2: Heave, roll and pitch elements of the hydrostatic restoring matrix of the WAMIT and NEMOH results, with and without additional stiffness.

	Heave ($\mathrm{N\,m^{-1}}$)	Roll & Pitch ($\mathrm{N\,m\,rad^{-1}}$)
WAMIT	3.82×10^{6}	-3.81×10^{8}
NEMOH	3.69×10^{6}	-3.39×10^{8}
Additional Stiffness	7.66×10^{4}	-4.14×10^{7}
Error w/out Additional Stiffness	3.32 %	10.88 %
Error w/ Additional Stiffness	1.32 %	0.01 %

7.1.4. NEMOH Mesh Convergence Study

To achieve a balance between precision and computational efficiency, a mesh convergence study was carried out. For this study, the frequency-dependent hydrodynamic coefficients and wave excitation forces are analysed for a series of simulations, each involving a different amount of mesh panels. Subsequently, the floating platform response was tested in the context of OpenFAST simulations, using these different mesh discretisations. The results of this study, including comparisons with the baseline WAMIT model, are presented in appendix D.

Looking at figures D.1 to D.3, there is a notable difference in the results between the coarse mesh of 518 panels, and those employing a finer mesh with a higher number of panels. On the other hand, the results show a comparatively minor difference between the NEMOH simulations with 1276 panels and those with 3026 panels. In all cases, even for the finest mesh, discrepancies persist between the NEMOH results and the reference data from WAMIT, for reasons explained previously in section 7.1.

However, it is worth pointing out that these observations do not directly apply to the results of the OpenFAST simulations in figures D.4 and D.5. In fact, there is hardly any noticeable influence of the mesh panel size on the OpenFAST simulation results. This observation implies that the sensitivity of the overall FOWT response to the hydrodynamic mesh size is relatively low when examining the fully coupled system. However, it remains uncertain whether this observation holds true for other floating platform concepts, where panel size may play a more critical role, or under different environmental conditions.

The CPU time required for hydrodynamic modelling with NEMOH (including both first- and second-order wave loads) is plotted in figure 7.7, where a polynomial curve has been fitted to the eight data points. The graph demonstrates that the computational cost increases exponentially with the number of mesh panels involved in the simulation. For the optimisation problem, a mesh with 1276 panels proved to be a good trade-off between accuracy and computational expense.

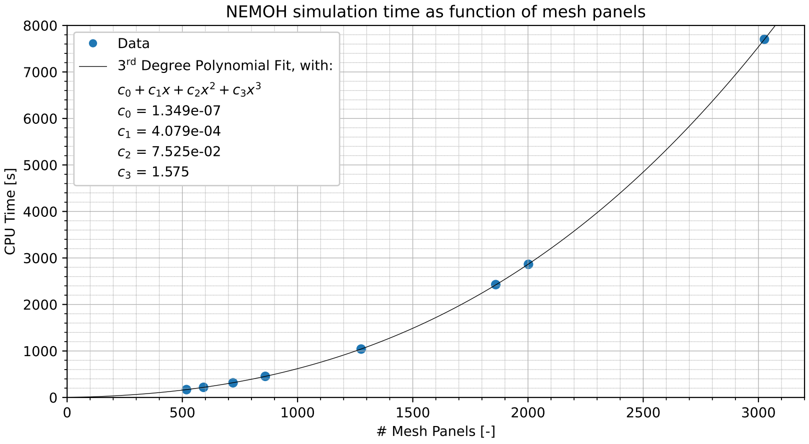

Figure 7.7: CPU time as function of mesh panel size

7.2. OpenFAST Simulation

Besides hydrodynamic modelling of the floating platform, the sub-structural dynamics have also been modelled in OpenFAST. Since the recent addition of substructural flexibility and member-level loads for floating platforms to OpenFAST, there are no public models available yet that support this functionality. Therefore a few verification runs with OpenFAST were required to test if the implementation is correct.

For this verification case, the same OC4 platform was modelled in OpenFAST for an existing test case: certification test # 25. The turbine included in this test is the NREL 5 MW offshore reference turbine, as described in [15]. The environmental conditions in this case are an aligned steady wind of 8 $\mathrm{m\,s^{-1}}$, and irregular white-noise waves propagating along the positive X-axis, with a maximum wave height of approximately 2 m. The initial surge offset is 5 m and the initial pitch offset 1.9 degrees. The simulation was carried out for 1000 seconds, but only the last 200 seconds are shown to enhance readability of the plots.

A total of three simulation results can be distinguished from the plots in figures 7.8 and 7.9. The blue curves correspond to the original certification test results: the reference case. The orange curves represent the reference case with the SubDyn module enabled. The platform is modelled as a rigid body in SubDyn. In the last case, the green curves correspond to the NEMOH-generated hydrodynamic data, using the combined potential flow and strip theory model in HydroDyn, and with SubDyn enabled.

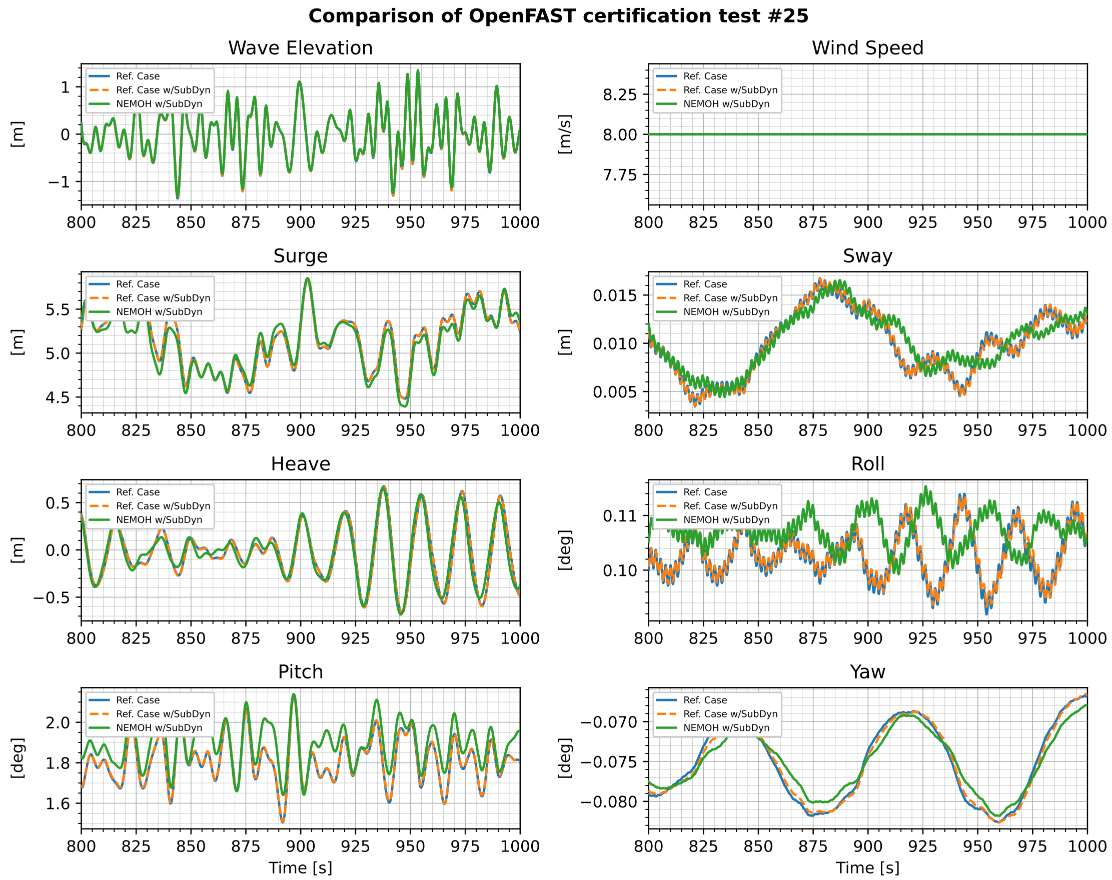

Figure 7.8: Comparison of simulations results for the surge, heave and pitch translations and rotations for steady wind and irregular waves.

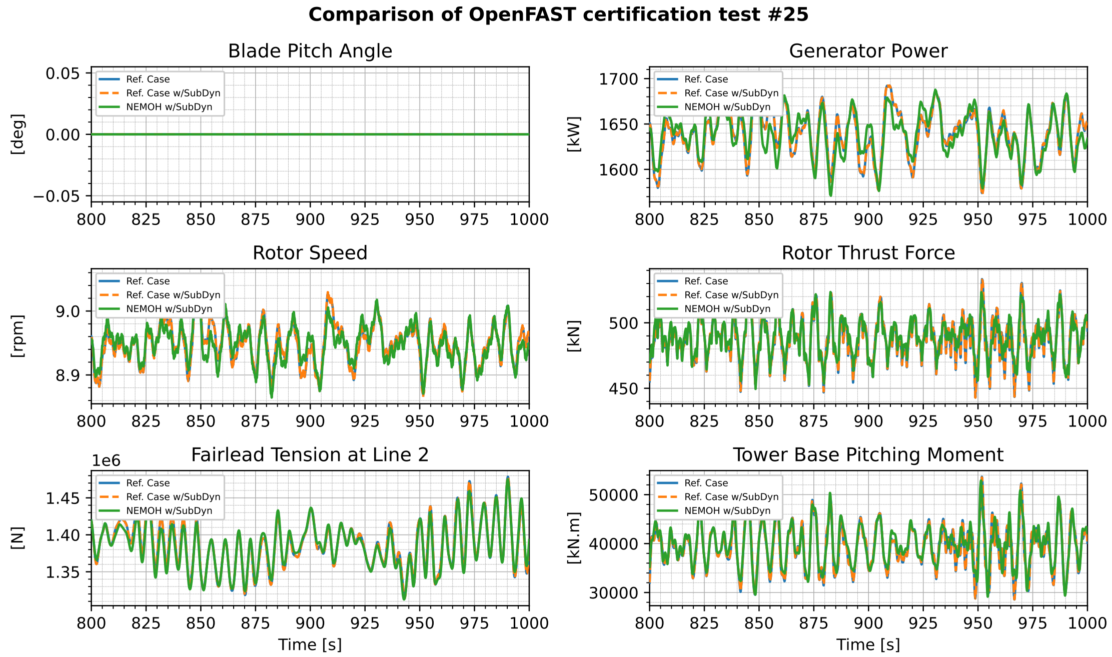

Figure 7.9: Comparison of simulations results for the turbine performance indicators for steady wind and irregular waves.

By looking at figure 7.8, two key observations can be made. Firstly, the blue and orange curves for the reference cases with and without SubDyn enabled coincide almost perfectly. This gives reason to believe that the physical representation of the floating platform has been properly modelled in SubDyn. On the contrary, there is a noticeable difference in the platform response between the WAMIT potential flow results and the combined NEMOH and strip theory results. While the overall trends are similar, there is a slight offset in the amplitudes of the surge, heave, and pitch signals. As for sway and roll motion, it could be argued that there is a minor phase difference in the signal, though it is worth noting that the magnitudes of the signals are negligible.

To verify the wind turbine performance in the OpenFAST model, the blade pitch angle, generator power, rotor speed, thrust force, fairlead tension and tower base pitching moment are plotted in figure 7.9. Upon analysis of these plots, the same conclusions can be made as for the platform motions. Enabling SubDyn did not yield a noticeable impact compared to the reference case. However, when considering the NEMOH results, disparities are evident in the curves representing turbine performance indicators. While the amplitude of the curves show a slight deviation, the general trends remain consistent. Although a perfect match is not achieved, the results are deemed satisfactory to proceed with the optimisation process.

8

Results

This chapter describes the results of the optimisation problem, as outlined in section 3.2. As mentioned, the main optimisation problem is executed twice. In the first case, the platform's structure is defined in SubDyn, which enables the possibility to perform structural analysis when the internal forces in the members are output. The results of the optimisation with SubDyn coupling are discussed in section 8.1. Subsequently, the results of the optimisation with the ElastoDyn-based substructure model are discussed in 8.2. Furthermore, the results of a sensitivity study on the influence of simulation length and inclusion of second-order wave forces are discussed in sections 8.3 and 8.4 respectively. Finally, the results of a small optimisation study on the cross-sectional dimensions of the pontoons are analysed in section 8.5.

8.1. Optimisation with SubDyn Coupling

The main optimisation routine, as described in section 3.2, terminates after 37 iterations. The total elapsed time amounts up to 125.4 hours, with an average CPU time of 3:22 hours per iteration, of which 3:05 hours is allocated to the parallel OpenFAST simulations. Figure 8.1 shows the convergence history of the optimisation problem. In the left plot in the figure, the objective function and design variable values are shown. In the right plot, the constraint values are visualised. For iterations 7 and 13, a simulation failure is signalled, which is represented by a red cross in the figures. From these plots, the following observations can be made.

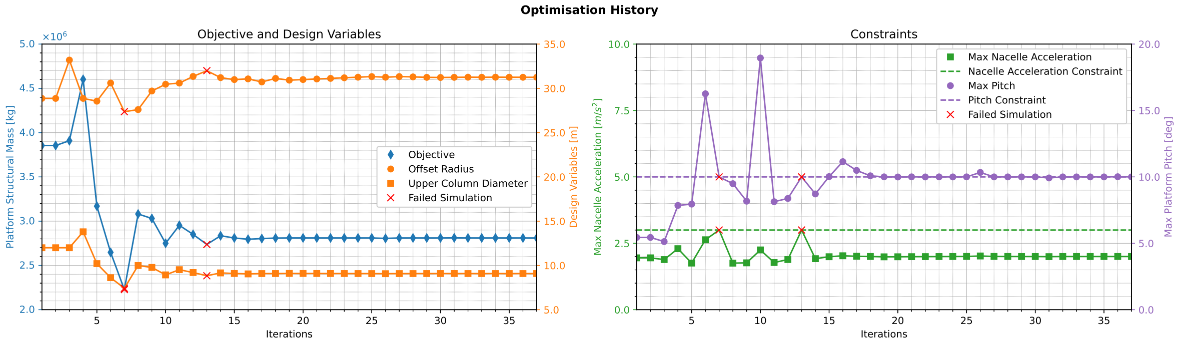

Figure 8.1: Convergence history of the main optimisation problem

Firstly, it can be observed that the optimised design is found for an offset radius that is higher than the initial radius, while the upper column diameter has reduced. By looking at the trends of the objective and constraint values, as a function of the design variables, it can be concluded that a reduction of the upper column diameter results in the greatest decline in structural mass, while the offset radius is increased to ensure that the maximum pitch constraint is satisfied.

Furthermore, the observation is made that after about twenty iterations, the solution approaches the optimal solution, whereas it can be stated that after thirty iterations, the solution can be considered to have converged. Hence, to improve computational efficiency, the termination criterion could be relaxed.

Regarding the constraints, it can be concluded that the limiting constraint is the maximum platform pitch angle. The maximum nacelle acceleration, on the other hand, never exceeds the predefined limit. Although the curve for the nacelle acceleration indicates that there is some variation in the maximum values observed, it is difficult to establish a clear and distinct correlation with any of the constraints or variables. In effect, the values for the initial and optimised design are very similar. This suggests that the nacelle acceleration is sensitive to a broader array of factors not directly explored in this study.

The final values for the objective function, constraints, independent and dependent design variables are summarised in table 8.1. The structural mass of the floating platform has reduced to a value of 2 810 501 kg, corresponding to a reduction of 37.1%. A visual representation of the optimised platform design compared to the initial design is provided in figure 8.3.

Table 8.1: Objective value, design variables (independent and dependent) and constraint values of the initial and optimised design

	Initial Design	Optimised Design	
Structural Mass	3854485	2810501	(kg)
R_{offset}	28.8675	31.2548	(m)
D_{UC}	12.0000	9.0823	(m)
D_{BC}	24.0000	18.1646	(m)
$\theta_{\max}$	5.4423	10.0000	(°)
$a_{\text{nac,max}}$	1.9526	2.0025	$(\mathrm{m\,s^{-2}})$
$z_{\text{ballast,UC}}$	6.17	11.16	(m)
$z_{\text{ballast,BC}}$	14.89	14.12	(m)

Annual Energy Production

In order to evaluate not just the cost of the platform, but also factor in the benefits in terms of energy production, the AEP is computed for each iteration. In effect, higher static pitch angles result in a greater inclination of the rotor with respect to the wind direction, thereby decreasing the effective rotor area and leading to a reduced power output.

The energy generated is computed firstly for each load case by integrating the instantaneous power signal over time. Subsequently, the AEP is determined by aggregating the energy generated across all simulations, accounting for the full year and factoring in the probability distribution of wind speeds, similar to the methodology described in section 6.4.1. For the original platform, the AEP is 26 287 MWh, while it is 26 066 MWh for the optimised platform, a reduction of 0.84%.

In order to test the sensitivity of the AEP, the values of the objective function have been divided by the AEP. They are illustrated in figure 8.2. It can be observed that the trend of the curve in this figure matches that of the objective values in figure 8.1 quite closely. This suggests that the slight reduction in terms of AEP is offset by the savings in structural mass. It would be interesting though, to see if a different optimal solution would be found if the AEP was incorporated into the objective function.

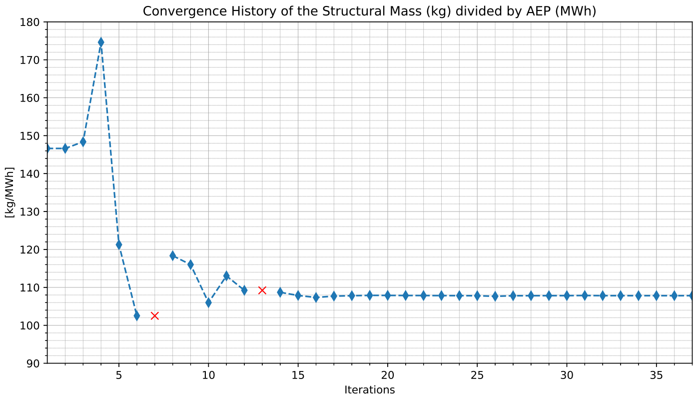

Figure 8.2: Cost function divided by the AEP

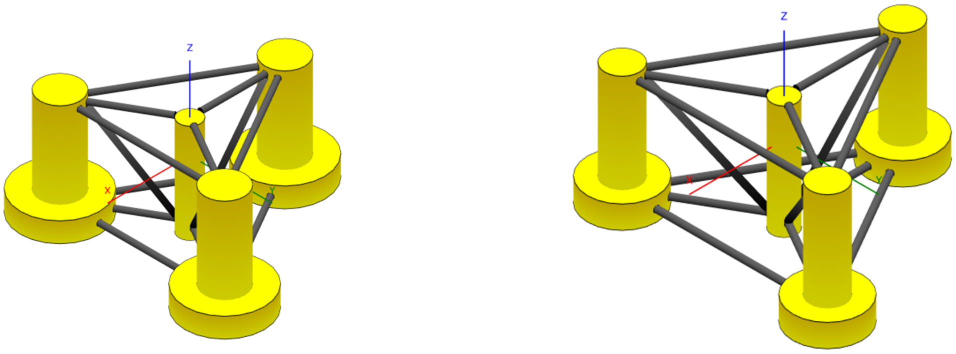

(a) Initial Design **(b)** Optimised Design

Figure 8.3: Visual representation of the initial and final design

Structural Analysis

As previously outlined in Section 6.4.1, the structural analysis was not directly included as a constraint within the optimisation process. Instead, it was utilised as a post-processing technique to calculate how the wall thickness of the outer columns should be adjusted to achieve the same structural performance with respect to the initial design. This choice was made because of two reasons. Firstly, the initial design exhibited questionable structural performance at full-scale dimensions, as reported in [15]. Secondly, the structural analysis employed considered only axial forces, disregarding the impact of shear forces, bending moments, and torsion. Figure 8.4 presents the maximum fatigue damage and maximum stress values observed in the outer columns of the floating platform for each iteration. It is noted, that again no values could be obtained for iterations 7 and 13, which correspond to failed simulations. The plotted data reveals that both the maximum fatigue damage and maximum stress decrease towards the optimal design.

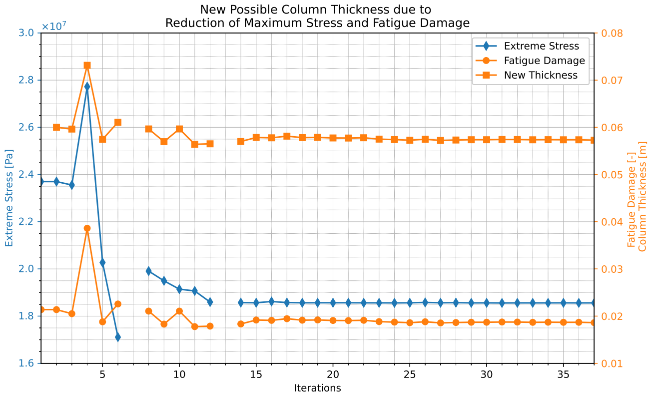

Figure 8.4: Results of the fatigue and stress analysis in the post-processing methods

The reduction in diameter of the outer columns results in a decrease in cross-sectional area, but it also leads to a reduction in internal axial forces. This reduction in forces is due to the decreased weight and buoyant force acting on the columns. Consequently, the stress values decline, resulting in lower levels of fatigue damage and extreme stresses compared to the initial design. This declining trend suggests the possibility of further reducing column thickness to achieve a lower platform mass. For the optimal design, a new thickness of 5.74 cm would result in the same structural performance in terms of fatigue and ultimate stress as the initial design. This reduction would result in a total structural mass of 2 709 390 kg.

It is important to note that this analysis assumes the columns to be rigid, and neglects the influence of a slight mass change on platform motion and internal member forces. To verify these assumptions, a new OpenFAST simulation was conducted using the adjusted thickness value. This led to a few insights. Because the platform mass was reduced but the buoyant force remained the same (maintaining the outer dimensions), additional ballast was required to maintain the same platform draft. This proved beneficial for stability, as it resulted in a lower centre of mass. However, the inclusion of ballast also increased internal forces, indicating that the assumption of negligible impact on internal forces was not entirely accurate.

Analysis of DLC impact on Results

In order to investigate the effects of different load cases on the constraint values, the mean platform pitch, maximum platform pitch, maximum nacelle acceleration and maximum axial stress have been plotted for each DLC in figures 8.5 and 8.6, for both the initial and optimal design. From the first figure, it can be observed that both the mean and maximum platform pitch values increase significantly when the initial design is compared to the optimal design.

As for the mean pitch, the distribution of the values over the different DLCs aligns with the expectation that the highest mean values occur at rated wind speed, where the thrust force is at its peak. This observation is no different for the optimised design. As for the maximum pitch values, it should be noted that the pitch values observed are a superposition of the mean pitch value due to the thrust force, and the excursion in response to wave loads. As higher wind speeds (and notably the storm case of DLC 6.1) correspond with increased significant wave height and period, it is plausible that the highest pitch values are observed for these load cases. It should be noted that DLC 6.3 was excluded from the results due to the occurrence of numerical instabilities at the rotor level. These instabilities were attributed to the high yaw misalignment angle, leading to unphysically high inertial forces.

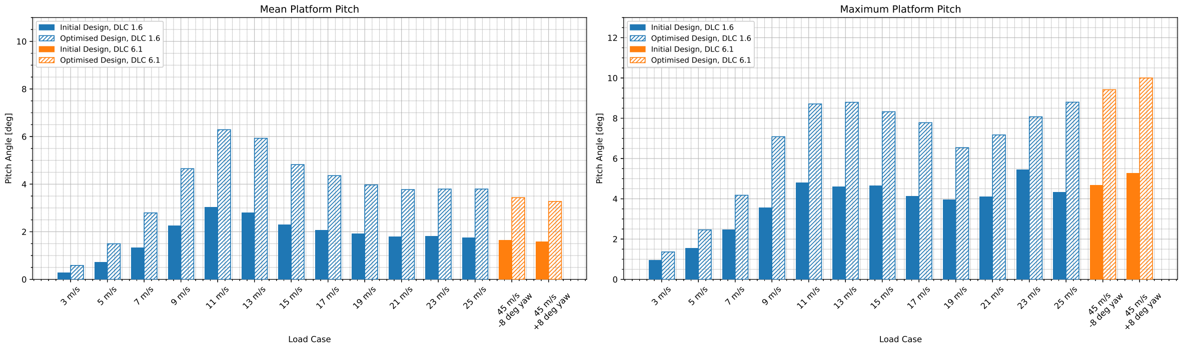

Figure 8.5: Average and maximum pitch values of the floating platform encountered for different DLCs

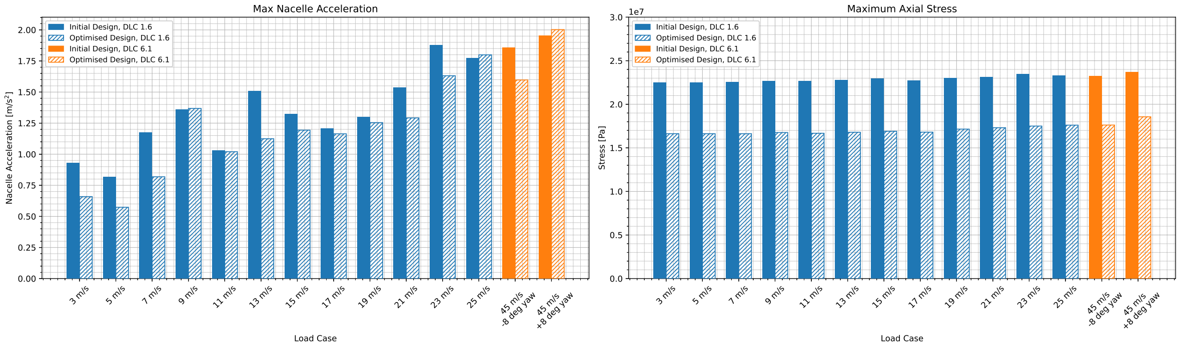

Figure 8.6: Maximum nacelle acceleration and axial stresses in the outer columns for different DLCs

As for the nacelle acceleration, the plot shows quite some variance in the maximum values among different load cases, although a general trend is identified that on average, the maximum observed acceleration increases with wind speed. An interesting observation is that for both the initial and optimised design, the maximum nacelle accelerations occur for DLC 6.1. This might be attributed to the fact that there is no aerodynamic damping when the rotor is parked and the blades are feathered to 90 degrees. But it could also be explained by the increased wave height and period, causing more excessive platfrom motion. Lastly, based on the data in the plot, it is impossible to make a statement about the sensitivity of the nacelle acceleration to the alterations in the platform geometry involved in the optimisation.

Regarding the axial stresses, it is observed that the maximum axial stresses are decreased for the optimised design, which suggests that the internal axial forces have decreased. This is likely due to the decrease in member self-weight and buoyant force.

Lastly, the plot showing which load case results in the maximum observed pitch angles in figure 8.7 reveals that the most critical load case in terms of pitch motion are the DLCs which exhibit the highest wave heights (and wave periods). For instance, in DLC 6.1, a wave height of 21 meter is observed. However, in some cases, the maximum pitch constraint is dominated by load case DLC 1.6 corresponding to a wind speed of 13 $\mathrm{m\,s^{-1}}$, which is close to the rated wind speed. Hence the conclusion can be drawn that the limit state in terms of floater pitch angle is mostly dominated by rotor thrust and the severity of the sea state.

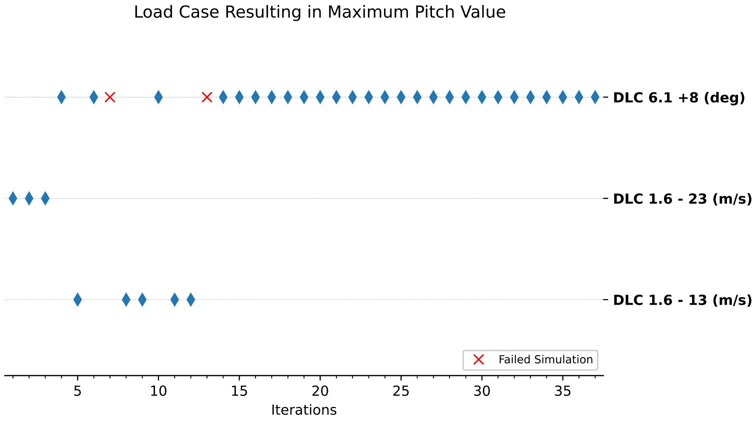

Figure 8.7: Load cases resulting in the maximum observed pitch value of the floating platform

Failed Simulations

To better understand the optimisation results, the failed iterations should be investigated. The reasons for the crashed OpenFAST simulations corresponding to iteration 7 and 13 can be understood by examining the time series and log files. Upon studying the log files, it becomes apparent that in both cases, the first load case to crash is the +8° yaw misalignment load case of DLC 6.1. The aborted simulation causes the remaining parallel simulations to terminate as well, such that the optimiser proceeds to the next iteration. Because the other simulations are halted prematurely, it remains uncertain whether they would have proven unstable, although this is a likely scenario. However, the platform design must be capable of withstanding all survival environmental conditions. Hence, the design is deemed inadequate, and it does not make sense to continue the simulation.

In both cases, the DLC 6.1 simulations of iteration 7 and 13 are terminated with the error message: `"The lowest element of a Morison member has become partially submerged! This is not allowed."` This means that one or more pontoons at the bottom side of the substructure are almost entirely above the waterline. This situation may occur as the result of excessive motion in the heave, roll or pitch DOF, possibly in combination with a very deep wave trough. Regardless of the specific cause, it represents an undesirable scenario and is proof of an inadequate platform design.

Figure 8.8 illustrates the time series of the relevant DLC. In iteration 7, a combination of small column diameter and reduced offset radius results in the restoring force being insuficient to counteract the overturning moment caused by the wind on the turbine (it is worth noting that this overturning moment is caused only due to drag, because the wind turbine is parked in DLC 6.1). This is clearly visible in the plots showing the pitch and roll behaviour, where the rotation angles increase steadily until they reach values that trigger the simulation to crash just before reaching the twenty second mark.

As for iteration 13, one would expect a better restoring behaviour, because the offset radius is increased with respect to the initial platform design. Although the pitch and roll behaviour show better performance within the same time span as iteration 7, the pitch excursion remains significant. However, the main problem here seems to originate from the heave signal: the platform heave displays negative damping, and the amplitude of the heave displacements grows unboundedly. This is a behaviour which is not observed for the same platform in less severe environmental conditions. This behaviour might be explained by the eigenfrequency of the platform in the heave DOF lying in the same range of the peak of the wave spectrum, although further analysis would be required to confirm this.

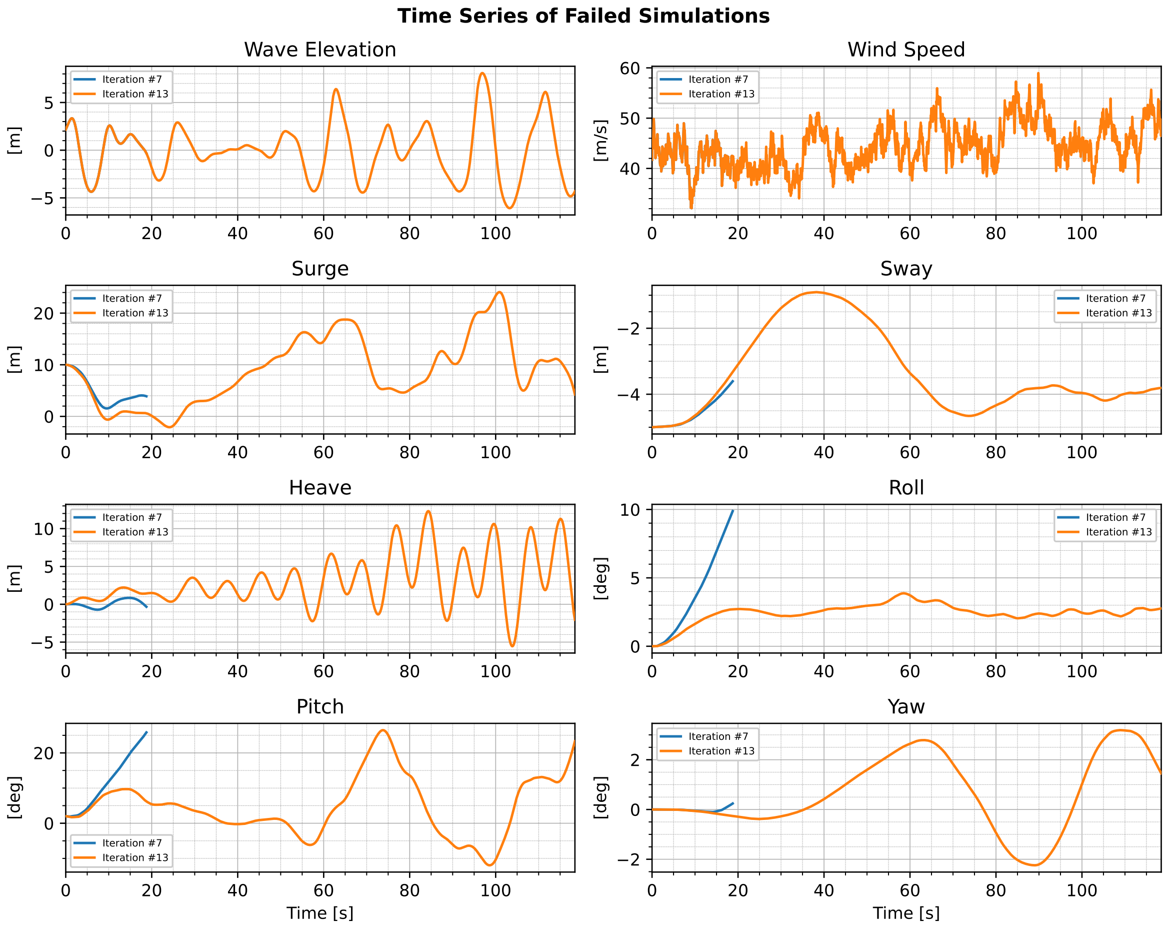

Figure 8.8: OpenFAST time series of failed iterations 7 and 13. Both curves represent the +8° yaw misalignment load case of DLC 6.1

Finally, an attempt was made to determine the natural periods of the six DOFs of the platform, using an approach to construct the RAO from the time series by dividing the cross-spectral density of the input and output signals by the auto-spectral density, and taking the ensemble average of all simulations [59]. However, this approach did not yield trustworthy results.

Firstly, the simulation duration was relatively short, and the wave spectrum too narrow, limiting the extent to which the platform's motion was excited. In order to obtain a better estimation of the RAOs, the platform response to a white-noise wave spectrum should have been simulated for longer simulation periods, to ensure broadband excitation of the hydrodynamic loads. And secondly, it is known that the presence of wind loading has an impact on the RAO curve. Given that the wind speed is different for each DLC, it would make more sense to specify an eigenfrequency range instead of identifying a distinct value.

8.2. Optimisation without SubDyn Coupling

The emphasis in the SubDyn-based substructure model has been on the capability to model the substructure as an elastic body rather than a rigid one, and to enable member-level loads to perform an ultimate loads and fatigue analysis. It has become evident from the previous section, that there is still room for improvement in the structural analysis. Both on the side of the OpenFAST software, but also in the post-processing methods. Furthermore, the structural analysis within the SubDyn model comes at a considerable expense in terms of CPU time required. This raises the incentive to re-run the same optimisation problem, this time without SubDyn coupling.

If the floating substructure is modelled rigidly in ElastoDyn following the approach described in section 6.2.2, the optimisation proceeds much faster, as the computational burden of analysing the structural dynamics of the platform is removed. Here, the maximum number of iterations was set to 30. The optimisation finishes in about 22.5 hours, which is considerably less than the case where SubDyn has been enabled. Figure 8.9 shows the convergence history of the optimisation problem. Comparing this figure to figure 8.1 reveals a nearly one-to-one match between the two optimisation problems. Furthermore, it is worth noting that the simulation crashes for exactly the same set of design variables.

Because the same seeds are used for generation of the wind- and wave signals, their time series remain identical for each simulation, resulting in a deterministic optimisation problem. Hence, the match in convergence behaviour between the two optimisation problems suggests that implementation of the structural properties (i.e. centre of mass, inertia, etc.) has been successful in the ElastoDyn-based substructure model. This also means that the latter may serve as a cheaper alternative for design optimisation of a floating platform, for example when the focus shifts towards optimising platform stability rather than structural mass minimisation. This highlights the flexibility of the developed optimisation framework, which can be extended to the desired level of detail.

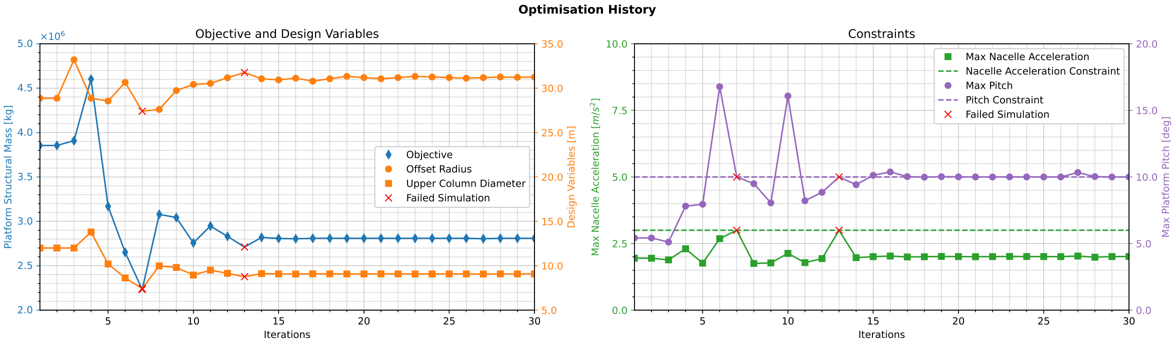

Figure 8.9: Convergence history of the optimisation problem without SubDyn coupling

8.3. Full Hour Simulation

In chapter 5, the OpenFAST setup has been described for a total simulation duration of 1000 seconds, with an exploitable window of ten minutes after trimming the data to remove the transient start-up phase. This choice was made to reduce the time needed to perform the OpenFAST simulations, and expedite the optimisation. To investigate the accuracy of the results compared to those obtained with a longer simulated time, an extended OpenFAST simulation has been performed, where the total simulation time has been extended to a full hour. The results of this simulation are plotted in figures 8.10 and 8.11.

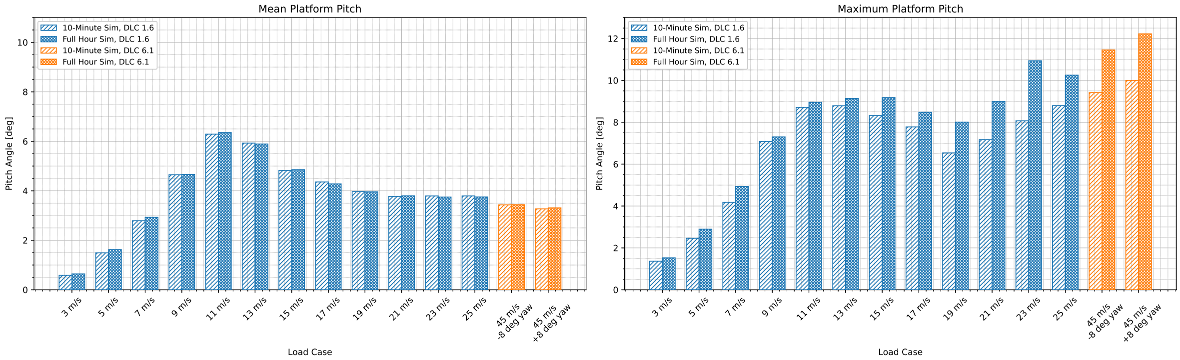

Figure 8.10: Average and maximum pitch values of the floating platform encountered for different DLCs for full hour simulations

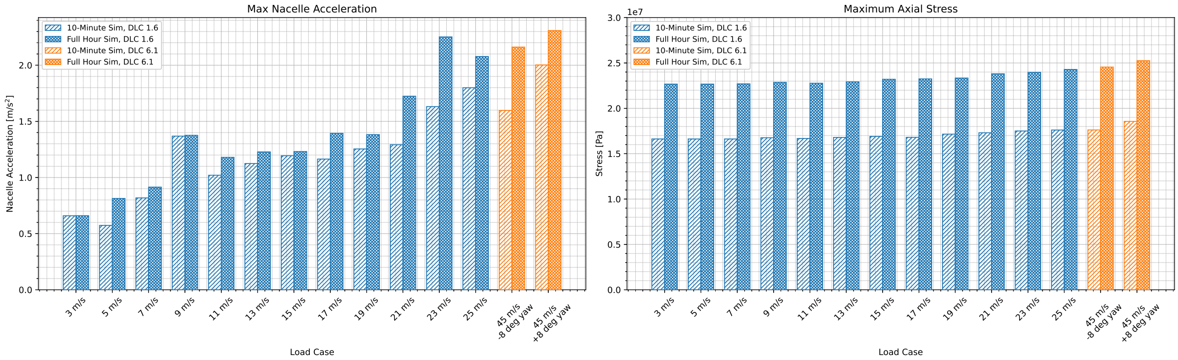

Figure 8.11: Maximum nacelle acceleration and axial stresses in the outer columns for different DLCs for full hour simulations

The above results show a trend where the maximum values for platform pitch, nacelle acceleration, and axial stress are systematically higher for each DLC when extending the simulation duration. While the maximum pitch value remained within the constraint for the ten-minute simulation, it exceeded the limit by over twenty percent during the full-hour simulation. This suggests that the assumption of ten-minute simulations being enough to adequately capture the overall system response and limit states is not valid. This poses a challenge, as extending the OpenFAST simulation window beyond ten minutes significantly increases the computational cost. However, a potential approach for future optimisations with ten-minute simulations could be to include a correcting factor into the values of the limit states.

8.4. Impact of Second Order Waves

Another interesting aspect to investigate is whether the floating platform response is significantly impacted by the inclusion of second-order waves. If they can be neglected, the simulations could potentially be expedited. Figures 8.12 to 8.14 show the results of two simulations with and without inclusion of second-order wave effects, for the initial design.

Looking at figure 8.12, there is a significant difference in the surge motion of the floating substructure. This is associated with the mean drift term, which is not captured by the first-order wave contributions. In effect, the surge excursion for the second-order wave case is higher. This phenomenon propagates to the fairlead tension of the main load-carrying line, for which the observed line tension is higher when considering second-order wave effects. Because of the coupling between the surge and pitch DOFs, there are minor differences visible in the pitch signal. The effect seems to be negligible in the context of this optimisation problem, however, especially considering the turbine performance indicators and internal stresses in the members.

It could thus be concluded that second-order wave effects are important to consider when performing mooring system co-design. However, as the mooring system properties are kept constant throughout the optimisation process in this project, it could be argued that it would suffice to only consider contributions from first order waves.

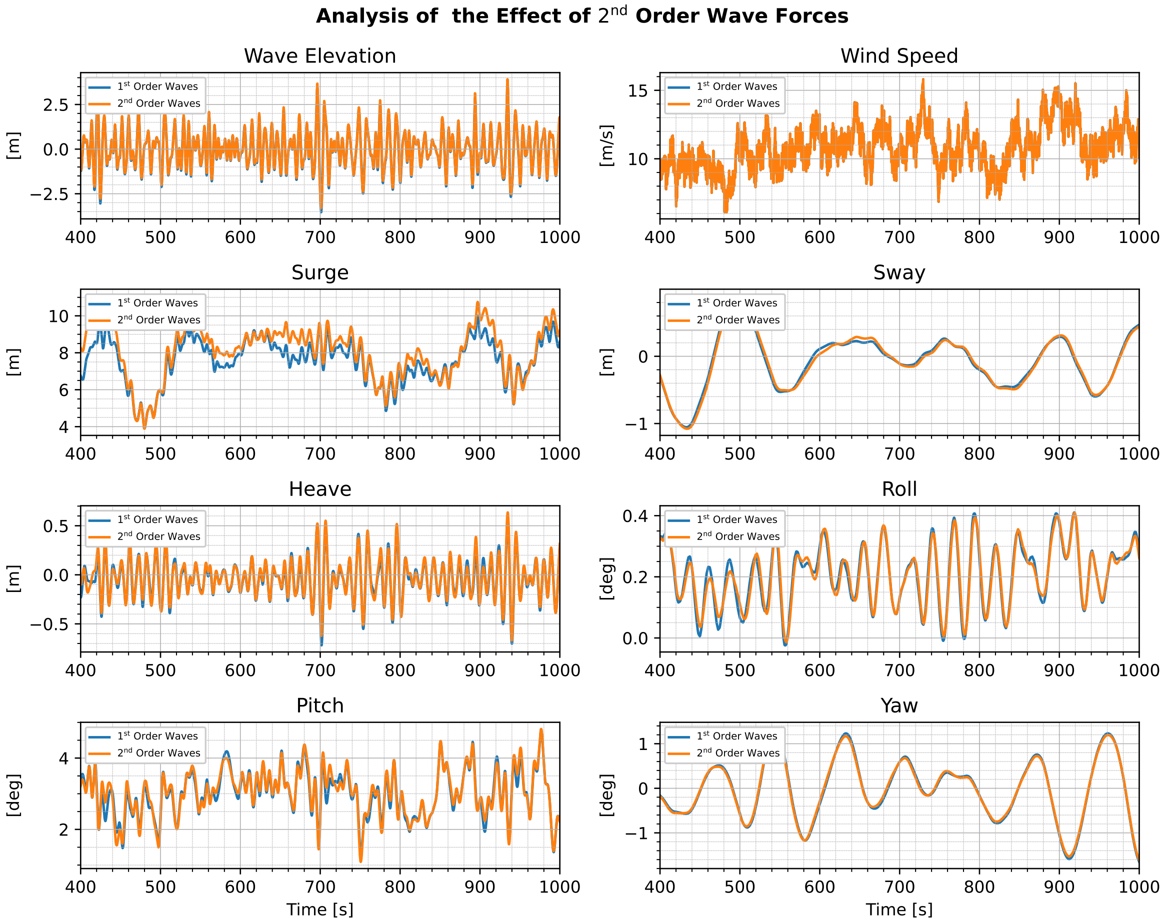

Figure 8.12: Comparison of the platform motion with and without inclusion of second-order wave effects, for the initial platform design at a mean wind speed of 11 $\mathrm{m\,s^{-1}}$ for DLC 1.6

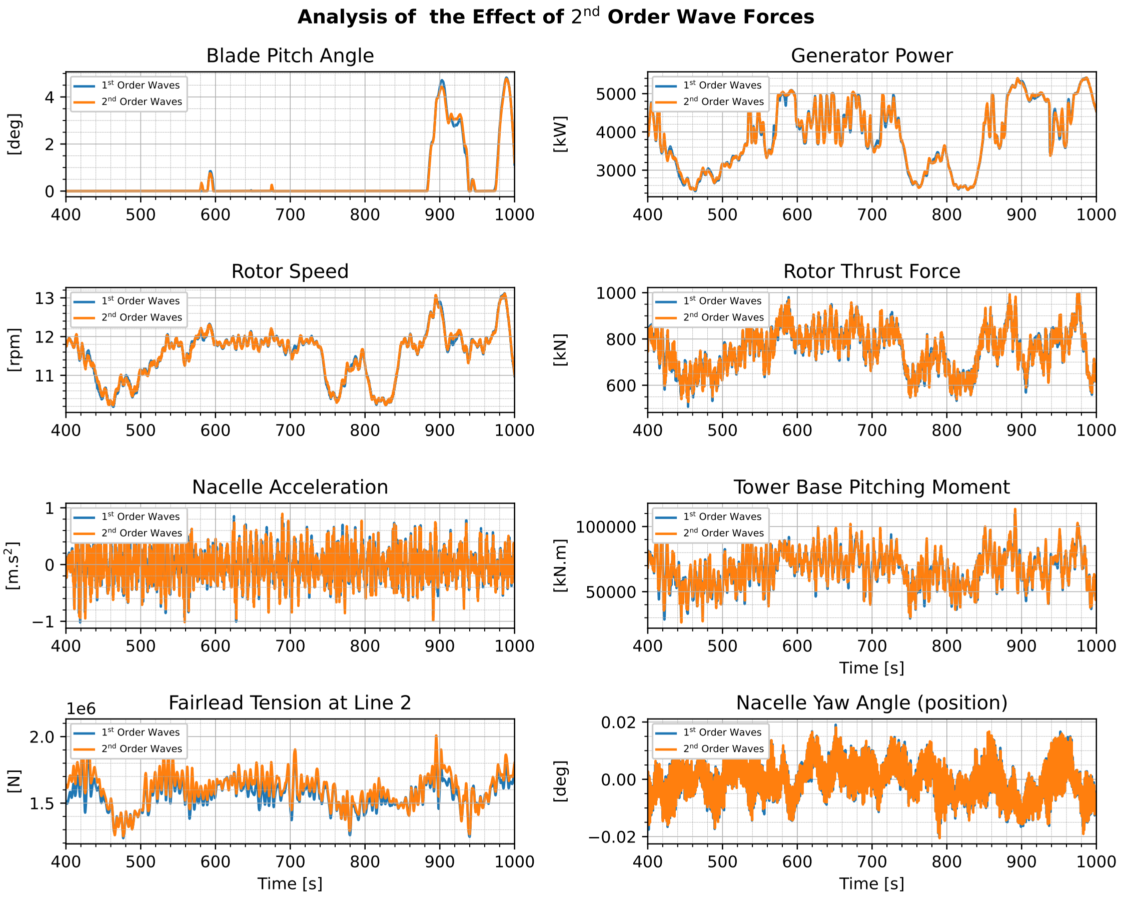

Figure 8.13: Comparison of the turbine performance indicators with and without inclusion of second-order wave effects, for the initial platform design at a mean wind speed of 11 m s^{-1} for DLC 1.6

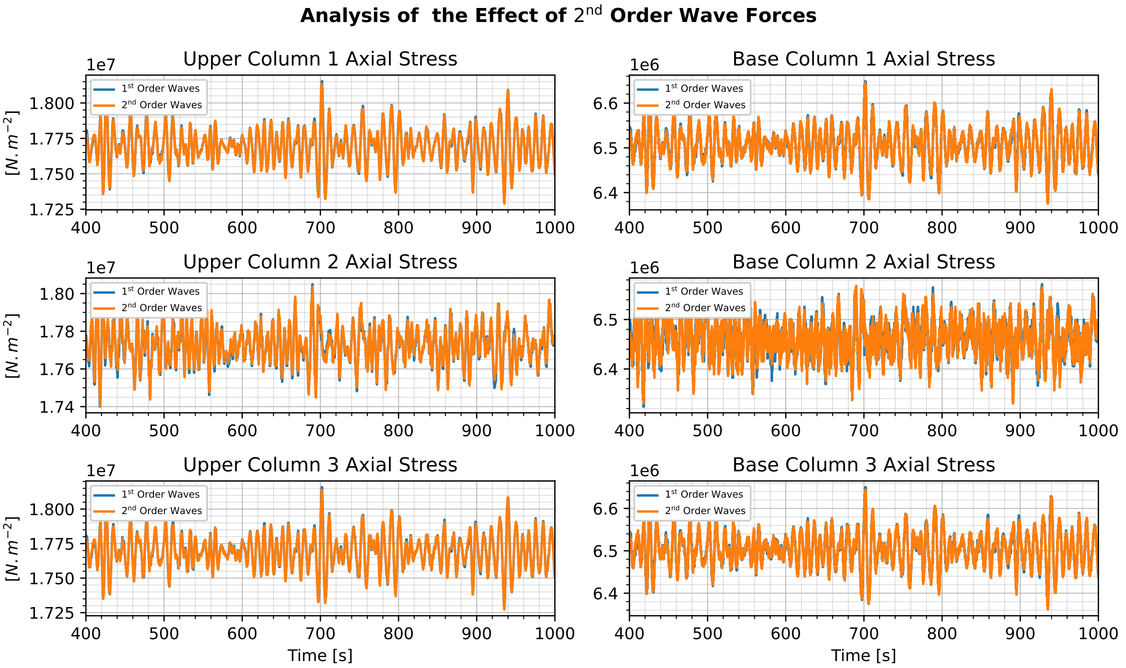

Figure 8.14: Comparison of the axial stresses in the outer columns with and without inclusion of second-order wave effects, for the initial platform design at a mean wind speed of 11 m s^{-1} for DLC 1.6

8.5. Pontoon Optimisation

As previously introduced in section 6.4.1, it was recognised in [15] that the pontoons and braces were reasonably sized for the model-scale platform but proved inadequate for the full-scale platform. This led to adjusting the scope of the structural analysis within the main optimisation problem. A comparison of the initial and optimal designs, as depicted in figure 8.3, reveals that the length of the pontoons and braces has been increased in the final design. Intuitively, this extension implies higher stresses in the slender components, which would require an increase of their cross-sectional dimensions to improve the bending stiffness.

To demonstrate the versatility of the developed optimisation framework, a new optimisation study is conducted, starting from the optimised platform design. The goal of this study is to redesign the diameter and wall thickness of the pontoons such that the overall observed fatigue damage and ultimate stresses inside the pontoons and braces remain within acceptable limits. The definition of this optimisation problem is similar to the one presented in section 3.2. However, the design variables are now the pontoon diameter and pontoon thickness, with appropriate boundaries. Additionally, the pitch and nacelle acceleration constraints have been replaced with a maximum allowable (yield) stress of 355 MPa and a maximum allowable fatigue damage of 0.75.

For this study, the structural members included in the output channels of SubDyn were the upper- and lower delta pontoons, and the y-pontoons and cross braces aligned with the negative x-direction. Furthermore, member flexibility was enabled in this optimisation by including six Craig-Bampton modes. The convergence history of the pontoon optimisation problem is illustrated in figure 8.15. The plot of the objective function demonstrates that in fact a substantial increase in pontoon diameter and thickness is necessary to mitigate fatigue damage and reduce the maximum stress inside the members, with higher structural mass as a result. It is worth noting that this would have been the case too if pontoon optimisation of the initial platform design had been done. In addition to this, it is observed from the figure that the fatigue damage shows a strong decline in the first ten iterations, but decreases only very slowly after this point.

Because of time constraints, the simulation was halted after 31 iterations. Nevertheless, it is apparent that additional iterations are necessary to achieve convergence towards the optimal design. A higher initial step in the design variables could also have helped in achieving faster convergence. However, by examining the trends of the design variables, it can be concluded that further increases in pontoon diameter and thickness are required to achieve a platform design that satisfies the fatigue damage constraint. It is important to note, that enlarging the pontoon diameter comes at a risk: as the outer dimensions of the pontoons increase relative to the typical wavelength, there will be a point where the strip theory is no longer applicable. This would require the pontoons to be modelled with NEMOH as well.

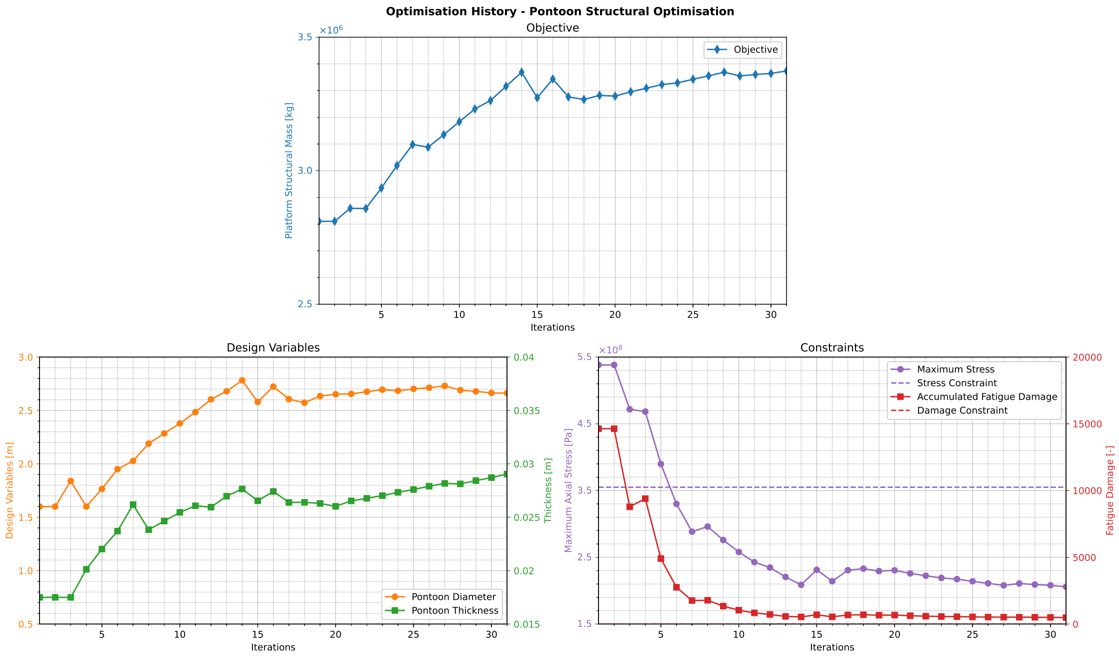

Figure 8.15: Convergence history of the pontoon optimisation problem, including 6 flexible modes

8.6. Limitations

Although the developed programming framework has demonstrated to be an effective method to obtain accurate optimisation results, a few limitations are still present and worth noting. Besides the ones already mentioned in the previous sections of the report, the most notable ones are summarised below.

- The structural analysis of platform members is currently limited to just nine members due to inherent limitations in the SubDyn module. In this project, an internal loads analysis was performed for each member by running the simulation multiple times with different member outputs. Subsequently, the internal forces were evaluated to identify the nine members with the most significant internal forces, which were then used in the optimisation process. This approach was suitable for the relatively simple load cases modelled, where wind and waves were co-directional and aligned with the platform's symmetry plane.

  However, this methodology may not be applicable to more complex load cases where wind and waves are not aligned. In such scenarios, it may be challenging to predict in advance which specific member experiences the highest loading or is subjected to cyclic loads resulting in high fatigue damage. Hence, there is a risk that the highest stresses and fatigue damage are not captured in a simulation which focuses on the outputs of just nine members.
- During the setup of the OpenFAST simulations, the model was prone to numerical instabilities. Understanding their underlying causes required extensive testing and tuning. For example, appropriate initial conditions were necessary in order to prevent the simulation from crashing at an early stage. But more importantly, defining accurate dimensions and properties (i.e. Young's modulus, mass etc.) for the structural members proved crucial; neglecting these aspects could lead to a stiff system without realising it. Hence, utilisation of the OpenFAST model within the optimisation framework requires a minimum amount of experience to troubleshoot the model in case of failure.

  Furthermore, it requires the initial platform design to be designed reasonably well to prevent crashes during the first iteration. Even if the first few iterations turn out successful, the OpenFAST model may be restrictive in terms of design exploration. This may be the case when simulations are aborted due to a bug or improper simulation setting as a results of the specific geometry modelled. This is because a failed simulation corresponds with a violation of the $failure$-flag constraint. This failure flag has been created to address the challenge of optimising a discontinuous function, where results are unavailable when the simulation crashes. However, by treating it as a boundary, the optimiser is constrained from fully exploring the design space beyond that point. A potential solution is to employ an evolutionary optimisation algorithm. These are better suited for optimising discontinuous functions, despite the fact that they are generally less efficient. Moreover, a trade-off may be necessary between population size and the number of DLCs simulated for each population member, to effectively allocate resources in terms of the limited availability of physical processors.
- The potential flow solution for the large-volume columns is an effective method for determining the overall hydrodynamic response of the platform. However, in the current approach, where the centre column and three outer columns are treated as a single rigid body, the global hydrodynamic loads are lumped to a single point. This prevents determination of the hydrodynamic load distribution along the individual members, which is essential for accurate internal force calculation. Currently, this can only be performed by the strip-theory method in HydroDyn. However, this is not suitable for the large volume columns.

  One way to address this issue is to model each large-volume column as individual potential-flow bodies with hydrodynamic interaction, which would provide a more accurate representation of the hydrodynamic load distribution. However, this approach adds complexity to setting up the NEMOH model and increases computational costs. Additionally, when using the rigid potential-flow representation, member flexibility should not be considered for the columns modelled with potential flow, as their deformation influences the hydrodynamic loads. Nonetheless, it is worth noting that large-volume columns tend to be stiff anyway, which mitigates this concern to some extent.

9

Conclusions

In this thesis, a programming framework has been developed to enable the design, analysis and optimisation of floating offshore wind substructures. The framework takes advantage of time-domain simulations in OpenFAST to analyse the fully coupled aero-hydro-servo-elastic response of the floating platform under a broad range of environmental and operational conditions, thereby enhancing the accuracy of the solution. The framework was developed exclusively using open-source software tools to ensure accessibility and reproducibility. It is entirely written in Python, which facilitated configuration of the simulation setup, seamless integration of various software modules, and post-processing of results. In addition, it offered good compatibility with the OpenMDAO optimisation library, utilising the COBYLA algorithm to perform gradient-free optimisation of the complex, non-linear problem. Leveraging the flexibility of the programming framework and the wealth of output data contained within the OpenFAST simulation results, this holistic approach offers opportunities to explore novel and cost-effective substructure designs with a high degree of reliability.

The focus of the project being on optimisation of the DeepCWind semi-submersible platform, not considering changes to the mooring system, control system or the wind turbine itself, most efforts were directed towards the hydrodynamic and structural model of this particular platform. A hybrid hydrodynamic model was created within HydroDyn to simulate the large-volume columns using a potential flow model, while representing the slender pontoons through Morison's equation. The potential flow model required modelling of the hydrodynamic coefficients with separate software in a pre-processing step, which was achieved by integrating the NEMOH software into the programming framework. The structural model was implemented in SubDyn, enabling computation of internal forces within the structural members and providing the possibility to perform extreme stress- and fatigue analysis in the post-processing stage. Although modelling of substructure flexibility has been made possible within SubDyn, the model in this project employs rigid members, because the flexible model did not always prove to be robust.

The main optimisation problem aimed at reducing the structural mass of the DeepCWind platform, while varying the diameter of the outer columns, and the distance between the centre column and the outer columns. Constraints were applied to limit the maximum pitch angle of the floating platform and the maximum allowable nacelle acceleration. An extra constraint was necessary to handle simulation failures that occurred when an unstable platform was modelled, causing OpenFAST to abort prematurely. Throughout the optimisation process, the platform response was simulated using 28 parallel OpenFAST simulations, each corresponding to a different load case with varying environmental conditions. Specifically, DLC 1.2 was modelled to conduct fatigue analysis and estimate the annual energy production, while DLCs 1.6, 6.1, and 6.3 were simulated for extreme value analysis. However, DLC 6.3 was excluded from the analysis due to instabilities observed in the OpenFAST results.

The optimisation results showed a significant reduction of 37.1% in the structural mass of the platform. The computational cost of the SubDyn coupling is substantial, and can be significantly decreased by employing an ElastoDyn-based rigid body model, for example when the focus of the optimisation is on platform stability, rather than weight minimisation. Although the static pitch of the optimal design is increased with respect to the initial design, the slight decrease of 0.84% in annual energy production is offset by the great mass reduction. In addition, the optimisation results showed that the pitch angle was the limiting constraint, which proved to be the highest for the load cases which exhibited the most severe environmental conditions in terms of wind speed, wave height and wave period. Extreme stresses and nacelle accelerations were also observed to achieve maximum values for these most severe load cases. This implies that other load cases with less severe metocean conditions could be excluded in future optimisation studies to reduce the computational effort. However, it remains uncertain how the optimisation would converge under scenarios involving misaligned wind and waves, because this is not taken into account in this study. In addition, it should be noted that if fatigue damage and annual energy production are to be considered in the analysis, a minimum distribution of operational load cases is required. Another important conclusion that is drawn from the results is that the mere ten-minute simulations proved to be insufficient to capture extreme values of the platform response in comparison with a simulation length of a full hour.

Although attempts have been made to include structural constraints in the optimisation, several challenges emerged when establishing the methods for structural analysis of the floating platform. Firstly, the number of output channels is limited within OpenFAST, which restricts the structural analysis to only nine members. Although for simple load cases it might be possible to identify the most critical members, this is less straightforward for complex load cases. Furthermore, a minimum amount of experience with OpenFAST is helpful to troubleshoot the model in the event of simulation failure, which proved to be necessary as the sub-structural model in the current version of OpenFAST is prone to numerical instabilities. While the optimisation process is designed to be able to cope with simulation failures, it may become overly constraining when incorrect simulation settings or an inadequate definition of the floating platform lead to such failures, limiting exploration of the full design space. Lastly, in order to accurately model the internal forces in the members, the potential flow model should be revised, modelling each column as a distinct potential flow body for a better distribution of hydrodynamic loads.

In conclusion, the developed programming framework, incorporating higher-fidelity analysis methods, provides an effective means to perform optimisation of floating substructures, taking into account a broad range of environmental conditions. However, its robustness can be further improved by addressing several aspects for further research and improvement, which are elaborated in the recommendations of chapter 10.

10

Recommendations

Building on the conclusions outlined in chapter 9, the following recommendations can be made, which can be subdivided into three categories: optimisation workflow, hydrodynamic modelling, and DLC simulation.

Optimisation Workflow

- The optimisation study in this thesis was focused on the DeepCWind semi-submersible platform, in conjunction with the 5 MW offshore reference turbine. To make it more universally applicable, methods should be incorporated to model different platform concepts, such as the spar-type or tension leg platform. Furthermore, the choice of the 5 MW reference turbine was based on its compatibility with the DeepCWind platform for verification purposes. However, considering the ongoing trend of increasing turbine size and capacity, it is recommended to include larger turbines in the optimisation problem, such as 15 MW or 20 MW, to provide a more representative analysis.

- Currently, the member definitions for the floating substructure must be provided manually in the configuration script, and once defined, members cannot be added or removed during the optimisation process. To allow experimenting with various design concepts, it is advised to incorporate a feature in the code that can automatically modify member definitions. However, it is acknowledged that this may be challenging, depending on the desired flexibility.

- Regarding the structural analysis, it is recommended to extend the methods to compute not only axial stress due to the axial forces but also the composite internal stresses resulting from forces and moments in the other directions: shear, bending, and torsion. Although this will inevitably require higher memory usage and processing capacity, it will provide a more accurate representation of internal stresses within the members.

- Given the lengthy OpenFAST simulations necessary to perform a thorough analysis of the FOWT system, the programming framework might benefit from ways to reduce the required CPU time. A possible way to achieve this is for example by employing a multi-fidelity approach, where the platform design is adjusted and analysed using simplified OpenFAST models (e.g. by disabling flexible DOFs of various components of the FOWT), and perform a higher-fidelity analysis only every i-th iteration.

- Lastly, concerning the optimisation algorithm, it is advised to investigate the impact of utilising different optimisation algorithms. For example, a genetic algorithm may be better suited to find a global optimum in the case where the COBYLA algorithm encounters discontinuities in the constraint functions due to simulation failures. However, this likely necessitates a trade-off between number of simulated DLCs and population size, because of the limited availability of CPU cores.

Hydrodynamic Model

- To address the concern that strip-theory becomes no longer applicable to pontoons and braces when their diameter grows in size, an additional feature could be added to the NEMOH wrapper script. This feature should determine for each member, based on their physical dimensions, whether it should be included in the potential flow model, or represented using Morison's equation in HydroDyn. Subsequently, the members should be meshed and analysed according to their categorisation and included in either the potential flow model or HydroDyn.

- For a more accurate representation of member internal forces, it is recommended to explore the option of modelling all large-volume columns as individual potential flow bodies. This possibility has been made available in the latest versions of both NEMOH and OpenFAST, including hydrodynamic interaction. This approach, as opposed to lumping hydrodynamic loads to a single point, enables the distribution of hydrodynamic loads across the different columns, leading to an improved representation of hydrodynamic loading. Nevertheless, it is important to evaluate whether the increased complexity is justified for the particular application.

DLC Simulation

- To address the issue of ten-minute simulations being insufficient to capture the extreme values of the platform response, a follow-up investigation is recommended. This study should include a series of simulations with multiple seeds and extended time frames to establish a correlation between ten-minute and full-hour simulations. This correlation should enable a safety factor to be imposed on the ten-minute simulations, in order to align them with the results obtained from the full-hour simulations.

- In order to further investigate the influence of particular DLCs on the optimal platform design, it is advised to study the simulation results in response to misaligned wind and waves, with heading angles that don't align with the platform symmetry plane. A comprehensive analysis will provide a more thorough understanding of the impact of extreme load cases, resulting in a better choice of critical load cases to incorporate into the optimisation process.

References

[1] International Energy Agency, “Offshore wind outlook 2019,” IEA, Paris, 2019. [Online]. Available: `https://www.iea.org/reports/offshore-wind-outlook-2019`.

[2] IRENA, “Floating foundations: A game changer for offshore wind power,” International Renewable Energy Agency, Abu Dhabi, 2016, pp. 1–8.

[3] R. James and M. Costa Ros, “Floating offshore wind: Market and technology review,” Carbon Trust, London, Jun. 2015.

[4] DNV GL, “Floating wind: The power to commercialize - insights and reasons for confidence,” DNV GL, Høvik, Norway, 2020. [Online]. Available: `https://www.dnv.com/focus-areas/floating-offshore-wind/commercialize-floating-wind-report.html`, (accessed Jan. 12, 2023).

[5] A. Ioannou, Y. Liang, M. L. Jalón, and F. P. Brennan, “A preliminary parametric techno-economic study of offshore wind floater concepts,” *Ocean Engineering*, vol. 197, Feb. 2020, ISSN: 00298018. DOI: `10.1016/j.oceaneng.2020.106937`.

[6] A. Ojo, M. Collu, and A. Coraddu, “Multidisciplinary design analysis and optimization of floating offshore wind turbine substructures: A review,” *Ocean Engineering*, vol. 266, Dec. 2022, ISSN: 00298018. DOI: `10.1016/j.oceaneng.2022.112727`.

[7] G. Barter, A. Robertson, and W. Musial, “A systems engineering vision for floating offshore wind cost optimization,” *Renewable Energy Focus*, vol. 34, pp. 1–16, 2020, ISSN: 17550084. DOI: `10.1016/j.ref.2020.03.002`.

[8] International Electrotechnical Commission, *IEC TS 61400-3-2:2019 Wind energy generation systems–Part 3-2: Design requirements for floating offshore wind turbines*, 2019. [Online]. Available: `https://webstore.iec.ch/publication/29244`, (accessed Nov. 18, 2023).

[9] M. Leimeister, A. Kolios, and M. Collu, “Critical review of floating support structures for offshore wind farm deployment,” *Journal of Physics: Conference Series*, vol. 1104, 2018, ISSN: 17426596. DOI: `10.1088/1742-6596/1104/1/012007`.

[10] K. Longridge. “Floating wind: What are the mooring options?” (2020), [Online]. Available: `https://acteon.com/blog/floating-wind-mooring-options/`. (accessed Feb. 16, 2023).

[11] J. Taboada, “Comparative analysis review on floating offshore wind foundations (FOWF),” *Ingeniería naval*, pp. 75–87, 949 2016, ISSN: 0020-1073. [Online]. Available: `https://sectormaritimo.es/comparative-analysis-review-on-floating-offshore-wind-foundations-fowf`, (accessed Jan. 12, 2023).

[12] Vryhof, *Vryhof Manual: The Guide to Anchoring*, 8th ed. 2018, ISBN: 9789090288017. [Online]. Available: `https://insights.vryhof.com/download-the-vryhof-manual`, (accessed Mar. 1, 2023).

[13] R. M. Raaijmakers, “The influence of mooring lines on the damping of low frequency motions of moored offshore structures,” Delft University of Technology, Netherlands, 1995. [Online]. Available: `https://repository.tudelft.nl/islandora/object/uuid%5C%3A0c78579c-a922-44cb-ab36-65a846f0ff53`, (accessed Mar. 1, 2023).

[14] J. Jonkman, “Definition of the floating system for phase iv of OC3,” National Renewable Energy Laboratory, Golden, Colorado, Tech. Rep. TP-500-47535, May 2010, (accessed Jun. 28, 2023).

[15] A. Robertson, J. Jonkman, M. Masciola, *et al.*, “Definition of the semisubmersible floating system for phase ii of oc4,” National Renewable Energy Laboratory, Golden, Colorado, Tech. Rep. TP-5000-60601, Sep. 2014.

[16] C. Allen, A. Viselli, H. D. A. Goupee, *et al.*, “Definition of the UMaine VolturnUS-S reference platform developed for the IEA Wind 15-Megawatt offshore reference wind turbine technical report,” National Renewable Energy Laboratory, Golden, Colorado, Tech. Rep. TP-5000-76773, 2020. [Online]. Available: `https://www.nrel.gov/docs/fy20osti/76773.pdf`, (accessed Apr. 12, 2023).

[17] A. Krieger, G. K. V. Ramachandran, L. Vita, *et al.*, “Qualification of innovative floating substructures for 10mw wind turbines and water depths greater than 50m,” 2015.

[18] J. Aldersey-Williams and T. Rubert, “Levelised cost of energy - a theoretical justification and critical assessment,” *Energy Policy*, vol. 124, pp. 169–179, Jan. 2019, ISSN: 03014215. DOI: `10.1016/j.enpol.2018.10.004`.

[19] UK Government (Department of Business, Energy & Industrial Strategy), “Electricity generation costs 2020,” 2020. [Online]. Available: `https://www.gov.uk/government/publications/beis-electricity-generation-costs-2020`, (accessed Mar. 15, 2023).

[20] A. Myhr, C. Bjerkseter, A. Ågotnes, and T. A. Nygaard, “Levelised cost of energy for offshore floating wind turbines in a lifecycle perspective,” *Renewable Energy*, vol. 66, pp. 714–728, 2014, ISSN: 09601481. DOI: `10.1016/j.renene.2014.01.017`.

[21] S. Santhakumar, C. Heuberger-Austin, H. Meerman, and A. Faaij, “Technological learning potential of offshore wind technology and underlying cost drivers,” 2022. DOI: `10.21203/rs.3.rs-1298062/v1`.

[22] J. Bosch, I. Staffell, and A. D. Hawkes, “Global levelised cost of electricity from offshore wind,” *Energy*, vol. 189, Dec. 2019, ISSN: 03605442. DOI: `10.1016/j.energy.2019.116357`.

[23] C. Maienza, A. M. Avossa, F. Ricciardelli, D. Coiro, G. Troise, and C. T. Georgakis, “A life cycle cost model for floating offshore wind farms,” *Applied Energy*, vol. 266, p. 114 716, 2020, ISSN: 03062619. DOI: `10.1016/j.apenergy.2020.114716`.

[24] L. Castro-Santos and V. Diaz-Casas, “Life-cycle cost analysis of floating offshore wind farms,” *Renewable Energy*, vol. 66, pp. 41–48, 2014, ISSN: 09601481. DOI: `10.1016/j.renene.2013.12.002`.

[25] M. Lerch, M. De-Prada-Gil, C. Molins, and G. Benveniste, “Sensitivity analysis on the levelized cost of energy for floating offshore wind farms,” *Sustainable Energy Technologies and Assessments*, vol. 30, pp. 77–90, 2018, ISSN: 22131388. DOI: `10.1016/j.seta.2018.09.005`.

[26] L. Castro-Santos and V. Diaz-Casas, “Economic influence of location in floating offshore wind farms,” *Ocean Engineering*, vol. 107, pp. 13–22, 2015, ISSN: 00298018. DOI: `10.1016/j.oceaneng.2015.07.025`.

[27] A. Martinez and G. Iglesias, “Mapping of the levelised cost of energy for floating offshore wind in the european atlantic,” *Renewable and Sustainable Energy Reviews*, vol. 154, Feb. 2022, ISSN: 18790690. DOI: `10.1016/j.rser.2021.111889`.

[28] A. Ghigo, L. Cottura, R. Caradonna, G. Bracco, and G. Mattiazzo, “Platform optimization and cost analysis in a floating offshore wind farm,” *Journal of Marine Science and Engineering*, vol. 8, pp. 1–26, 11 Nov. 2020, ISSN: 20771312. DOI: `10.3390/jmse8110835`.

[29] V. Sykes, M. Collu, and A. Coraddu, “A review and analysis of optimisation techniques applied to floating offshore wind platforms,” *Ocean Engineering*, vol. 285, p. 115 247, 2023, ISSN: 0029-8018. DOI: `https://doi.org/10.1016/j.oceaneng.2023.115247`.

[30] S. Dou, A. Pegalajar-Jurado, S. Wang, H. Bredmose, and M. Stolpe, “Optimization of floating wind turbine support structures using frequency-domain analysis and analytical gradients,” vol. 1618, IOP Publishing Ltd, Sep. 2020. DOI: `10.1088/1742-6596/1618/4/042028`.

[31] N. Pollini, A. Pegalajar-Jurado, S. Dou, H. Bredmose, and M. Stolpe, “Gradient-based optimization of a 15 mw wind turbine spar floater,” vol. 2018, IOP Publishing Ltd, Sep. 2021. DOI: `10.1088/1742-6596/2018/1/012032`.

[32] M. Hall, B. Buckham, and C. Crawford, “Evaluating the importance of mooring line model fidelity in floating offshore wind turbine simulations,” *Wind Energy*, vol. 17, pp. 1835–1853, 12 Dec. 2014, ISSN: 10991824. DOI: `10.1002/we.1669`.

[33] D. Zhao, N. Han, E. Goh, J. Cater, and A. Reinecke, “Chapter 5 - offshore wind turbine aerodynamics modelling and measurements,” in *Wind Turbines and Aerodynamics Energy Harvesters*, Academic Press, 2019, pp. 373–400, ISBN: 978-0-12-817135-6. DOI: `https://doi.org/10.1016/B978-0-12-817135-6.00005-3`.

[34] M. Borg, A. M. Hansen, and H. Bredmose, “Floating substructure flexibility of large-volume 10MW offshore wind turbine platforms in dynamic calculations,” 8, vol. 753, 2016. DOI: `10.1088/1742-6596/753/8/082024`.

[35] National Renewable Energy Laboratory, *OpenFAST v3.4.1 documentation*, Feb. 2023. [Online]. Available: `https://openfast.readthedocs.io/en/v3.4.1/`, (accessed Jun. 28, 2023).

[36] M. J. Todd, "Analysis of interior-point methods for linear programming problems with variable upper bounds," in *Advances in Optimization and Numerical Analysis*, S. Gomez and J.-P. Hennart, Eds. Dordrecht: Springer Netherlands, 1994, pp. 1–23, ISBN: 978-94-015-8330-5. DOI: `10.1007/978-94-015-8330-5_1`.

[37] M. Leimeister, A. Kolios, and M. Collu, "Development of a framework for wind turbine design and optimization," *Modelling*, vol. 2, no. 1, pp. 105–128, 2021, ISSN: 2673-3951. DOI: `10.3390/modelling2010006`.

[38] OpenFAST v3.4.1, Accessed Apr. 8, 2023. Available at `https://github.com/openfast/openfast/`.

[39] R. Kurnia, G. Ducrozet, and J.-C. Gilloteaux, "Second Order Difference- and Sum-Frequency Wave Loads in the Open-Source Potential Flow Solver NEMOH," International Conference on Offshore Mechanics and Arctic Engineering, vol. Volume 5A: Ocean Engineering, Jun. 2022, V05AT06A019. DOI: `10.1115/OMAE2022-79163`.

[40] J. S. Gray, J. T. Hwang, J. R. R. A. Martins, K. T. Moore, and B. A. Naylor, "OpenMDAO: An Open-Source Framework for Multidisciplinary Design, Analysis, and Optimization," *Structural and Multidisciplinary Optimization*, vol. 59, pp. 1075–1104, 4 2019. DOI: `10.1007/s00158-019-02211-z`.

[41] M. B. Bessone, M. Zaaijer, D. V. Terzi, K. Dykes, E. Jump, and A. Vire, "Including installation logistics costs in the optimal sizing of semi-submersibles for floating wind farms," *Journal of Physics: Conference Series*, vol. 2265, 4 2022, ISSN: 17426596. DOI: `10.1088/1742-6596/2265/4/042018`.

[42] A. Ojo, M. Collu, and A. Coraddu, "Parametrisation scheme for multidisciplinary design analysis and optimisation of a floating offshore wind turbine substructure - oc3 5mw case study," vol. 2265, Institute of Physics, Jun. 2022. DOI: `10.1088/1742-6596/2265/4/042009`.

[43] J. M. J. Journée and W. W. Massie, *Offshore Hydromechanics*. Delft University of Technology, 2008, vol. 2.

[44] R. Kurnia and G. Ducrozet, *NEMOH v3.0 User Manual*. Ecole Centrale de Nantes, Dec. 2022. [Online]. Available: `https://www.researchgate.net/publication/366166860_NEMOH_v30_User_Manual`, (accessed Jul. 13, 2023).

[45] J. Jonkman, E. Branlard, M. Hall, G. Hayman, A. Platt, and A. Robertson, "Implementation of substructure flexibility and member-level load capabilities for floating offshore wind turbines in openfast," National Renewable Energy Laboratory, Golden, Colorado, TP-5000-76822, 2020.

[46] L. E. S. Stieng and M. Muskulus, "Load case reduction for offshore wind turbine support structure fatigue assessment by importance sampling with two-stage filtering," *Wind Energy*, vol. 22, no. 11, pp. 1472–1486, 2019. DOI: `https://doi.org/10.1002/we.2382`.

[47] D. Matha, F. Sandner, and D. Schlipf, "Efficient critical design load case identification for floating offshore wind turbines with a reduced nonlinear model," in *Journal of Physics Conference Series*, ser. Journal of Physics Conference Series, vol. 555, Dec. 2014, 012069, p. 012 069. DOI: `10.1088/1742-6596/555/1/012069`.

[48] B. J. Jonkman, "TurbSim user's guide: Version 1.5," National Renewable Energy Laboratory, Golden, Colorado, Tech. Rep. TP-500-46198, 2009. [Online]. Available: `https://www.nrel.gov/docs/fy09osti/46198.pdf`, (accessed Aug. 22, 2023).

[49] M. Mathiesen, A. K. Meyer, and B. Kvengedal, "Hywind Buchan Deep metocean design basis," Statoil, Tech. Rep. RE2014-002, May 2014. [Online]. Available: `https://marine.gov.scot/sites/default/files/metocean_design_basis_hywind_buchan_deep_mdb_rev2_0.pdf`, (accessed Aug. 7, 2023).

[50] T. Burton, N. Jenkins, D. Sharpe, and E. Bossanyi, *Wind energy handbook*. John Wiley & Sons, 2011, pp. 14–15, ISBN: 9781119992714. DOI: `10.1002/9781119992714`.

[51] J. Jonkman, S. Butterfield, W. Musial, and G. Scott, "Definition of a 5-MW reference wind turbine for offshore system development," National Renewable Energy Laboratory, Golden, Colorado, Tech. Rep. TP-500-38060, Feb. 2009. [Online]. Available: `https://www.nrel.gov/docs/fy09osti/38060.pdf`, (accessed Jun. 14, 2023).

[52] J. Jonkman, [Jason.Jonkman], *FAST integrator, step size & precision*, Forum Post, 2010. [Online]. Available: `https://forums.nrel.gov/t/fast-integrator-step-size-precision/247/3`, (accessed Oct. 2, 2023).

[53] J. Nunemaker and N. Abbas, *pCrunch v1.0.5*, Accessed Aug. 4, 2023. Available at `https://github.com/NREL/pCrunch`.

[54] G. J. Hayman, *Mlife theory manual for version 1.00*, 2012. [Online]. Available: `https://www.nrel.gov/wind/nwtc/assets/pdfs/mlife-theory.pdf`, (accessed Oct. 16, 2023).

[55] DNV GL, "Fatigue design of offshore steel structures," DNV GL, Recommended Practice DNVGL-RP-C203, Apr. 2016.

[56] R. Kurnia and G. Ducrozet, "Computation of second-order wave loads on floating offshore wind turbine platforms in bi-chromatic bi-directional waves using open-source potential flow solver NEMOH.," ser. 18èmes Journées de l'Hydrodynamique, 2022. [Online]. Available: `https://jh2022.sciencesconf.org/420480`, (accessed Jun. 18, 2023).

[57] Y.-H. Lin and C.-H. Yang, "Hydrodynamic simulation of the semi-submersible wind float by investigating mooring systems in irregular waves," *Applied Sciences*, vol. 10, no. 12, 2020, ISSN: 2076-3417. DOI: `10.3390/app10124267`.

[58] T. Kelly, I. Zabala, Y. Peña-Sanchez, *et al.*, "A post-processing technique for addressing irregular frequencies and other issues in the results from bem solvers," 2021. [Online]. Available: `https://mural.maynoothuniversity.ie/16248/`, (accessed Nov. 20, 2023).

[59] G. K. V. Ramachandran, A. Robertson, J. M. Jonkman, and M. D. Masciola, "Investigation of response amplitude operators for floating offshore wind turbines: Preprint," Jul. 2013. [Online]. Available: `https://www.osti.gov/biblio/1087800`, (accessed Aug. 4, 2023).

A

OpenFAST Input Files

A.1. SubDyn

```
----------- SubDyn MultiMember Support Structure Input File ------------
OC4           ’Semisubmersible’ - SubStructure Input File.
------------------------- SIMULATION CONTROL ---------------------------------
True          Echo          - Echo input data to "<rootname>.SD.ech" (flag)
"DEFAULT"     SDdeltaT      - Local Integration Step. If "default", the glue-code step will be used.
3             IntMethod     - Integration Method [1/2/3/4 = RK4/AB4/ABM4/AM2].
True          SttcSolve     - Solve dynamics about static equilibrium point
True          GuyanLoadCorrection - Include extra moment from lever arm at interface
                                    and rotate FEM for floating.
-------------------- FEA and CRAIG-BAMPTON PARAMETERS---------------------------
3             FEMMod        - FEM switch: element model in the FEM. [3= 2-node Timoshenko]
1             NDiv          - Number of sub-elements per member
True          CBMod         - [T/F] If True perform C-B reduction, else full FEM dofs will be retained.
0             Nmodes        - Number of internal modes to retain. If Nmodes=0 --> Guyan Reduction.
1             JDampings     - Damping Ratios for each retained mode (% of critical)
0             GuyanDampMod  - Guyan damping {0=none, 1=Rayleigh Damping, 2=user specified 6x6 matrix}
0.0, 0.0      RayleighDamp  - Mass and stiffness proportional damping coefficients [Rayleigh Damping = 1]
6             GuyanDampSize - Guyan damping matrix (6x6) [only if GuyanDampMod=2]
              0             0              0              0              0              0
              0             0              0              0              0              0
              0             0              0              0              0              0
              0             0              0              0              0              0
              0             0              0              0              0              0
              0             0              0              0              0              0
---- STRUCTURE JOINTS: joints connect structure members (~Hydrodyn Input File) ---
49    NJoints    -    Number of joints (-)
JointID  JointXss  JointYss  JointZss  JointType  JointDirX  JointDirY  JointDirZ  JointStiff
(-)        (m)        (m)        (m)      (-)        (-)        (-)        (-)      (Nm/rad)
1        0.0000     0.0000    10.0000      1          0          0          0          0
2        0.0000     0.0000   -20.0000      1          0          0          0          0
3        0.0000     0.0000     9.9990      1          0          0          0          0
4        0.0000     0.0000   -17.0000      1          0          0          0          0
5      -28.8675     0.0000    12.0000      1          0          0          0          0
6      -28.8675     0.0000   -14.0000      1          0          0          0          0
7      -28.8675     0.0000   -20.0000      1          0          0          0          0
8      -22.8675     0.0000     9.9990      1          0          0          0          0
9      -23.6714    -3.0000     9.9990      1          0          0          0          0
10     -23.6714     3.0000     9.9990      1          0          0          0          0
11      -3.2500     0.0000     9.9990      1          0          0          0          0
12     -22.8675     0.0000     9.1990      1          0          0          0          0
13     -28.8675     0.0000     9.9990      1          0          0          0          0
14     -16.8675     0.0000   -17.0000      1          0          0          0          0
15     -18.4752    -6.0000   -17.0000      1          0          0          0          0
16     -18.4752     6.0000   -17.0000      1          0          0          0          0
17      -3.2500     0.0000   -17.0000      1          0          0          0          0
18      -3.2500     0.0000   -16.2000      1          0          0          0          0
19     -28.8675     0.0000   -17.0000      1          0          0          0          0
20      14.4338   -25.0000    12.0000      1          0          0          0          0
21      14.4338   -25.0000   -14.0000      1          0          0          0          0
22      14.4338   -25.0000   -20.0000      1          0          0          0          0
23      11.4338   -19.8038     9.9990      1          0          0          0          0
24      14.4338   -19.0000     9.9990      1          0          0          0          0
25       9.2376   -22.0000     9.9990      1          0          0          0          0
26       1.6250    -2.8146     9.9990      1          0          0          0          0
27      11.4338   -19.8038     9.1990      1          0          0          0          0
28      14.4338   -25.0000     9.9990      1          0          0          0          0
29       8.4338   -14.6077   -17.0000      1          0          0          0          0
30      14.4338   -13.0000   -17.0000      1          0          0          0          0
```

```
31       4.0415   -19.0000   -17.0000      1          0          0          0          0
32       1.6250    -2.8146   -17.0000      1          0          0          0          0
33       1.6250    -2.8146   -16.2000      1          0          0          0          0
34      14.4338    25.0000   -17.0000      1          0          0          0          0
35      14.4338    25.0000    12.0000      1          0          0          0          0
36      14.4338    25.0000   -14.0000      1          0          0          0          0
37      14.4338    25.0000   -20.0000      1          0          0          0          0
38      11.4338    19.8038     9.9990      1          0          0          0          0
39       9.2376    22.0000     9.9990      1          0          0          0          0
40      14.4338    19.0000     9.9990      1          0          0          0          0
41       1.6250     2.8146     9.9990      1          0          0          0          0
42      11.4338    19.8038     9.1990      1          0          0          0          0
43      14.4338    25.0000     9.9990      1          0          0          0          0
44       8.4338    14.6077   -17.0000      1          0          0          0          0
45       4.0415    19.0000   -17.0000      1          0          0          0          0
46      14.4338    13.0000   -17.0000      1          0          0          0          0
47       1.6250     2.8146   -17.0000      1          0          0          0          0
48       1.6250     2.8146   -16.2000      1          0          0          0          0
49      14.4338    25.0000   -17.0000      1          0          0          0          0
------------------ BASE REACTION JOINTS: 1/0 for Locked/Free DOF @ each Reaction Node -----------------
0             NReact        - Number of Joints with reaction forces
RJointID      RctTDXss      RctTDYss     RctTDZss      RctRDXss      RctRDYss      RctRDZss     SSIfile
(-)            (flag)        (flag)       (flag)        (flag)        (flag)        (flag)       (string)
---------------- INTERFACE JOINTS: 1/0 for Locked (to the TP)/Free DOF @each Interface Joint  ---------
1             NInterf       - Number of interface joints locked to the Transition Piece (TP)
IJointID      ItfTDXss      ItfTDYss     ItfTDZss      ItfRDXss      ItfRDYss      ItfRDZss
(-)            (flag)        (flag)       (flag)        (flag)        (flag)        (flag)
1                1             1            1             1             1             1
----------------------------------- MEMBERS --------------------------------------
60            NMembers      - Number of frame members
MemberID      MJointID1     MJointID2    MPropSetID1   MPropSetID2   MType
(-)             (-)           (-)          (-)           (-)           (-)
1                 1             3            1             1             1
2                 3             4            1             1             1
3                 4             2            1             1             1
4                 5            13            3             3             1
5                13             6            3             3             1
6                 6            19            2             2             1
7                19             7            2             2             1
8                20            28            3             3             1
9                28            21            3             3             1
10               21            34            2             2             1
11               34            22            2             2             1
12               35            43            3             3             1
13               43            36            3             3             1
14               36            49            2             2             1
15               49            37            2             2             1
16                8            11            4             4             1
17               23            26            4             4             1
18               38            41            4             4             1
19               14            17            4             4             1
20               29            32            4             4             1
21               44            47            4             4             1
22                9            25            4             4             1
23               24            40            4             4             1
24               39            10            4             4             1
25               15            31            4             4             1
26               30            46            4             4             1
27               45            16            4             4             1
28               12            18            4             4             1
29               27            33            4             4             1
30               42            48            4             4             1
31                8            13            1             1             3
32                9            13            1             1             3
33               10            13            1             1             3
34               12            13            1             1             3
35               14            19            1             1             3
36               15            19            1             1             3
37               16            19            1             1             3
38               23            28            1             1             3
39               24            28            1             1             3
40               25            28            1             1             3
```

```
41              27            28            1             1             3
42              29            34            1             1             3
43              30            34            1             1             3
44              31            34            1             1             3
45              38            43            1             1             3
46              39            43            1             1             3
47              40            43            1             1             3
48              42            43            1             1             3
49              44            49            1             1             3
50              45            49            1             1             3
51              46            49            1             1             3
52               3            11            1             1             3
53               3            26            1             1             3
54               3            41            1             1             3
55               4            17            1             1             3
56               4            32            1             1             3
57               4            47            1             1             3
58               4            18            1             1             3
59               4            33            1             1             3
60               4            48            1             1             3
-------- MEMBER X-SECTION PROPERTY data 1/2 [isotropic material for now: circular members] ------------
4             NPropSets     - Number of structurally unique x-sections
PropSetID     YoungE         ShearG       MatDens       XsecD         XsecT
(-)           (N/m2)        (N/m2)        (kg/m3)        (m)           (m)
1            210.00E+11    80.769E+09      7850          6.5         0.0300
2            210.00E+11    80.769E+09      7850         24.0         0.0600
3            210.00E+11    80.769E+09      7850         12.0         0.0600
4            210.00E+11    80.769E+09      7850          1.6         0.0175
------- MEMBER X-SECTION PROPERTY data 2/2 [isotropic material for now: non-circular members] ---------
0             NXPropSets    - Number of structurally unique non-circular x-sections
PropSetID  YoungE   ShearG    MatDens    XsecA   XsecAsx   XsecAsy   XsecJxx   XsecJyy   XsecJ0
(-)        (N/m2)   (N/m2)    (kg/m3)    (m2)     (m2)      (m2)      (m4)      (m4)      (m4)
-------------------------- CABLE PROPERTIES  -------------------------------------
0             NCablePropSets - Number of cable cable properties
PropSetID     EA             MatDens        T0        CtrlChannel
(-)           (N)            (kg/m)         (N)          (-)
----------------------- RIGID LINK PROPERTIES ------------------------------------
1             NRigidPropSets - Number of rigid link properties
PropSetID     MatDens
(-)           (kg/m)
1             1
---------------------- MEMBER COSINE MATRICES COSM(i,j) ------------------------
0             NCOSMs        - Number of unique cosine matrices (i.e., of unique member alignments)
COSMID     COSM11    COSM12    COSM13    COSM21    COSM22    COSM23    COSM31    COSM32    COSM33
(-)         (-)       (-)       (-)       (-)       (-)       (-)       (-)       (-)       (-)
------------------------ JOINT ADDITIONAL CONCENTRATED MASSES--------------------------
13            NCmass    - Number of joints with concentrated masses; Global Coordinate System
CMJointID  JMass       JMXX        JMYY        JMZZ      JMXY     JMXZ     JMYZ    MCGX   MCGY   MCGZ
(-)        (kg)      (kg*m^2)    (kg*m^2)    (kg*m^2)  (kg*m^2) (kg*m^2) (kg*m^2)   (m)    (m)    (m)
 2      7.6710e+03  1.0164e+06  1.0164e+06  3.9768e+04   0        0        0        0      0      0
 2      7.6710E+03  1.0164E+06  1.0164E+06  3.9768E+04   0        0        0        0      0      0
 7      2.1095E+05  3.4922E+07  2.1071E+08  1.9083E+08   0        0        0        0      0      0
22      2.1095E+05  1.6677E+08  7.8870E+07  1.9083E+08   0        0        0        0      0      0
37      2.1095E+05  1.6677E+08  7.8870E+07  1.9083E+08   0        0        0        0      0      0
 6      1.5768E+05  1.1633E+07  1.4303E+08  1.4548E+08   0        0        0        0      0      0
21      1.5768E+05  1.1018E+08  4.4483E+07  1.4548E+08   0        0        0        0      0      0
36      1.5768E+05  1.1018E+08  4.4483E+07  1.4548E+08   0        0        0        0      0      0
 6      5.3269E+04  2.0314E+06  4.6422E+07  4.5350E+07   0        0        0        0      0      0
21      5.3269E+04  3.5324E+07  1.3129E+07  4.5350E+07   0        0        0        0      0      0
36      5.3269E+04  3.5324E+07  1.3129E+07  4.5350E+07   0        0        0        0      0      0
 5      5.2209E+04  2.2621E+07  6.6128E+07  4.4428E+07   0        0        0        0      0      0
20      5.2209E+04  5.5251E+07  3.3498E+07  4.4428E+07   0        0        0        0      0      0
35      5.2209E+04  5.5251E+07  3.3498E+07  4.4428E+07   0        0        0        0      0      0
---------------------------- OUTPUT: SUMMARY & OUTFILE ------------------------------
True          SumPrint      - Output a Summary File (flag)
1             OutCBModes    - Output Guyan and Craig-Bampton modes (flag)
1             OutFEMModes   - Output first 30 FEM modes (flag)
False         OutCOSM       - Output cosine matrices with the selected output member forces (flag)
False         OutAll        - [T/F] Output all members' end forces
2             OutSwtch      - [1/2/3] Output requested channels to: 2=<rootname>.out (generated by FAST)
True          TabDelim      - Generate a tab-delimited output in the <rootname>.SD.out file
1             OutDec        - Decimation of output in the <rootname>.SD.out file
"ES11.4e2"    OutFmt        - Output format for numerical results in the <rootname>.SD.out file
"A11"         OutSFmt       - Output format for header strings in the <rootname>.SD.out file
```

```
------------------------- MEMBER OUTPUT LIST ------------------------------------------
6             NMOutputs     - Number of members whose forces/displacements/... will be output (-)
MemberID      NOutCnt    NodeCnt
(-)           (-)        (-)
13            2          1  2
14            2          1  2
5             2          1  2
6             2          1  2
9             2          1  2
10            2          1  2
---------- SDOutList: The next line(s) contains a list of output parameters that will be output  ------
"M1N1FKxe, M1N1FKye, M1N1FKze, M1N1MKxe, M1N1MKye, M1N1MKze"
"M1N2FKxe, M1N2FKye, M1N2FKze, M1N2MKxe, M1N2MKye, M1N2MKze"
"M2N1FKxe, M2N1FKye, M2N1FKze, M2N1MKxe, M2N1MKye, M2N1MKze"
"M2N2FKxe, M2N2FKye, M2N2FKze, M2N2MKxe, M2N2MKye, M2N2MKze"
"M3N1FKxe, M3N1FKye, M3N1FKze, M3N1MKxe, M3N1MKye, M3N1MKze"
"M3N2FKxe, M3N2FKye, M3N2FKze, M3N2MKxe, M3N2MKye, M3N2MKze"
"M4N1FKxe, M4N1FKye, M4N1FKze, M4N1MKxe, M4N1MKye, M4N1MKze"
"M4N2FKxe, M4N2FKye, M4N2FKze, M4N2MKxe, M4N2MKye, M4N2MKze"
"M5N1FKxe, M5N1FKye, M5N1FKze, M5N1MKxe, M5N1MKye, M5N1MKze"
"M5N2FKxe, M5N2FKye, M5N2FKze, M5N2MKxe, M5N2MKye, M5N2MKze"
"M6N1FKxe, M6N1FKye, M6N1FKze, M6N1MKxe, M6N1MKye, M6N1MKze"
"M6N2FKxe, M6N2FKye, M6N2FKze, M6N2MKxe, M6N2MKye, M6N2MKze"
END
```

A.2. HydroDyn

```
------- HydroDyn Input File ----------------------------------------------------
NREL          MW            - offshore baseline floating platform HydroDyn input properties
False         Echo          - Echo the input file data (flag)
---------------------- ENVIRONMENTAL CONDITIONS --------------------------------
"default"     WtrDens       - Water density (kg/m^3)
"default"     WtrDpth       - Water depth (meters)
"default"     MSL2SWL       - Offset between still-water- and mean sea level (meters) [positive upward]
---------------------- WAVES ---------------------------------------------------
2             WaveMod       - Incident wave kinematics model {2: JONSWAP/Pierson-Moskowitz spectrum}
0             WaveStMod     - Model for stretching incident wave kinematics to instantaneous free surface
4600          WaveTMax      - Analysis time for incident wave calculations (sec)
0.2           WaveDT        - Time step for incident wave calculations (sec)
1.8           WaveHs        - Significant wave height of incident waves (meters)
7.7           WaveTp        - Peak-spectral period of incident waves (sec)
1.44          WavePkShp     - Peak-shape parameter of incident wave spectrum (-)
0.314159      WvLowCOff     - Low cut-off frequency of the wave spectrum (rad/s)
1.570796      WvHiCOff      - High cut-off frequency of the wave spectrum (rad/s)
0.0           WaveDir       - Incident wave propagation heading direction (degrees)
0             WaveDirMod    - Directional spreading function {0: none, 1: COS2S} (-)
1             WaveDirSpread - Wave direction spreading coefficient ( > 0 ) (-)
1             WaveNDir      - Number of wave directions (-)
0             WaveDirRange  - Range of wave directions (full range: WaveDir +/- 1/2*WaveDirRange) (deg)
834081084     WaveSeed(1)   - First random seed of incident waves [-2147483648 to 2147483647] (-)
RANLUX        WaveSeed(2)   - Second random seed of incident waves, or an alternative pRNG: "RanLux" (-)
False         WaveNDAmp     - Flag for normally distributed amplitudes (flag)
""            WvKinFile     - Root name of externally generated wave data file(s) (quoted string)
1             NWaveElev     - Number of points where the incident wave elevations can be computed (-)
0             WaveElevxi    - List of xi output coordinates for the incident wave elevations (meters)
0             WaveElevyi    - List of yi output coordinates for the incident wave elevations (meters)
---------------------- 2ND-ORDER WAVES -----------------------------------------
True          WvDiffQTF     - Full difference-frequency 2nd-order wave kinematics (flag)
True          WvSumQTF      - Full summation-frequency 2nd-order wave kinematics (flag)
0             WvLowCOffD    - Low frequency cutoff used in the difference-frequencies (rad/s)
1.256637      WvHiCOffD     - High frequency cutoff used in the difference-frequencies (rad/s)
0.618319      WvLowCOffS    - Low frequency cutoff used in the summation-frequencies (rad/s)
3.141593      WvHiCOffS     - High frequency cutoff used in the summation-frequencies (rad/s)
---------------------- CURRENT -------------------------------------------------
0             CurrMod       - Current profile model {0: none=no current} (switch)
0             CurrSSV0      - Sub-surface current velocity at still water level (m/s)
"DEFAULT"     CurrSSDir     - Sub-surface current heading direction (degrees) or DEFAULT (string)
20            CurrNSRef     - Near-surface current reference depth (meters)
0             CurrNSV0      - Near-surface current velocity at still water level (m/s)
0             CurrNSDir     - Near-surface current heading direction (degrees)
0             CurrDIV       - Depth-independent current velocity (m/s)
0             CurrDIDir     - Depth-independent current heading direction (degrees)
---------------------- FLOATING PLATFORM ---------------------------------------
1             PotMod        - Potential-flow model {1: freq-to-time-domain based on WAMIT output}
1             ExctnMod      - Wave-excitation model {1: DFT} (switch)
1             RdtnMod       - Radiation memory-effect model {1: convolution} (switch)
60            RdtnTMax      - Analysis time for wave radiation kernel calculations (sec)
0.0125        RdtnDT        - Time step for wave radiation kernel calculations (sec)
1             NBody         - Number of WAMIT bodies to be used (-)
1             NBodyMod      - Body coupling model
"..\_HydroData\run_1"  PotFile - Root name of potential-flow model data;
1             WAMITULEN     - Characteristic body length scale to redimensionalize WAMIT output (meters)
0.0           PtfmRefxt     - The xt offset of the body reference point(s) from (0,0,0) (meters)
0.0           PtfmRefyt     - The yt offset of the body reference point(s) from (0,0,0) (meters)
0.0           PtfmRefzt     - The zt offset of the body reference point(s) from (0,0,0) (meters)
0.0           PtfmRefztRot  - The rotation about zt of the body reference frame(s) from xt/yt (degrees)
13556.76      PtfmVol0      - Displaced water volume when the body is in its undisplaced position (m^3)
0.0           PtfmCOBxt     - The xt offset of the center of buoyancy (COB) from (0,0) (meters)
0.0           PtfmCOByt     - The yt offset of the center of buoyancy (COB) from (0,0) (meters)
---------------------- 2ND-ORDER FLOATING PLATFORM FORCES ----------------------
0             MnDrift       - Mean-drift 2nd-order forces computed {WAMIT file to use}
0             NewmanApp     - Mean- and slow-drift 2nd-order forces computed with Newman's approximation
12            DiffQTF       - Full difference-frequency 2nd-order forces computed with QTF {WAMIT file}
12            SumQTF        - Full summation -frequency 2nd-order forces computed with QTF {WAMIT file}
```

```
---------------------- PLATFORM ADDITIONAL STIFFNESS AND DAMPING  --------------
0   AddF0    - Additional preload (N, N-m)
0
0
0
0
0
0          0          0          0          0          0   AddCLin  - Additional linear stiffness
0          0          0          0          0          0
0          0        76610.51     0          0          0
0          0          0     -41370632       0          0
0          0          0          0     -41370632       0
0          0          0          0          0          0
0          0          0          0          0          0   AddBLin  - Additional linear damping
0          0          0          0          0          0
0          0          0          0          0          0
0          0          0          0          0          0
0          0          0          0          0          0
0          0          0          0          0          0
0          0          0          0          0          0   AddBQuad - Additional quadratic drag
0          0          0          0          0          0
0          0          0          0          0          0
0          0          0          0          0          0
0          0          0          0          0          0
0          0          0          0          0          0
---------------------- AXIAL COEFFICIENTS --------------------------------------
2             NAxCoef       - Number of axial coefficients (-)
AxCoefID      AxCd          AxCa          AxCp
(-)           (-)           (-)           (-)
1              0             0             1
2            9.6             0             1
---------------------- MEMBER JOINTS -------------------------------------------
44            NJoints       - Number of joints (-) [must be exactly 0 or at least 2]
JointID       Jointxi       Jointyi       Jointzi       JointAxID     JointOvrlp
(-)             (m)           (m)           (m)            (-)         (switch)
1              0.0000        0.0000       10.0000           1              0
2              0.0000        0.0000      -20.0000           1              0
5            -28.8675        0.0000       12.0000           1              0
6            -28.8675        0.0000      -14.0000           1              0
7            -28.8675        0.0000      -20.0000           1              0
8            -22.8675        0.0000        9.9990           1              0
9            -23.6714       -3.0000        9.9990           1              0
10           -23.6714        3.0000        9.9990           1              0
11            -3.2500        0.0000        9.9990           1              0
12           -22.8675        0.0000        9.1990           1              0
14           -16.8675        0.0000      -17.0000           1              0
15           -18.4752       -6.0000      -17.0000           1              0
16           -18.4752        6.0000      -17.0000           1              0
17            -3.2500        0.0000      -17.0000           1              0
18            -3.2500        0.0000      -16.2000           1              0
20            14.4338      -25.0000       12.0000           1              0
21            14.4338      -25.0000      -14.0000           1              0
22            14.4338      -25.0000      -20.0000           1              0
23            11.4338      -19.8000        9.9990           1              0
24            14.4338      -19.0000        9.9990           1              0
25             9.2376      -22.0000        9.9990           1              0
26             1.6250       -2.8140        9.9990           1              0
27            11.4338      -19.8000        9.1990           1              0
29             8.4338      -14.6000      -17.0000           1              0
30            14.4338      -13.0000      -17.0000           1              0
31             4.0414      -19.0000      -17.0000           1              0
32             1.6250       -2.8140      -17.0000           1              0
33             1.6250       -2.8140      -16.2000           1              0
35            14.4338       25.0000       12.0000           1              0
36            14.4338       25.0000      -14.0000           1              0
37            14.4338       25.0000      -20.0000           1              0
38            11.4338       19.8000        9.9990           1              0
39             9.2376       22.0000        9.9990           1              0
40            14.4338       19.0000        9.9990           1              0
41             1.6250        2.8140        9.9990           1              0
42            11.4338       19.8000        9.1990           1              0
44             8.4338       14.6000      -17.0000           1              0
45             4.0414       19.0000      -17.0000           1              0
46            14.4338       13.0000      -17.0000           1              0
47             1.6250        2.8140      -17.0000           1              0
48             1.6250        2.8140      -16.2000           1              0
50           -28.8675        0.0000      -19.9400           1              0
51            14.4338      -25.0000      -19.9400           1              0
52            14.4338       25.0000      -19.9400           1              0
```

```
---------------------- MEMBER CROSS-SECTION PROPERTIES -------------------------
4             NPropSets     - Number of member property sets (-)
PropSetID     PropD           PropThck
(-)            (m)             (m)
1              6.5            0.0300
2             24.0            0.0600
3             12.0            0.0600
4              1.6            0.0175
---------------------- SIMPLE HYDRODYNAMIC COEFFICIENTS (model 1) --------------
SimplCd  SimplCdMG  SimplCa  SimplCaMG  SimplCp  SimplCpMG  SimplAxCd  SimplAxCdMG  SimplAxCa
(-)         (-)       (-)       (-)       (-)       (-)        (-)        (-)          (-)
0            0         0         0         1         1          0          0            0
SimplAxCaMG  SimplAxCp  SimplAxCpMG
(-)             (-)        (-)
0                1          1
---------------------- DEPTH-BASED HYDRODYNAMIC COEFFICIENTS (model 2) ---------
0             NCoefDpth     - Number of depth-dependent coefficients (-)
Dpth  DpthCd  DpthCdMG  DpthCa  DpthCaMG  DpthCp  DpthCpMG  DpthAxCd  DpthAxCdMG  DpthAxCa
(m)    (-)      (-)      (-)      (-)      (-)       (-)       (-)        (-)        (-)
DpthAxCaMG  DpthAxCp  DpthAxCpMG
(-)             (-)      (-)
---------------------- MEMBER-BASED HYDRODYNAMIC COEFFICIENTS (model 3) --------
25            NCoefMembers  - Number of member-based coefficients (-)
MemberID      MemberCd1       MemberCd2
(-)              (-)             (-)
1               0.56            0.56
2               0.61            0.61
3               0.61            0.61
4               0.61            0.61
5               0.68            0.68
6               0.68            0.68
7               0.68            0.68
23              0.68            0.68
24              0.68            0.68
25              0.68            0.68
8               0.63            0.63
9               0.63            0.63
10              0.63            0.63
11              0.63            0.63
12              0.63            0.63
13              0.63            0.63
14              0.63            0.63
15              0.63            0.63
16              0.63            0.63
17              0.63            0.63
18              0.63            0.63
19              0.63            0.63
20              0.63            0.63
21              0.63            0.63
22              0.63            0.63
-------------------- MEMBERS -------------------------------------------------
25            NMembers      - Number of members (-)
MemberID      MJointID1     MJointID2     MPropSetID1   MPropSetID2   MDivSize     MCoefMod     PropPot
(-)             (-)           (-)           (-)           (-)          (m)        (switch)     (flag)
1                1             2             1             1            1            3             TRUE
2                5             6             3             3            1            3             TRUE
3                6            50             2             2            1            3             TRUE
4               20            21             3             3            1            3             TRUE
5               21            51             2             2            1            3             TRUE
6               35            36             3             3            1            3             TRUE
7               36            52             2             2            1            3             TRUE
8                8            11             4             4            1            3            FALSE
9               23            26             4             4            1            3            FALSE
10              38            41             4             4            1            3            FALSE
11              14            17             4             4            1            3            FALSE
12              29            32             4             4            1            3            FALSE
13              44            47             4             4            1            3            FALSE
14               9            25             4             4            1            3            FALSE
15              24            40             4             4            1            3            FALSE
16              39            10             4             4            1            3            FALSE
17              15            31             4             4            1            3            FALSE
18              30            46             4             4            1            3            FALSE
19              45            16             4             4            1            3            FALSE
20              12            18             4             4            1            3            FALSE
21              27            33             4             4            1            3            FALSE
22              42            48             4             4            1            3            FALSE
23              50             7             2             2            1            3             TRUE
24              51            22             2             2            1            3             TRUE
25              52            37             2             2            1            3             TRUE
```

```
---------------------- FILLED MEMBERS ------------------------------------------
2             NFillGroups   - Number of filled member groups (-) [FillFSLoc is related to MSL2SWL]
FillNumM      FillMList       FillFSLoc       FillDens
(-)             (-)             (m)           (kg/m^3)
3              2 4 6           -6.17            1025
3              3 5 7          -14.89            1025
---------------------- MARINE GROWTH -------------------------------------------
0             NMGDepths     - Number of marine-growth depths specified (-)
MGDpth          MGThck          MGDens
(m)             (m)             (kg/m^3)
---------------------- MEMBER OUTPUT LIST --------------------------------------
0             NMOutputs     - Number of member outputs (-) [must be < 10]
MemberID        NOutLoc         NodeLocs
(-)             (-)             (-)
---------------------- JOINT OUTPUT LIST ---------------------------------------
0             NJOutputs     - Number of joint outputs [Must be < 10]
0             JOutLst       - List of JointIDs which are to be output (-)
---------------------- OUTPUT --------------------------------------------------
True          HDSum         - Output a summary file [flag]
False         OutAll        - Output all user-specified member and joint loads (not interior locations)
2             OutSwtch      - Output requested channels to: [2=GlueCode.out]
"E15.7e2"     OutFmt        - Output format for numerical results (quoted string)
"A11"         OutSFmt       - Output format for header strings (quoted string)
----------------------- OUTPUT CHANNELS -----------------------------------------
"Wave1Elev"               - Wave elevation at the platform reference point (0,  0)
"HydroFxi"
"HydroFyi"
"HydroFzi"
"HydroMxi"
"HydroMyi"
"HydroMzi"
"B1Surge"
"B1Sway"
"B1Heave"
"B1Roll"
"B1Pitch"
"B1Yaw"
END
---------------------------------------------------------------------------------------
```

B

Derivations

In section B.1 of this appendix, the derivation of the additional linear stiffness matrix of section 5.4.5 is provided. Subsequently, the derivation of the platform mass moment of inertia of the ElastoDyn-based substructure model of section 6.2.2 is given in section B.2.

B.1. Additional Linear Stiffness Matrix

The coefficients for the additional linear stiffness matrix are given by the following matrix:

$$\texttt{AddCLin} = \begin{bmatrix} 0 & 0 & 0 & 0 & 0 & 0 \\ 0 & 0 & 0 & 0 & 0 & 0 \\ 0 & 0 & c_{3,3} & c_{3,4} & c_{3,5} & 0 \\ 0 & 0 & c_{4,3} & c_{4,4} & c_{4,5} & c_{4,6} \\ 0 & 0 & c_{5,3} & c_{5,4} & c_{5,5} & c_{5,6} \\ 0 & 0 & 0 & 0 & 0 & 0 \end{bmatrix} \tag{B.1}$$

$$\begin{aligned} \text{with:}\quad & c_{3,3} = \rho g A_0 \\ & c_{3,4} = \rho g \iint_{A_0} y dA \\ & c_{3,5} = -\rho g \iint_{A_0} x dA \\ & c_{4,3} = \rho g \iint_{A_0} y dA \\ & c_{4,4} = \rho g \iint_{A_0} y^2 dA + \rho g V_0 z_\mathrm{b} - m_\mathrm{mg} g z_\mathrm{mg} - m_\mathrm{f} g z_\mathrm{f} \\ & c_{4,5} = -\rho g \iint_{A_0} xy dA \\ & c_{4,6} = -\rho g V_0 x_\mathrm{b} + m_\mathrm{mg} g x_\mathrm{mg} - m_\mathrm{f} g x_\mathrm{f} \\ & c_{5,3} = -\rho g \iint_{A_0} x dA \\ & c_{5,4} = -\rho g \iint_{A_0} xy dA \\ & c_{5,5} = \rho g \iint_{A_0} x^2 dA + \rho g V_0 z_\mathrm{b} - m_\mathrm{mg} g z_\mathrm{mg} - m_\mathrm{f} g z_\mathrm{f} \\ & c_{5,6} = -\rho g V_0 y_\mathrm{b} + m_\mathrm{mg} g y_\mathrm{mg} - m_\mathrm{f} g y_\mathrm{f} \end{aligned}$$

where A_0 is the undisplaced waterplane area of all strip-theory members combined (m^2), V_0 is the undisplaced volume of all strip-theory members combined (m^3), $(x_\mathrm{b}, y_\mathrm{b}, z_\mathrm{b})$ are the coordinates of the center of buoyancy of the undisplaced structure composed by all strip-theory members (m), m_mg is the total mass of marine growth (kg), $(x_{\mathrm{mg}}, y_{\mathrm{mg}}, z_{\mathrm{mg}})$ are the coordinates of the center of mass of the undisplaced marine growth mass (m), m_{f} is the total ballast mass present in the strip-theory members (kg), and $(x_{\mathrm{f}}, y_{\mathrm{f}}, z_{\mathrm{f}})$ are the coordinates of the center of mass of the ballast (m).

Now, because marine growth is neglected in this project, all the terms related to m_{mg} are nullified. Furthermore, as there is no ballast present in the pontoons/braces, the terms with m_{f} reduce to zero as well. Lastly, as the platform has three planes of symmetry, which coincide with the z-axis, the following simplifications can be made:

$$\iint_{A_0} x dA = 0, \quad \iint_{A_0} y dA = 0, \quad \iint_{A_0} xy dA = 0, \quad x_{\mathrm{b}} = 0, \quad y_{\mathrm{b}} = 0$$

hence the off-diagonal terms disappear, and the matrix from equation B.1 finally reduces to:

$$\texttt{AddCLin} = \begin{bmatrix} 0 & 0 & 0 & 0 & 0 & 0 \\ 0 & 0 & 0 & 0 & 0 & 0 \\ 0 & 0 & \rho g A_0 & 0 & 0 & 0 \\ 0 & 0 & 0 & \rho g \iint_{A_0} y^2 dA + \rho g V_0 z_b & 0 & 0 \\ 0 & 0 & 0 & 0 & \rho g \iint_{A_0} x^2 dA + \rho g V_0 z_b & 0 \\ 0 & 0 & 0 & 0 & 0 & 0 \end{bmatrix} \tag{B.2}$$

B.2. Platform Mass Moment of Inertia

The process to compute the platform mass moments of inertia involves several steps. Initially, the inertia tensor for each individual member is determined with respect to its centre of gravity in the element frame of reference, using the relations in equation B.3. These cylindrical hollow elements are symmetric, thus only the diagonal elements need computing: I_{xx}, I_{yy}, and I_{zz}.

$$\begin{aligned} I_{\mathrm{xx}} &= \frac{1}{4} m \left(r^2 + (r-t)^2\right) + \frac{1}{12} m L^2 \\ I_{\mathrm{yy}} &= I_{\mathrm{xx}} \\ I_{\mathrm{zz}} &= \frac{1}{2} m \left(r^2 + (r-t)^2\right) \end{aligned} \tag{B.3}$$

where m is the member mass (kg), r is the member radius (m), t is the member wall thickness (m), and L is the member length (m). In the subsequent step, the direction cosine matrix for each member is used to transform the member's inertia tensor from its local frame to the global reference frame of the undisplaced platform. The direction cosine matrix is given by the following relation [35]:

$$\mathbf{D}_{\mathrm{c}} = \begin{bmatrix} \frac{y_2 - y_1}{L_{xy}} & \frac{(x_2 - x_1)(z_2 - z_1)}{L_{xy} L} & \frac{x_2 - x_1}{L} \\ \frac{x_1 - x_2}{L_{xy}} & \frac{(y_2 - y_1)(z_2 - z_1)}{L_{xy} L} & \frac{y_2 - y_1}{L} \\ 0 & -\frac{L_{xy}}{L} & \frac{z_2 - z_1}{L} \end{bmatrix} \tag{B.4}$$

$$\text{with:} \quad L_{xy} = \sqrt{(x_2 - x_1)^2 + (y_2 - y_1)^2} \tag{B.5}$$

$$L = \sqrt{(x_2 - x_1)^2 + (y_2 - y_1)^2 + (z_2 - z_1)^2} \tag{B.6}$$

where (x_1, y_1, z_1) and (x_2, y_2, z_2) are the start- and endpoints of the members, respectively. In the special case where the member is in parallel with the z-axis (i.e., $x_1 = x_2$ and $z_1 = z_2$), the cosine matrix is reduced to:

$$\begin{aligned} &\text{if } z_1 \leq z_2 \quad \mathbf{D}_{\mathrm{c}} = \begin{bmatrix} 1 & 0 & 0 \\ 0 & 1 & 0 \\ 0 & 0 & 1 \end{bmatrix} \\ &\text{else} \quad \mathbf{D}_{\mathrm{c}} = \begin{bmatrix} 1 & 0 & 0 \\ 0 & -1 & 0 \\ 0 & 0 & -1 \end{bmatrix} \end{aligned} \tag{B.7}$$

The element inertia tensor can then be transformed to the global reference frame by performing the following matrix operation:

$$I_{\text{global}} = \mathbf{D}_{\text{c}} \cdot \begin{bmatrix} I_{\text{xx}} & 0 & 0 \\ 0 & I_{\text{yy}} & 0 \\ 0 & 0 & I_{\text{zz}} \end{bmatrix} \cdot \mathbf{D}_{\text{c}}^{T} \tag{B.8}$$

In the last step, the total roll, pitch and yaw inertia of the floating platform are computed by summing the inertia of the members expressed in the global reference frame, taking into account the parallel axis theorem:

$$I_{\text{roll}} = \sum_{i=1}^{N} \left(I_{\text{global},i}(1,1) + m_i \left(d_y^2 + d_z^2 \right) \right) \tag{B.9}$$

$$I_{\text{pitch}} = \sum_{i=1}^{N} \left(I_{\text{global},i}(2,2) + m_i \left(d_x^2 + d_z^2 \right) \right) \tag{B.10}$$

$$I_{\text{yaw}} = \sum_{i=1}^{N} \left(I_{\text{global},i}(3,3) + m_i \left(d_x^2 + d_y^2 \right) \right) \tag{B.11}$$

where N is the total number of members, m_i is the mass of the i-th member, and d_x, d_y, d_z are the distances in (m) between the member centroids and the platform centre of mass, in their respective directions.

C

Axial Stresses In the Structural Members of the DeepCWind Platform

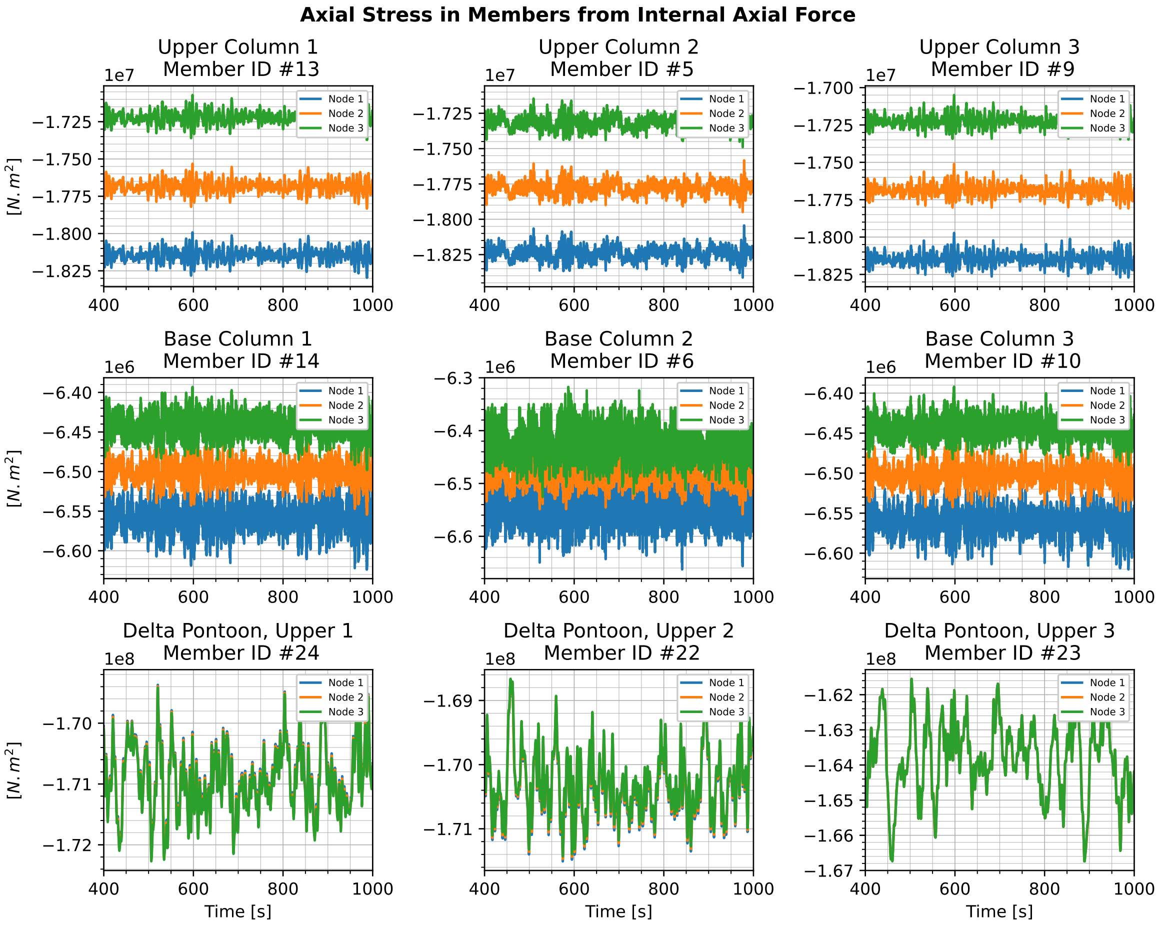

Figure C.1: Internal stresses in the structural members, processed from the results of load case 11 $\mathrm{m\,s^{-1}}$ of DLC 1.2 (1)

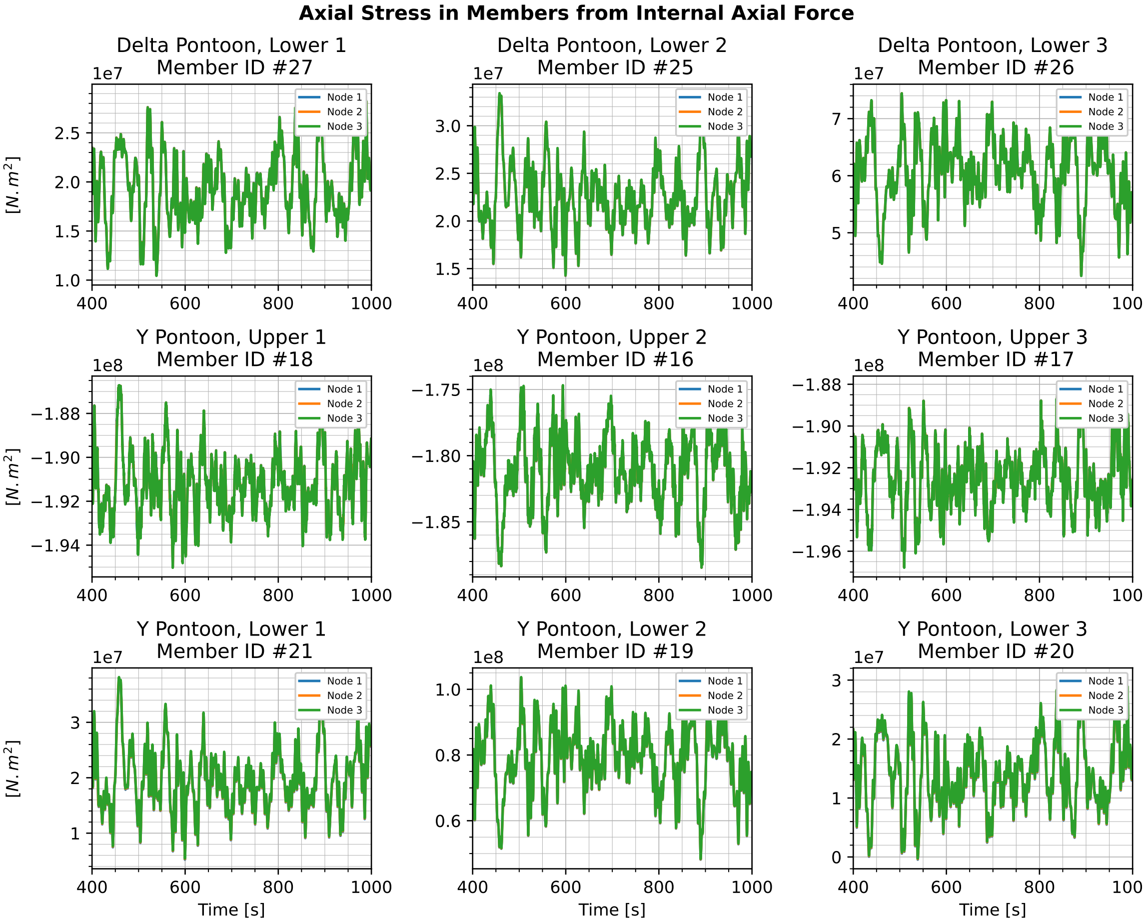

Figure C.2: Internal stresses in the structural members, processed from the results of load case 11 m s^{-1} of DLC 1.2 (2)

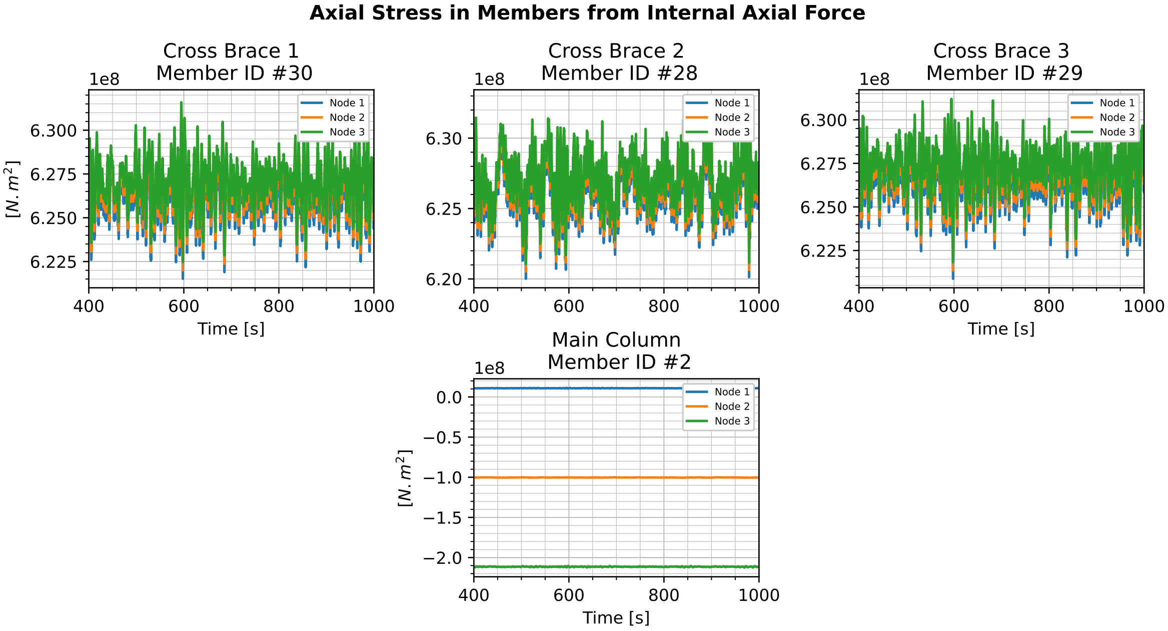

Figure C.3: Internal stresses in the structural members, processed from the results of load case 11 m s^{-1} of DLC 1.2 (3)

D

NEMOH Mesh Convergence Plots

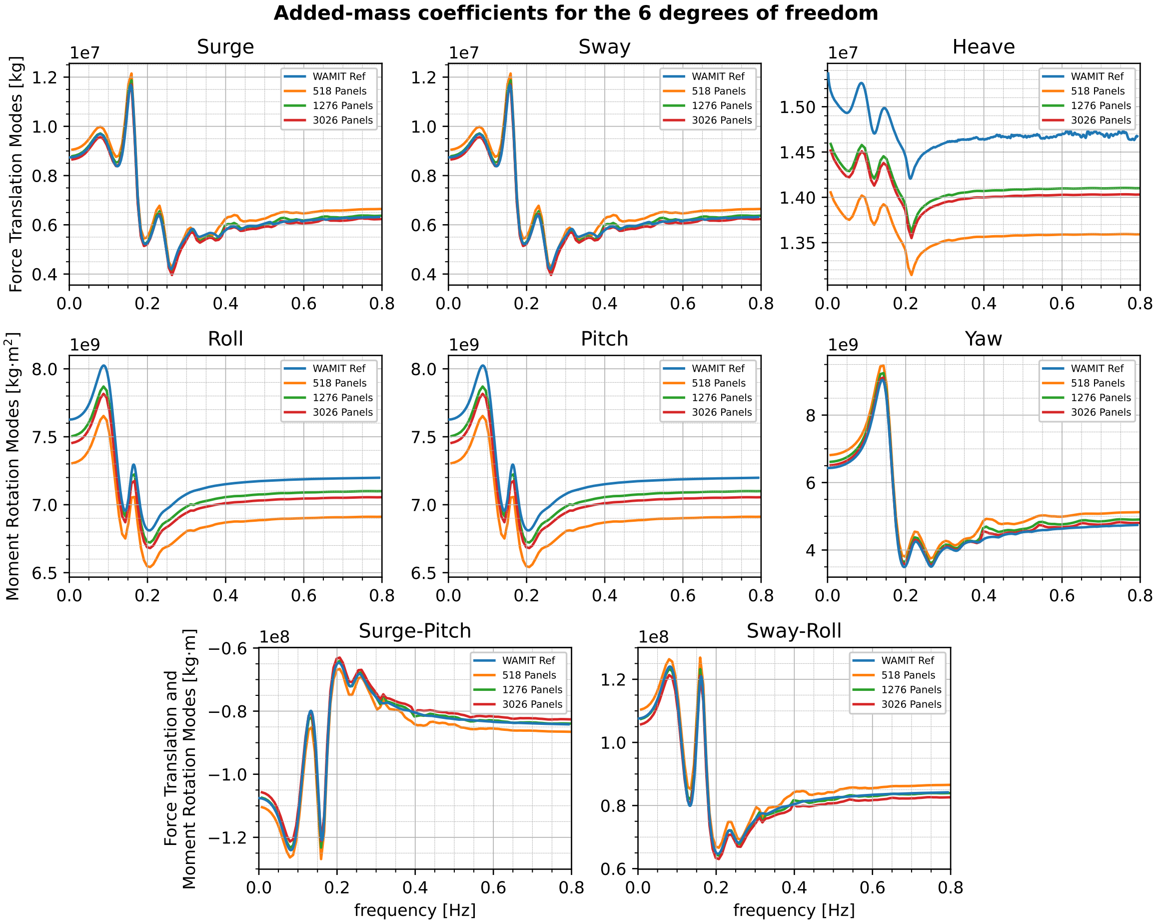

Figure D.1: Influence of mesh panel size on the added mass coefficients

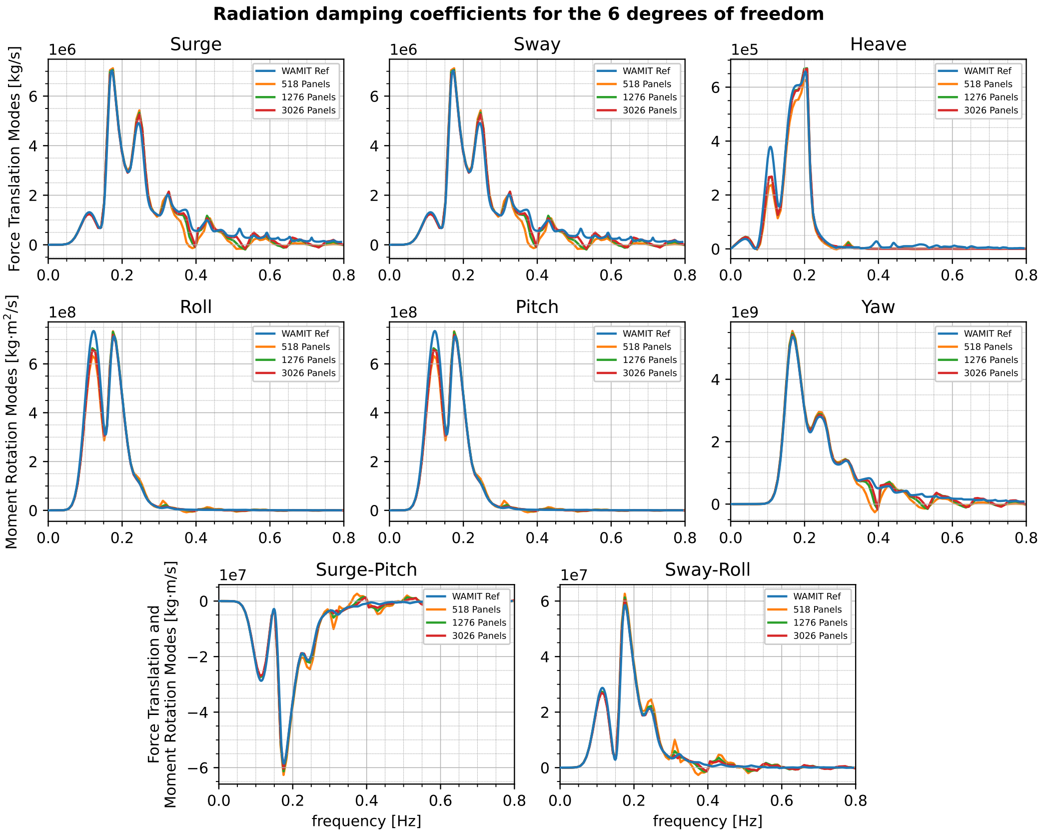

Figure D.2: Influence of mesh panel size on the radiation damping coefficients

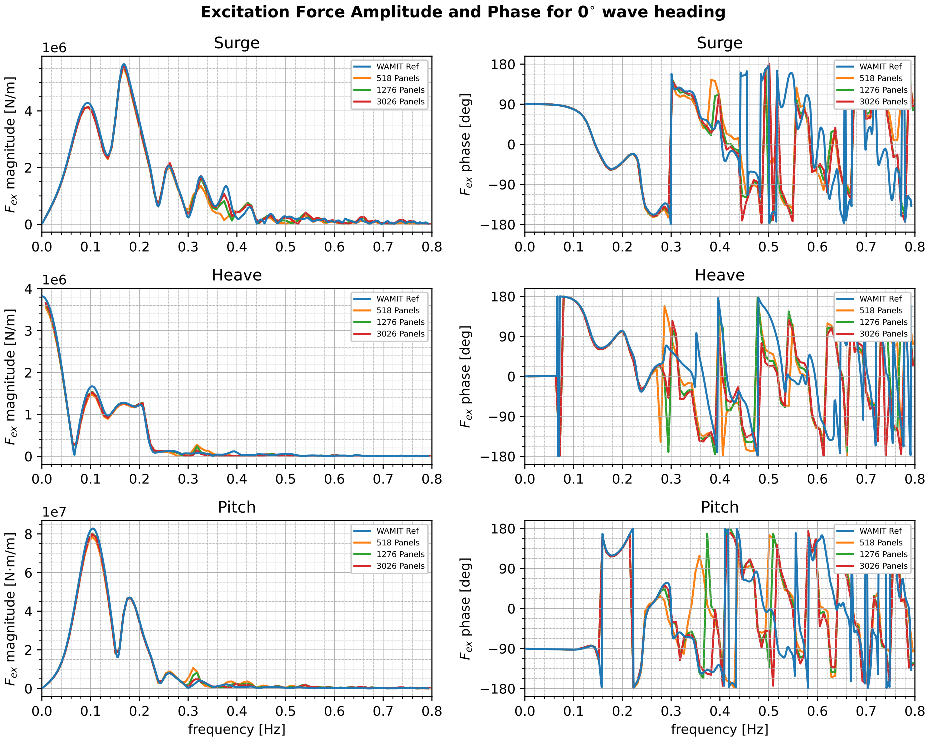

Figure D.3: Influence of mesh panel size on the wave excitation force

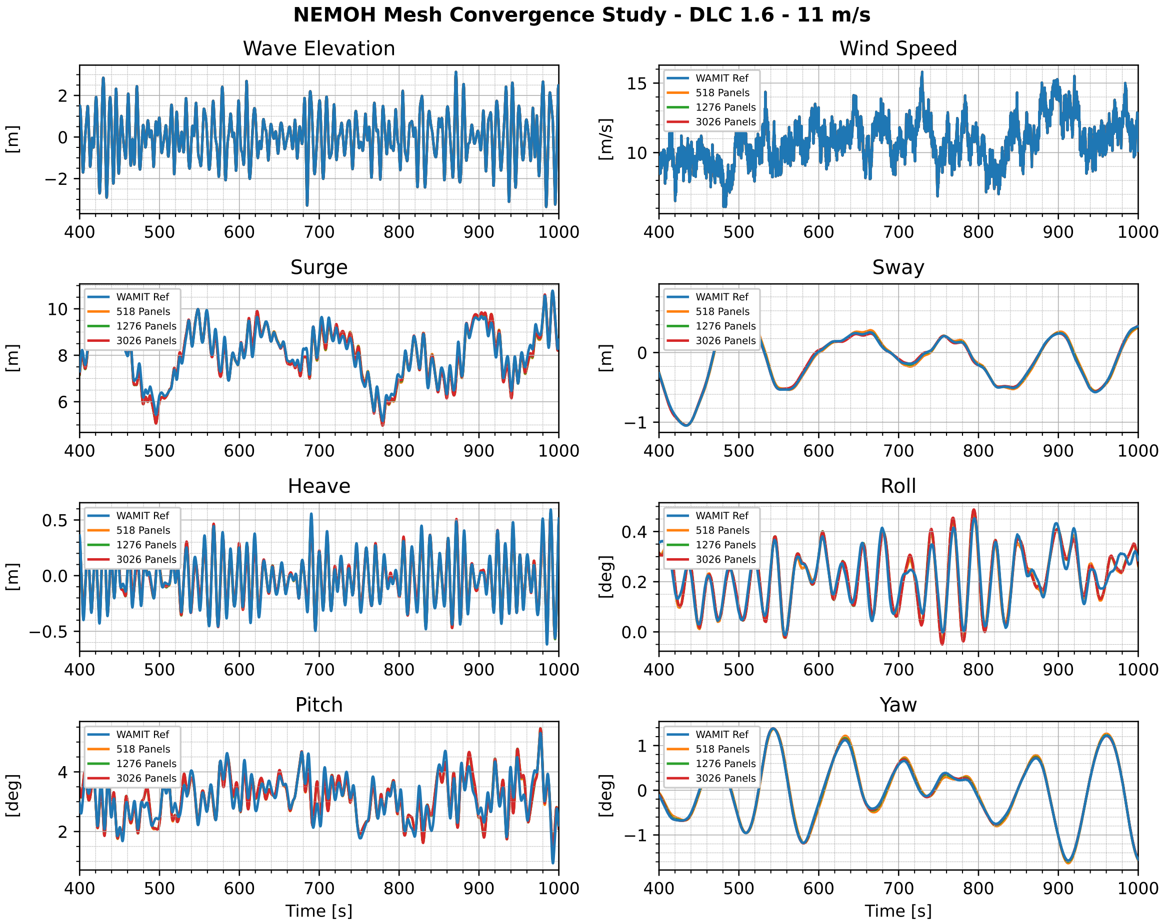

Figure D.4: Influence of mesh panel size on FOWT motion

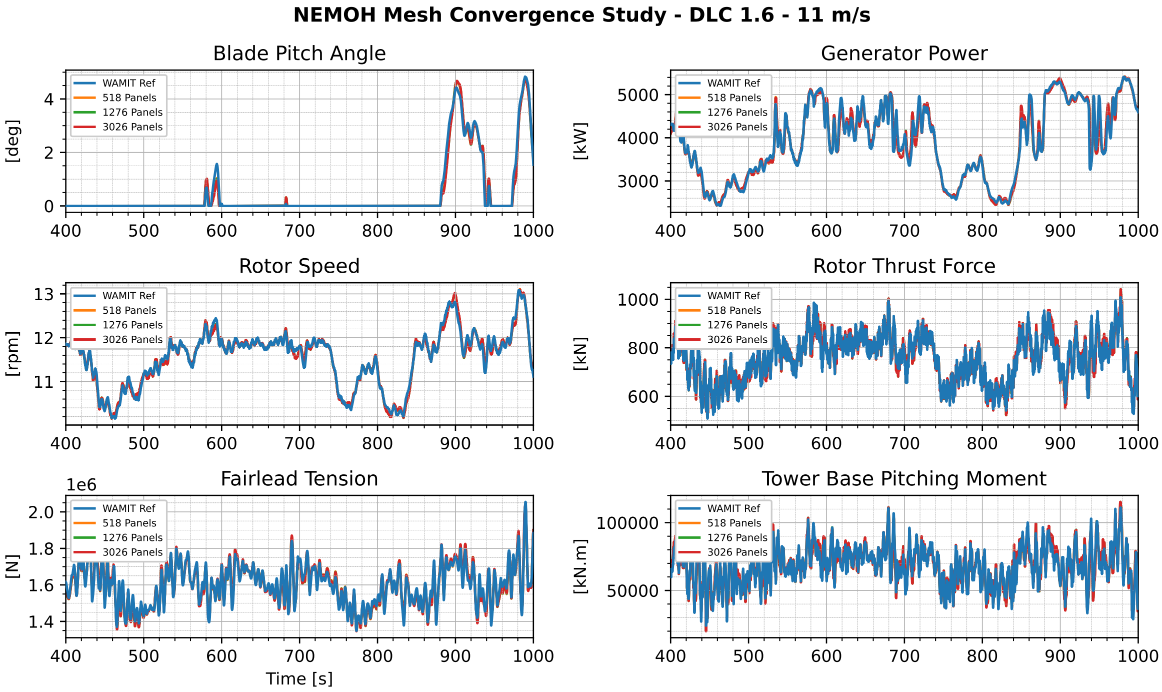

Figure D.5: Influence of mesh panel size on FOWT performance